12-2007

Fundamental Investigation of Vesicle Bilayer Membrane Dynamics

Okumu

FUNDAMENTAL INVESTIGATION OF VESICLE BILAYER MEMBRANE DYNAMICS

by
Wilson Okumu

A Thesis
Submitted to the
Faculty of the Graduate College
in partial fulfillment of the
requirements for the
Degree of Master of Science
Department of Chemistry

Western Michigan University
Kalamazoo, Michigan
December 2007

ACKNOWLEDGEMENTS

First, I thank Chemistry Department, Western Michigan University for the continuous support towards my graduate studies in Chemistry.

A special thanks to my research advisor Prof. Subra Muralidharan for the guidance, support, and patience throughout this research. He gave the support and confidence to present my research data in American Chemical Society (ACS) national conferences. Thanks to the Postdoc Narayan Srividya for her guidance in laser spectroscopy, optical trapping, analysis of kinetic data and equipping the lab.

I extend a special thanks to Prof. Ekkehard Sinn who accepted to Chair my thesis committee and in writing the thesis. Thanks to Dr. Reinhold for accepting to be a committee member, writing of this thesis and the challenging research that lies behind it. Also thanks to the folks who made up the KECK group for the valuable contributions towards this project. I am greatly indebted to my mum Margaret for her patience and unconditional support, my brother Michael and my wife Mildred.

This research was supported by grants from W. M. KECK Foundations and the Department of Defense.

Wilson Okumu

FUNDAMENTAL INVESTIGATION OF VESICLE BILAYER MEMBRANE DYNAMICS

Wilson Okumu, M.S.

Western Michigan University, 2007

We studied the bilayer of vesicles from dimyristolyphosphatidylcholine (DMPC), using nitrobenzoxadiazole (NBD) probes, attached to the head (NBD-PE) and the tail (NBD-PC) of phospholipid derivatives. We characterized the bilayer as it underwent reversible transition from the gel to the fluid through a phase transition range. The main phase transition was characterized by steady state and time-resolved fluorescence anisotropy, fluorescence intensity decrement and kinetics of dithionite reduction. We also studied DMPC with dihydrocholesterol. Differences between the surface and interior regions of the bilayer region were obtained. The activation barrier was enthalpic in the gel, entropic in the fluid phase and anomalous at the transition region. In addition, the rate coefficient of NBD PC was higher than the NBD PE. The studies have developed rapid preparation method for generating giant vesicles from phosphatidylcholines. The studies show for the first time that the dithionite reduction of the NBD involves a pre-equilibrium association step based on Eyring kinetic model.

TABLE OF CONTENTS

Table of Contents -Continued

CHAPTER

Table of Contents - Continued

CHAPTER

Table of Contents – Continued

CHAPTER

LIST OF TABLES

LIST OF FIGURES

List of Figures- Continued

List of Figures- Continued

LIST OF ABBREVIATIONS

NBD	Nitro-2,1,3-benzoxadiazol-4-yl
NBD PC	1-palmitoyl-2-[12-[(7-nitro-2-1, 3-benzoxadiazol-4-yl) amino] dodecanoyl]-*sn*-glycero- 3-phosphocholine, 16:0-12:0
NBD PE	(1, 2-dipalmitoyl-*sn*-glycero-3-phosphoethanolamine-N-(7-nitro-2-1, 3-benzoxadizol-4-yl) (ammonium salt), (16:0)
DMPC	1, 2-dimyristoyl-sn-glycero-3-phosphocholine, (14:0)
DPPN	L-α-1,2-dipalmitoyl-*sn*-glycero-3-phospho-[*N*-(4-nitrobenz-2-oxa-1,3-diazole)-ethanolamine]
DPPC	Dipalmitoylglycerophosphocholine, (16:0)
Dchol	Dihydrocholesterol, 3β-hydroxy-5α-cholestane
GUV	Giant Unilamellar Vesicles
SUV	Small Unilamellar Vesicles
MLV	Multi-lamellar Vesicles
LED	Light emitting diode
TCSPC	Time-Correlated Single Photon Counting
DPH	Diphenylhextriene
QEL	Quasi Elastic Light Scattering
POPC	1-palmitoyl 2-oleoyl phosphatidylcholine
DOPC	Dioeoylphosphatidylcholine
k_1	Rate coefficient for the fast reduction
HEPES	N-2-Hydroxyethylpiperazine-N'-2-ethanesulfonic acid

CHAPTER 1

INTRODUCTION

1.1The Lipid Bilayer as a Simple Model System

The dynamic property of biological membranes is best understood by studying the kinetics and thermodynamics of interactions of molecules in a model lipid bilayer system. In addition, studies conducted may provide useful information on the physical and chemical properties of the bilayer of lipid membranes. The ultimate goal is to determine rate of interactions and activation barriers associated with these interactions in model systems.

The lipid bilayer is the oldest and still valid molecular model of biological structure [1]. It is interesting to study lipid bilayers, since they display thermodynamically stable [2], self-organized non covalent aggregates to the study of cell membrane properties and dynamics. As an organized structure, the lipid bilayer of cell membranes fulfils a critical role as a barrier that marks the boundary of the cell, and a carrier and passive transporter of mostly water, solutes and ions. To a large extent, the lipid bilayer region has membrane constituents which are heterogeneously distributed contributing to the diverse membrane environment that enables lipid bilayer performs its roles.

A membrane is a two dimensional fluid embedding integral proteins in a mosaic manner and undergoes Brownian motion that was first hypothesized by Singer

and Nicholson [3]. It envisions proteins floating in a sea of a lipid bilayer like icebergs with much of the protein submerged in a globular mass in the bilayer.

A membrane is diverse in structure and function in order to implement a vast complexity of cellular functions. Structural constituents of membranes are lipids categorized into five components: fatty acids, triacylgylcerol, glycerosphospholipid, sphingolipids and steroids. These lipid classes are distributed in an asymmetric fashion in the lipid bilayer region serving a pivotal role in regulating membrane structure and function [4, 5]. The major phospholipid in a cell membrane is phosphatidylcholine (PC). PC account for 46.3 to 60.8 % of the total lipid in the red cell membranes of mammalian species [6].

Studies on cellular membrane dynamics have concentrated on using model systems that provide novel platforms for biophysical studies. Model membranes can be formed as a result of aggregation of phospholipids. Their stability and form are fundamentally determined by the aggregation behavior of phospholipids in an aqueous environment, which encapsulates a small volume of water at the core. The result is a hydrophobic core that functions as an insulator with a very low dielectric constant value of 2, surrounded by a high dielectric constant on the inside and outside that is close to the value 78 for water [7]. Thus, the lipid bilayer region of a membrane is endowed with the ability to influence flow of water, solutes and ions.

Phospholipids are amphiphiles that can assemble spontaneously forming vesicles that are between 50 nanometer (nm) to 10 micrometer (μm) or greater in size [8]. This range is comparable to the size of a typical cell. Vesicles are distinguished depending on size. Multi-lamellar vesicles (MLV) are defined as vesicles with a size range between 0.1 to10 μm and smaller unilamellar vesicles (SUV) can be less that 100 nm. Large unilamellar vesicles (LUV) are between 100 and 500 nm. Giant unilamellar vesicles (GUV) are greater than 1 μm. Giant vesicles greater than 10 μm possess low curvature and can withstand thermal fluctuations.

Vesicles are formed as a result of the alignment on the inside of the bilayer of the double chain hydrophobic tails of phospholipids interdigitate while the polar head groups face out. Such an arrangement results in a bilayer with an encapsulated inner aqueous cavity called a liposome. Liposomes have been used as model systems to study cell membranes as a micro-reactor in biochemical reactions [9, 10]. This concept has been extended to manipulation under an optical tweezer [11]. In optical tweezer, a focused laser is used to trap objects within the region of high intensity and focal volume of a high numerical aperture microscope objective [12, 13]. Giant vesicles have been employed in studying microcompartmentation and cellular crowding [14, 15]. They have been used as model systems to study cell membranes that have a wide range of applications in drug delivery [16, 17] and in the emerging field of Lipidomics in encapsulating both hydrophilic and hydrophobic substances [18]. Liposomes offer an opportunity to study membranes in physiologically relevant conditions. X-ray

diffraction studies on concentrated lipid dispersions have shown that vesicles exist as stacks of lamellar sheets [19, 20] or in a closed form [21] resembling an 'onion'.

Detailed knowledge on the structural and dynamic properties of lipid bilayers is required to better understand its functional roles. Numerous biophysical approached have been employed in studying general membrane properties based on model systems. Neutron scattering has been employed in determining the internal membrane structure of DMPC as pertains to the thickness of the bilayers, hydrophobic and hydrophilic parts of the bilayers and water distribution behavior [22-25]. Nuclear magnetic resonance (NMR) was among the first techniques used to resolve the structure of lipid bilayers. NMR has been used to investigate the molecular ordering and conformations of membrane lipids [25].

The large sizes of vesicles have allowed real time observations and manipulations under optical microscopy [26-28]. The recent developments in detection techniques in microscopy and spectroscopy measurement have opened up the possibility of single molecule level detection [29]. Therefore, it is now possible to determine the structure of a lipid bilayer and interactions at the molecular level. Single molecule optical microscopy enables the study of molecular heterogeneities as opposed to average ensemble measurements that is characteristic of bulk experiments [30]. Thus, one can determine on a nanoscale level the behavior of one molecule at a time in a complex environment matrix.

Laser and fluorescence spectroscopy and microscopy techniques can monitor single molecules in the smallest possible volume. The epifluorescence mode of the microscopy operating under a wide-field mode has made it possible to monitor emission from a single molecule embedded in a membrane. The Optical microscopy techniques have brought about direct visualization of giant unilamellar vesicles as model systems of biomembranes. In addition, Kolarch *et al* recently showed the potential of applying confocal microscopy technique to study phase behavior of membranes [31] which can provide a platform to elucidate formation of a raft within a lipid bilayer. In fact, known behavior of lipid rafts in cell membranes is predominantly defined by the behavior of lipid mixtures in model systems [32]. Phase separated regions in a lipid bilayer can lead to raft formation [33]. These regions have been implicated in cell signaling [34] and virus entry into cells [35]. Raft formation in cell and model membranes, as revealed by optical microscopy, has been implicated in the structure and function of membranes. These studies have been done in model membranes in the presence of cholesterol [36], sphingolipids [37] and recently protein caveolin [38]. Therefore, giant vesicles, optical microscopy technique and fluorescent probes provide a powerful combination to demonstrate cellular processes in real time.

The conventional optical microscopy techniques (bright field, phase contrast and differential interference contrast microscopy (DIC)) image vesicles as a result of the difference between the membrane and the solution refractive indices. Phase

contrast, in particular is an imaging technique that relies on the refractive indices of the solutions inside and outside of the vesicles to resolve specimen under focus. For example, using isotonic solutions of sucrose inside and glucose outside create contrast or shadowing that brings the specimen under focus and better resolution. Therefore, novel techniques and applications in florescence microscopy has lead to the possibility of achieving miniaturization, enhanced resolution and reduction of detection volumes required in lipid bilayer studies.

1.2 Self-Assembly of Phosphatidylcholines

The typical structure of a phospholipid is summarized in Figure 1.1. Two saturated hydrocarbons are esterified to a glycerol constituting the hydrophobic part [16]. The hydrophobic region of the structure is attached to the hydrophilic headgroup containing a phosphate and linked to a choline moiety in phosphatidylcholines. Phosphatidylcholines are biologically relevant zwitterionic lipid headgroup. The saturated hydrocarbon chains vary in length from 12 to 22 carbon atoms [39].

Cholesterol possesses molecular structure that is different from phospholipids. It has a four-ring steroid structure with a short hydrocarbon side-chain and hydroxyl group. Cholesterol is also amphipathic as a result of its hydrophobic rings and side-chain, and its hydrophilic hydroxyl group. It can be incorporated into phospholipids bilayer but cannot form bilayer by itself.

The self-assembly of phospholipids is driven by a hydrophobic effect as a result of molecular interactions at close proximity (Figure 1.3). The effect is influenced by environmental factors that include temperature, ionic strength, concentration and the water/lipid mixing ratio. It has been shown that size can be controlled by temperature and solvent composition [2]. For example, increasing water content increases vesicle size [40]. At low temperature, the hydrocarbon tails of the bilayer pack closely together to form an ordered arrangement (gel state) that is rigid. As the temperature is increased the lipid molecules vibrate rapidly causing the bilayer to 'melt' to a more disordered flexibly state (liquid) or fluid. There is a region of gel and fluid coexistence. This temperature region is characterized by chain melting which is also referred to as transition temperature.

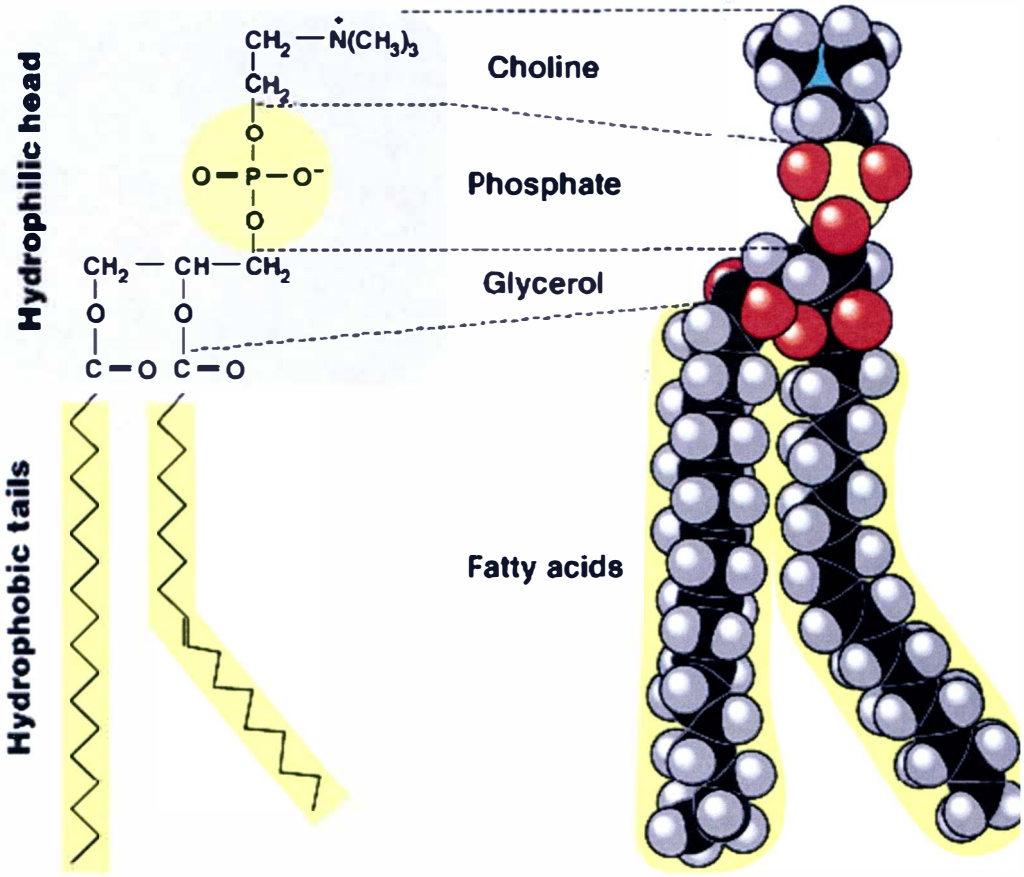

Figure 1.1. Structure of phosphatidylcholine. On the left is structural formula and on the left is the space-filling model. Choline and the phosphate groups are oriented in the head displaying the hydrophilic region while the acyl chain in the tail forming the hydrophobic region
http://bioweb.usc.edu/courses/2004-spring/documents/bisc221-watts_lecture3.pdf

1.3 Vesicle Formation Methods

The spontaneously assembly of lipids leading to formation of lipid vesicles has been studied previously. The mechanism of vesicle formation has been proposed and the spontaneity of formation determined by time-resolved static and dynamic light scattering [41]. They found out that the kinetic rate constants and the properties of the final liposome formation are strongly correlated with the lipid concentration and the ionic strength. The model of vesicle formation based on detergent depletion was proposed by Lasic who predicted disk-like phospholipid

micelle structures as intermediates in vesicle formation [42]. Phospholipids have low permeability to electrolytes and thus are strongly influenced by electric fields. In some cases, electroformation methods, first proposed by Angelova et al [43] are used to generate vesicles *via* electric fields. The procedure generates mainly giant vesicles greater than 10 μm in size. In this method, alternating current fields are employed to form liposomes from thin films of lipids deposited on the surface of a platinum wire or indium tin oxide (ITO) plate. This procedure generates giant vesicles that are predominantly unilamellar. Sonication technique that involves first hydration of lipid films and then subjecting the films to an ultrasound generates small unilamellar vesicles [44]. Moreso, Akashi *et al* developed an improved gentle hydration method that resulted in giant unilamellar vesicles under physiological conditions [45]. Furthermore, it has been found that large vesicle sizes correspond to a wide size distribution, whereas a narrow distribution is observed in small vesicles [2]. Thus a range of methods produce various sizes and size distribution of vesicles for different applications.

1.4 Width of a Lipid Bilayer

The width of the bilayer constitutes an important area to consider when studying model membranes. It represents a minute percentage of the overall lipid bilayer of thickness approximately 5 nm (Figure 1.2) that varies linearly with the acyl chain length [46]. The bilayer thickness is also affected by temperature. Studies have yielded bilayer thickness of 44.5 Å at 30 °C [47]. Nagle *et al* estimated the fluid bilayer thickness at 44.2 Å in DMPC at 30 °C [48] suggesting the significance of

temperature in modulating membrane properties such as volume, thickness of the bilayer and the membrane phase transitions. The volume of membrane increases by about 3 to 4 % [49-51] while the thickness decreases by 20 to 25 % that implies an overall increase in the surface area by about 23 % [52].

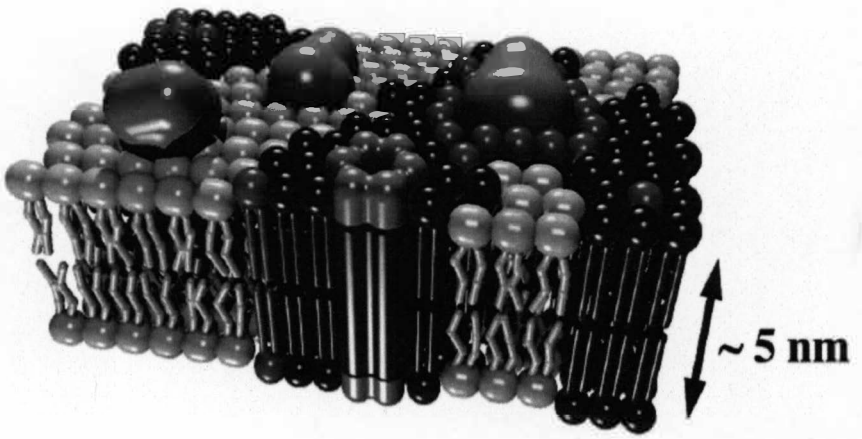

Figure 1.2. Fluid mosaic model of lipid bilayer. The figure shows thickness of the bilayer region [53].

1.5 Phase Behavior of a Lipid Bilayer

The phase behavior of phospholipids in a lipid bilayer controls the motion of membrane constituents. This is accompanied by changes in permeability of intra and extra cellular materials. The phase behavior of phospholipid vesicles are connected by phase transitions that drives phase segregation. Phase transitions have been widely studied and understood. Biomembranes exists in fluid phase above the phase transition. Therefore, it is important and interesting to study hydrocarbon–chain disordering transitions, which constitute phase behavior in

lipid bilayers. The phase behavior of phospholipids is determined by the main lipid composition and by environmental factors. Among these factors are hydrocarbon chain length; impurities present in the phospholipids and the level of saturation of the acyl chain. These factors, therefore, dictate a polymorphic nature of lipids that is controlled by temperature.

Cellular functions are determined by lipid polymorphism [54, 55] and highly controlled by electrostatic factors [56]. Lipids exist as a gel, ripple or fluid phase depending on temperature. Transitions between these phases are accompanied by lateral diffusion and decrease in conformational ordering. The gel to fluid phase transition has been studied in model systems either in unilamellar or multilamellar systems [57] due to the complexities of biological systems. The gel phase is characterized by relatively low rate of lateral diffusion, a high degree of neighboring lipid interactions and increased bilayer thickness. The opposite is true for the fluid phase region. Ripple phase occurs between the gel and fluid phase that display 'ripple' surface phenomenon and having all *trans* configuration. The changes in molecular orientation from the more rigid *trans* to a more flexible gauche isomerism define gel to fluid transitions in the bilayer.

The lipid bilayer fluidity is critical for biological functions. The rich phase behavior contributes significantly to molecular movement that influences fluidity [58, 59]. Cholesterol added to the membrane has significant effect on the membrane fluidity and the phase transition temperature. It acts as a plasticizer by

increasing rigidity of the fluid phase and fluidity of the gel phase when its concentration increases in the membrane. It forms a nonideal mixing behavior with phospholipids that can associate with the phospholipid-rich phase and cholesterol rich phase [60-62]. This behavior had been investigated by epifluorescence microscopy of monolayers mixture of phospholipid and dihydrocholesterol [61, 63].

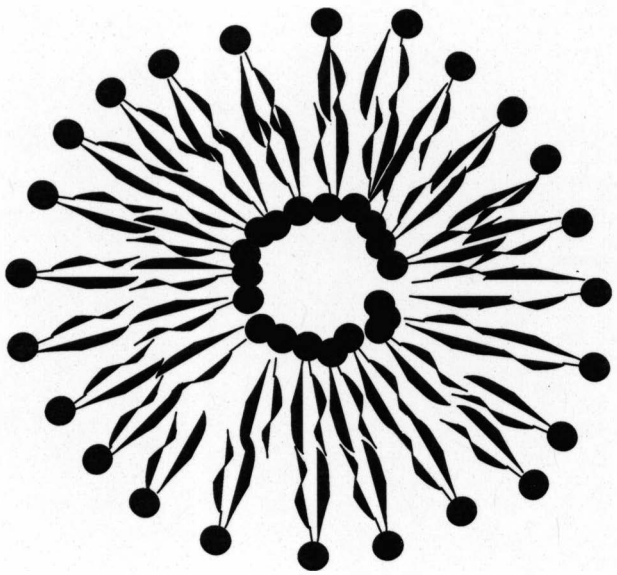

Figure 1.3. Orientation of phospholipids in a bilayer. The hydrophilic head groups coalesce facing the aqueous environment while the hydrophobic region self associate facing away from the aqueous environment.

Several techniques have been used to determine the phase transition phenomenon in the presence or absence of 'impurities'. Recently Raman spectroscopic technique has been employed to study this region as a function of temperature [64, 65]. The phase transition occurs as a result of the melting of acyl chain. This region of the transition is greatly influenced by the presence of small impurities that can broaden or shift phase transition [66, 67]. Among the 'impurities' previously reported include cholesterol [68], alcohols [69, 70], proteins and carbohydrates.

1.6 Dielectric Constant of a Bilayer Region

Electrostatic properties of a lipid bilayer are controlled by the dielectric constant of the bilayer itself. Some acidic or charged lipids present in naturally occurring lipid membranes contribute to electrostatic properties of the cell membranes. The dielectric property of a lipid bilayer influences the lipid ion association, the ion - binding and transport, and thus the chemical activity and electrical conductivity of the membrane surface. The dielectric constant of a zwitterionic lipid bilayer has been determined from both experimental and theory approaches based on the spectroscopic and kinetics studies. These values obtained depend on the technique used. Marked variation is observed in dielectric constant and its profile from the interface to the hydrocarbon core of the membrane. There is a stiff gradient of polarity in the transition between the hydrophobic and hydrophilic region (Figure 1.4). The dielectric constant increases from a value of 2 in the hydrophobic core up to its value of 80 in water over a distance of approximately 1 nm. Levitt and Huang [71] used a theoretical approach to obtain the dielectric constant of the hydrocarbons core of the bilayer as 2.06. Cametti and Di Biasio [72] obtained a measured permittivity value between 2 and 3. The data presented by Toccane and Teissie [73] gave the polar head group region dielectric constant value in the range between 10 and 45 depending on the technique used.

The region between the aqueous phase and the membrane lipid head group (interfacial region) presents a strong dipole moment with the possibility of that region attracting the counter ions from the environment bulk medium. It has been suggested that the first layer of water molecules bound by hydrogen bonds to the

membrane is polar. The second one has no preferential orientations and thus may have a significant influence on the permeability of the polar compounds [7, 74, 75]. The membrane-water interfacial region has a dielectric constant environment which approximates that of the aqueous phase at 25 °C. They reported dielectric constant value in this region of roughly 78 and reduces to 2 over a distance of 10 to 15 Å.

The dielectric constants profile of a lipid bilayer has been investigated by a variety of techniques. NMR and X-ray diffraction techniques have produced an effective dielectric constant value of approximately 30 [76]. Low frequency impedance measurements that are consistent with hydrocarbon dielectric constants values between 2 and 3 while the head group region and the ester–group regions have dielectric environment values between 20 and 30 [77]. The relationship between the dielectric constant value and temperature has been previously reported and showed an anomalous behavior at the phase transition [78]. They observed an abrupt change in real and imaginary permittivity around the phase transition. This was attributed to hydration changes in the bilayer coupled with the amount of lipid and water interactions. A sharp increase in permittivity is also observed at pre-transition and the transition temperature which could be attributed to strong dipolar interactions. This can influence head group mobility behavior of the probes embedded in the membrane bilayer specifically those with strong dipole interactions.

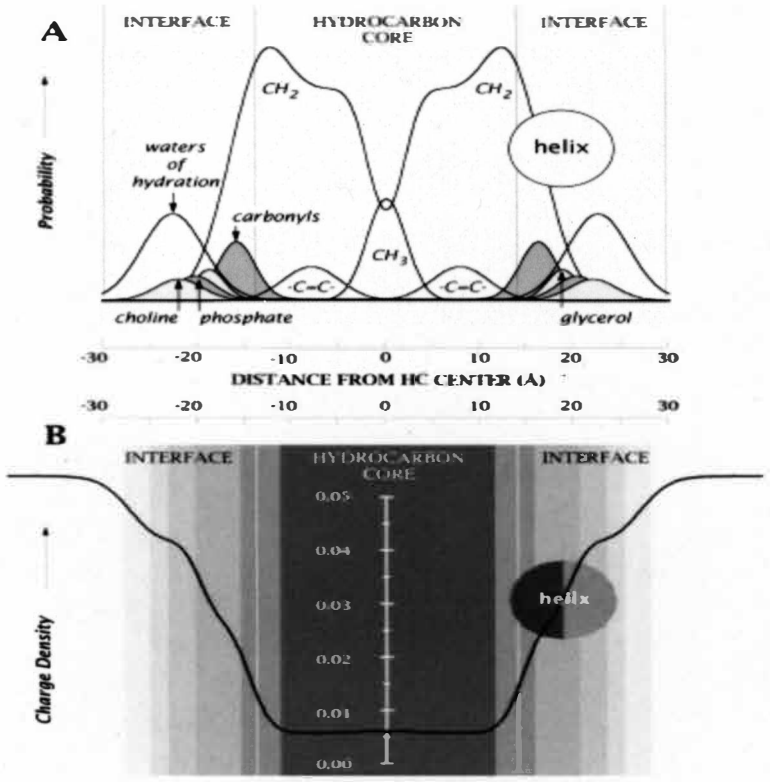

Figure 1.4. Dielectric constant profile of the lipid bilayer. The figure shows the thickness of the hydrocarbons core and the interface regions. Part B is a representation of the variations in the dielectric constant within a lipid bilayer [18].

1.7 Study of Dynamics by Fluorescence Spectroscopy

The dynamics of the bilayer region occur as a result of changes in physical properties. These properties include phase transition temperature, lateral phase separations, rotational diffusion and local dielectric properties. The changes in the physical properties can influence the fluorescence anisotropies, quantum yields, lifetimes, and emission spectra of an excited state of an embedded fluorophore. Time-resolved and steady state fluorescence spectroscopy techniques have proved useful in studying lipid vesicles [79, 80]. Furthermore, fluorescence spectroscopy

and fluorescence imaging have met the criteria to study membranes properties that have widened knowledge in the field of biochemistry and biophysics [81]. The sensitivity and simplicity of fluorescence have provided useful clues to molecular features of a particular sample since one can correlate the spectral changes of a given probe to local environment. The local environment can also be affected by the proximity to quenchers or acceptors that can influence fluorescence emission. Fluorescence quenching is defined as a process that diminishes florescence intensity. Quenching is a result of excited state reactions, molecular arrangements, ground state complex formation, energy transfer and collision quenching. It can be used to investigate fundamental problems in biochemical systems. Quenching can be used to investigate the partition and mobility of small molecules used as quenchers in the bilayer.

1.8 Probing Bilayer Region by Fluorescent Probes

The lipid bilayer region has been studied based on the environment- sensitive fluorescent probes embedded in low concentrations in the bilayer [82] yielding excellent results on phospholipids bilayer [83]. The results have shown a remarkable heterogeneity in the spectroscopic properties of the fluorescent dyes concerning a particular location of the probe or its distribution between several locations having different properties [84]. The heterogeneity is attributed to the different forms of the probe, such as H-bonded or non-H-bonded, that can influence the interactions with water at different depths of the membrane. Thus,

one can determine the bilayer region by probing the microenvironment around the fluorophore.

The most crucial criteria in choosing a fluorescent probe depend on the region of the bilayer of interest. As discussed above, the bilayer region consists of the hydrophobic backbone of limited water of hydration [85] and the interface that experience solvation dynamics in broad time scale [86]. Fluorescence lipophilic dyes are ideally suited for studying the lipid bilayer structure and the changes in their fluorescence can be attributed to changes in the polarity, viscosity or hydration of the bilayer itself [84, 87]. Previous studies on the bilayer region have employed fluorescent dyes with the anthroyloxy chromophore which is highly sensitive to solvent dynamics at different depths of the bilayer region and can serve as sensitive polarity probes [88]. Different depths within a lipid bilayer have been measured by fluorescence changes as a result of the changes in environment of a diphenylhextriene (DPH) fluorophore [80]. The rod-like shape of this probe provides minimal disruptions of the bilayer while it gives a high quantum yield and stability. These properties make it an excellent potential membrane probe. DPH can be localized within the membrane-water interface by attaching a trimethylammonium group to one of the phenyl rings (TMA-DPH) [89]. Texas Red – PE can also play similar role in determining the nature of membrane-water interface. Diffusion processes can be assessed by excimer formation using pyrene fluorophore attached to a lipid. This fluorophore is highly sensitive to temperature changes. Other probes sensitive to polarity and solvent

relaxations in lipid bilayer include, Laurdan, Dansyl and Prodan [75]. These probes sense polarity and the solvent dynamics around the hydration sites of the carbonyl and phosphates. Ultimately it is the behavior of a fluorophore and its environment that is used to determine the bilayer profile using a variety of probing techniques.

1.9 Fluorescence Spectroscopy Methods

Careful evaluation of fluorescence emission spectra can provide reliable interpretations of intensity values, anisotropy, or lifetimes obtained either in steady state or time-resolved measurements. Time-resolved measurements provide more detailed information than steady state [81]. Their use is currently recognized as a result of the availability of time-correlated single photon counting technology (TCSPC). Time-resolved measurements can be either time or frequency-domain measurements. Time-domain is widely used. Here the sample is excited with a pulse width shorter than the decay time of the sample. In time-resolved anisotropy measurement the fluorescence intensity decreases exponentially (Equation 1.0). In the process molecule can undergo a wobbling motion rather than free rotation. Time-resolved fluorescence anisotropy measurement can measure simultaneously the rate and range of rotational diffusion in the nanoscale range [90] and this can be used to resolve the motion of a particular moiety of phospholipid molecule. The rate is determined by the frequency of fluctuations of molecular orientations in the membrane while the

stationary value is attributed to orientational constraint imposed by the neighboring molecules [91].

$$I(t) = I_O \exp(-t / \tau) \qquad (1.0)$$

where τ is decay time, Io is the initial intensity at time 0 and I(t) is the intensity at time t.

The bilayer region can be studied either in steady state or time-resolved fluorescence anisotropy mode. The orientation of a fluorescent fluorophore within a bilayer can be determined from fluorescence polarization measurements. Rotations parallel and perpendicular to the plane of the bilayer that occur in nanosecond time scale can be resolved through time-resolved measurements. The local dielectric constant can be determined from the Stokes shift of fluorescence spectra of lipophilic dyes in the bilayer. Therefore fluorescence spectroscopy becomes a powerful tool to resolve the dynamics of the lipid bilayer.

2.0 Probing Lipid Bilayer using Fluorescent Analogs of Phospholipids

In this study, the use of fluorescent analogs of phospholipids is presented. A detailed study of DMPC bilayer region using fluorescence steady state, time-resolved measurements and fluorescent analogs of phospholipids is reported. In the present work, we have systematically performed fluorescence steady state, time-resolved measurements and microscopy techniques based on the behavior of two fluorescent molecules 7-nitrobenz-2-oxa-1, 3-diazol-4-yl (NBD) attached to the head (NBD-PE) or tail (NBD-PC) of the phospholipids. These probes are readily incorporated in the vesicle bilayer region. NBD moiety is a widely used extrinsic fluorophore in biophysical, biochemical, and in cellular biology serving both in spectroscopic and microscopic investigations [84]. The unique properties of NBD have been exploited in lipid membrane studies [92]. These include a) the ability to strongly fluoresce in organic solvents and lipids and weakly in water, b) its easy conversion to non- fluorescence products and c) its ability to reside in a more polar environment within the bilayer [93]. The NBD fluorescence in the bilayer region can be modulated by physical state of the membrane (structure and composition) and the concentration-dependent self quenching [94]. The nitro group in position 4 (see Figure 1.5.) is electron-withdrawing that can possible delocalize π-electrons in the conjugated ring system. The reduction of a nitro-group to an electron-donating amine can alter the electronic transition of NBD affecting the fluorescence properties. McIntyre and Sleight [95] demonstrated this reaction by using NBD-lipid analogs and sodium dithionite in measuring lipid asymmetry by fluorescence spectroscopy methods. They presented a method that

can preferentially eliminate the fluorescence of NBD-lipid analogs in the outer leaflets of a lipid bilayer. Thus, they were able to gauge the distribution of these dyes in the outer and inner leaflets of the bilayer region of the membrane. They proposed this mechanism as a potential means to study transmembrane migration and fusion of lipid vesicles. This mechanism has been extended to investigations of a variety of membrane properties such as defects within the bilayer and membrane permeability [96].

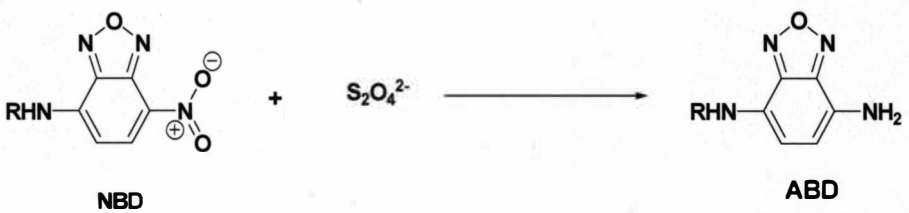

Figure 1.5. Quenching of NBD fluorescence by dithionite. NBD is fluorescent while ABD (Aminobenzoxadiazole) is nofluorescent.

2.1 Kinetics and Thermodynamics of Dithionite Reduction

The rate of reduction of NBD by dithionite in a lipid bilayer has been determined previously. The rate constant of the reduction for tail labeled NBD PC and head group DPPN, studied in a stopped-flow spectrofluorometer as a functional of dipole potential, was found to be negatively correlated with dipole potential [97]. The study was conducted in a sonicated 100 nm size-extruded liquid-crystalline state DPPC vesicles with 16 carbon chain lengths. The resulting rate coefficients were treated via a sum of two exponentials due to quenching of outer followed by inner leaflets NBD moiety. Similar studies were conducted to determine spectral

characteristics and dithionite reduction of membrane undergoing phase transitions [98]. Here, a comparative study of NBD PC and DPPN in DPPC was made on the basis of activation energy for the reduction process and spectral properties of NBD. They concluded that the NBD in DPPN is transiently immersed deeper in the hydrophobic region of the bilayer. This slowed down the rate of reduction by dithionite. Conversely, the NBD PC was higher due to change in the vertical distribution and therefore, projects the NBD moiety into the interface.

The kinetics and thermodynamic of association of phospholipid derivatives with lipid at different phases has been reported [99]. Recently a detailed study of kinetics and thermodynamics of translocation and permeability of one and two acyl chains with similar head group labeled NBD phospholipid derivatives were reported [100]. The study was conducted as a function of temperature using liquid-disordered state POPC and liquid-ordered state POPC with cholesterol lipid bilayer. The measurements taken in stopped-flow fluorimeter, using vesicles a 100 nm diameter size distribution, gave rate constants of translocation of the acyl chains and permeability of dithionite. Using the transition state theory they reported the standard free energies, entropy and enthalpy of associated with the activation complex formed between dithionite and NBD.

Previous reports on the kinetics and thermodynamics of dithionite reduction of NBD have mainly been evaluated based on the Arrhenius model. Here, we present the kinetics and thermodynamic parameters for the reduction of NBD by

dithionite in pure DMPC lipid bilayer with a wide range of size distribution from nanometer to micron sizes. The activation parameters, entropy and enthalpy, were derived in the gel, around the phase transition and fluid phase using Eyring model. It is known that DMPC presents a sharp phase transition temperature close to room temperature (23 °C) [52]. The nature of DMPC presents an interesting behavior to explore phase transitions. One can derive the activation parameters in the gel and fluid from a pure lipid system. In this report we derive these parameters based on the kinetics of dithionite quenching. We also report on the steady state and time-resolved anisotropy and lifetime measurements. We explore the phase behavior of DMPC by exercising temperature control above and below the phase transition of DMPC ranging from 0 to 45 °C. In addition, we present bright field, phase contrast and fluorescence microscopy images to demonstrate quality of the preparation method employed in vesicle production. We extended excited state lifetime measurement of the two probes in single vesicles in a microscope.

2.2 Specific Objectives of the Study

The following were specific objectives of the study reported here.

1. To characterize nanometer size vesicles of DMPC by light scattering and micron sizes by microscopy techniques.

2. To elucidate the dynamics of DMPC bilayer region using head group NBD PE and tail labeled NBD PC. This is done by sodium dithionite quenching kinetics, steady state anisotropy, time- correlated anisotropy, lifetime and fluorescence intensity changes as a function of temperature.

3. To elucidate the single vesicle and ensemble behavior with respect to lifetime and time-resolved anisotropy studies in DMPC vesicles

4. To study DMPC bilayer region in the presence of variable amount of dihydrocholesterol. Dihydrocholesterol was proposed since it is less affected by oxidation than is cholesterol [101].

CHAPTER 2

EXPERIMENTAL METHODS

2.1 Reagents

Saturated synthetic phospholipids 1,2-dimyristoyl-sn-glycero-3-phosphocholine (DMPC), (Figure 2.0), NBD PE (1,2-dipalmitoyl-*sn*-glycero-3-phosphoethanolamine-N-(7-nitro-2-1,3-benzoxadizol-4-yl) (ammonium salt) (16:0) , (Figure 2.1) and 16:0-12:0 NBD-PC 1-palmitoyl-2-[12-[(7-nitro-2-1,3-benzoxadiazol-4-yl)amino]dodecanoyl]-*sn*-glycero-3-phosphocholine(Figure 2.2) were all purchased from Avanti Polar Lipids (Alabaster,AL) and were used without further purification and kept at a -20 °C. Dihydrocholesterol 3β-hydroxy-5α-cholestane, (Figure 2.3) was purchased from Sigma Chemical Company, St Louis MO, and stored at room temperature and was used without further modification. Sodium dithionite (sodium hydrosulfite), chloroform, methanol and ethanol (HPLC grade) were obtained from Fisher Scientific. Triton X-100 was obtained from Fluka. Magnesium chloride hexahydrate was obtained from OmniPur while Trizima base was purchased from Sigma Aldrich. Nanopure water made with a Barnstead NANOpure Diamond water purification system was used in all the experimental procedures.

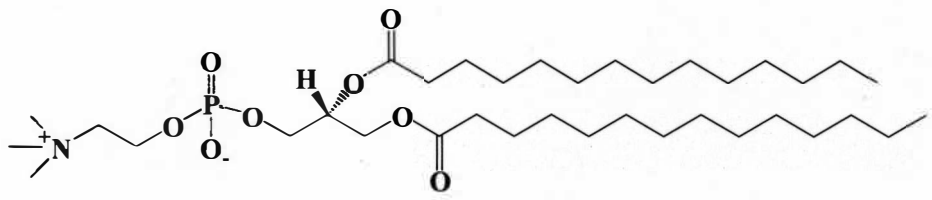

Figure 2.0. Structure of DMPC

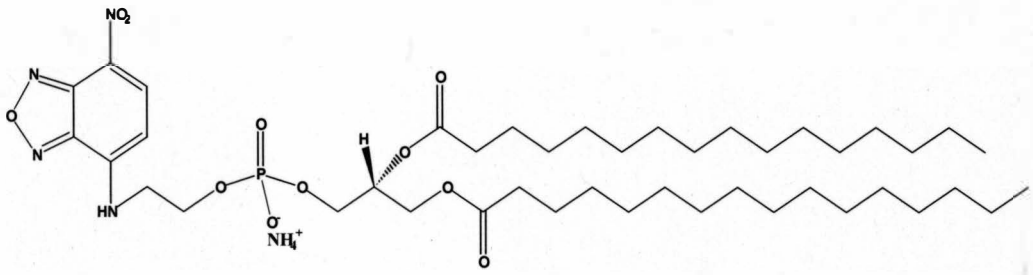

Figure 2.1. Structure of NBD PE

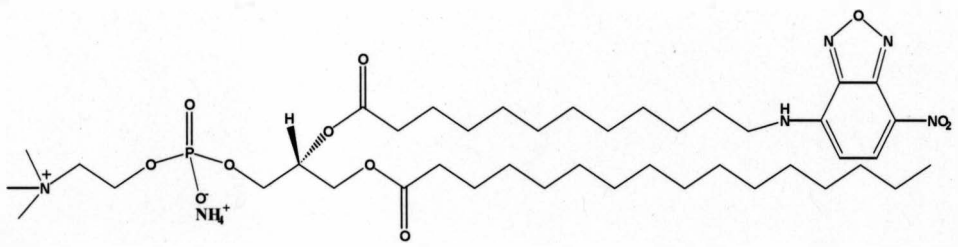

Figure 2.2. Structure of NBD PC

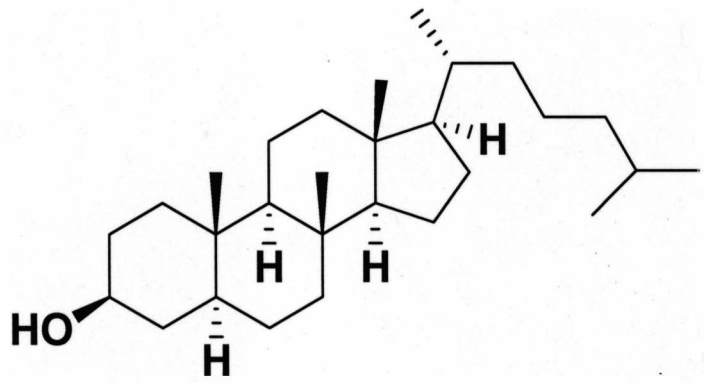

Figure 2.3. Structure of dihydrocholesterol. The shows hydrophilic head with hydroxyl group at the end, steroid ring and the alkyl chain tail

2.2 Apparatus

2.2.1 Avanti Mini-Extruder for Extrusion of Vesicles

Avanti mini-extruder from Avanti Polar Lipids (Alabaster, AL) was used to extrude vesicles from synthetic procedure into nanometer size range. The mini-extruder had the following components

1. Heating block for extrusions of vesicles that were done at 50 °C,
2. Gas tight syringes used to withdraw samples of the vesicles to be extruded,
3. Polycarbonate membranes used for controlling sizes of vesicles (from 50 nm to 3 μm). This allowed vesicles to pass through pores of predetermined size and with maximum size distribution,
4. O- ring and the filter supports that prevented linkage of sample during extrusion (Figure 2.4).

A 1 ml sample of the vesicles was pumped in a 1 ml gas tight syringe that was previously cleaned with ethanol and dried. The syringe was placed on one side while an empty syringe of the same size was placed in the opposed side of the assembled mini-extruder with a heating block placed on heating mantle set at 50 °C far above the phase transition of DMPC phospholipids. The heating mantle was left to equilibrate with the set temperature for about 10 minutes before putting on the mini-extruder. The vesicles were passed through two 1μm size polycarbonate membranes (Avanti Polar, Lipids) back and forth 15 times. The mini-extruder was disassembled and cleaned in ethanol and Millipore water and re-assembled with two 100 nm size polycarbonate membranes instead of the 1 μm size. The extrusion procedure was repeated the same number of times and the sample size distribution were determined by quasi elastic light scattering instrument as described below.

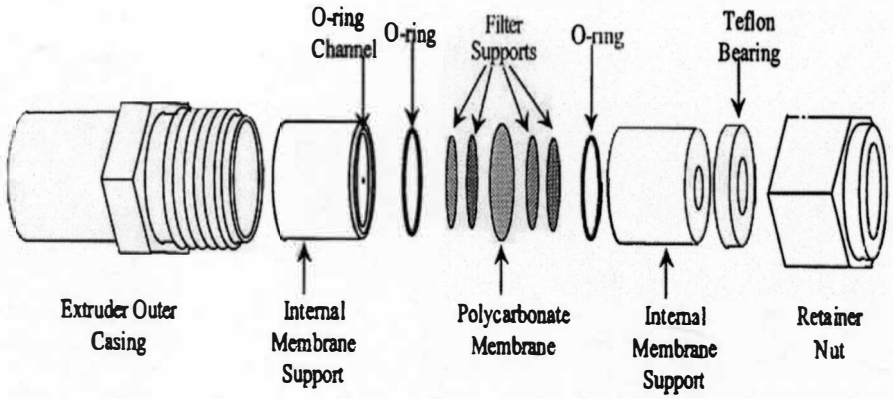

Figure 2.4. Assembly parts of Avanti mini-extruder. The figure shows polycarbonate and O-ring that are essentials for the extrusion process. http://www.ncnr.nist.gov/userlab/pdf/E134extruder.pdf

2.2.2 Quasi Elastic Light Scattering

The extruded vesicles were characterized by a quasi -elastic light scattering QELS detector (Wyatt Technology Corporation, Santa Barbara, CA) with a 630 nm laser wavelength and measurements were taken at 25 °C. Software ASTRA 5.1.8.0 from Wyatt Technology was used to acquire data from QELS that measured scattering intensity at eleven different angles.

A 40 µl solution of extruded vesicle in l lMm magnesium chloride was added to 10 ml Millipore water in a 20ml scintillations vial (from Barnstead NANOpure Diamond water purification system) that had previously passed through 0.2 µm polycarbonate membrane filters. Prior to the transfer, the vial was thoroughly rinsed with filtered solution. The diluted sample suspensions and the scintillation cell were placed in the optical system of QELs and the measurements acquired were delayed for 5 minutes to allow the sample to equilibrate with the bath temperature. The dynamic light scattering measurements was run for 10 minutes at 25 ± 0.1 °C. The average decay rate of the electric field autocorrelation function was estimated by the cumulant method. The apparent diffusion coefficient was accounted for by the solvent refractive index and the wavelength of the laser light. The corresponding hydrodynamic radius was electronically calculated by the software using the Stokes-Einstein relationship.

2.2.3 Microscopy

The micron sizes of vesicles were investigated under brightfield, phase contrast and epifluorescence modes of microscope techniques employing a multi-port design Nikon eclipse TE2000U inverted microscope, coupled to a cooled CCD color camera from Arryx, Inc. Chicago, IL (Figure 2.5). The set-up was all assembled on top of a vibration-free table. All vesicles samples were observed under high-magnification 60X N.A. 1.4, in oil immersion objective. In a typical specimen, a 50 ul of 4 mg / ml sample of DMPC vesicles was transferred onto a hydrophilic depression slide, covered with a cover-slip and then mounted onto the microscope stage. The oil immersed objective was moved upwards in close proximity and within range of the working distance set for microscope. This was made possible by independently controllable motions along the x, y and z directions under the control of the joystick in a user- configurable stage speed. Images were acquired with acquisition settings in the Arryx software upon capture by CCD color camera.

DMPC vesicles labeled with 0.5 % NBD PE or NBD PC were illuminated with ultra violet light from a mercury arc lamp supplied through a fiber optic cable. About 10 minutes was allowed for the lamp to stabilize before use. The amount of light entering the sample was controlled through the adjustable lamphouse while the shutter was used to block the excitation light from the specimen when not under view to minimize the photobleaching effect of the mercury lamp. Further control of light intensity and wavelength was achieved by selective wavelength

neutral density (ND) filters in the path of light. The ND filters used were as follows; ND4 has a transmittance of 25% and ND8 with a transmittance of 12.5%. The light passes through a filter block that houses an excitation filter, a dichromatic mirror beam-splitter and an emission filter. A standard fluorescein filter cube (470 nm, 20 nm band pass) was used as an excitation filter and 537 nm long pass as emission filter.

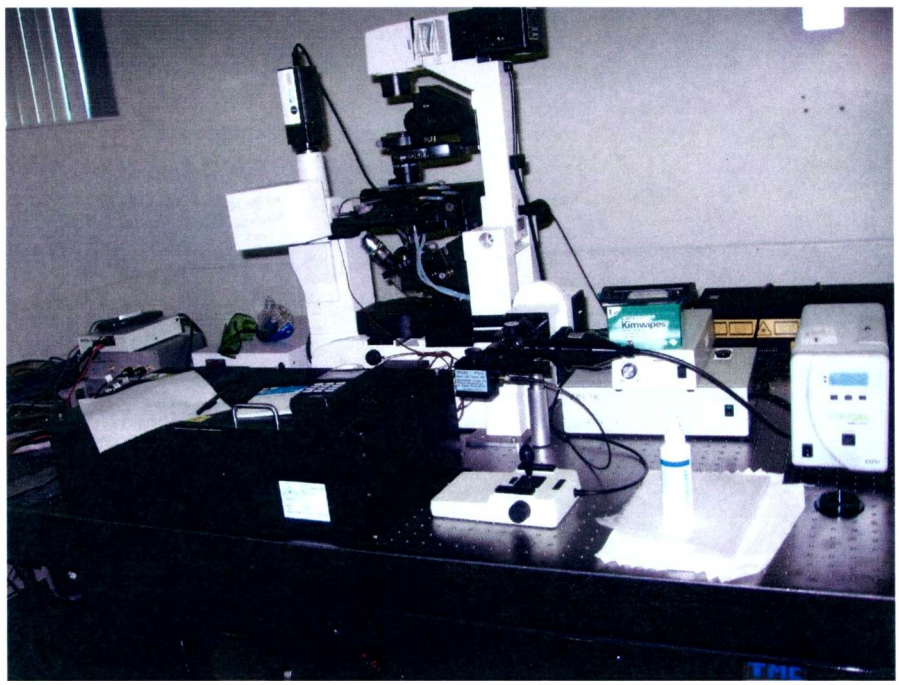

Figure 2.5. Laser tweezer and lifetime instrument set-up

2.2.4 Shimadzu RF-5301 Spectrofluorometer

Steady state fluorescence, fluorescence anisotropy and quenching studied were performed in a Shimadzu RF-5301 spectrofluorometer with temperature-controlled polarization and magnetic stirrer accessories. This instrument employs a 150W Xenon lamp that was capable of producing 220-900 nm range of wavelength and a square cuvette was used to maximize output for emission capture. The emission was observed perpendicular to the direction of exciting beam.

In summary, a 150 ul of 4mg/ml DMPC vesicles sample were added to sodium buffer at pH 7.4 to make a total volume of 3 ml. 'Sodium buffer' composition was prepared according Gruber and Schindler [102]. The composition was made by accurately weighing 100 mM of sodium chloride and 10 mM of Hepes buffer and pH was brought to 7.4 in a pH meter using 1M sodium hydroxide. Fluorescence emission spectra were obtained by setting an excitation wavelength beam at 470 nm and observing the emission at wavelength range between 480 to 650 nm. The excitation spectra were determined by holding the wavelength at 540 nm emission while scanning wavelength range between 200 to 530 nm. The emission and excitation of NBD were obtained using a 5 nm slit width and the data plotted using Origin software (Figure 2.6). Further studies were done to determine the influence of temperature on the same excitation and emission as shown in Figure 2.7.

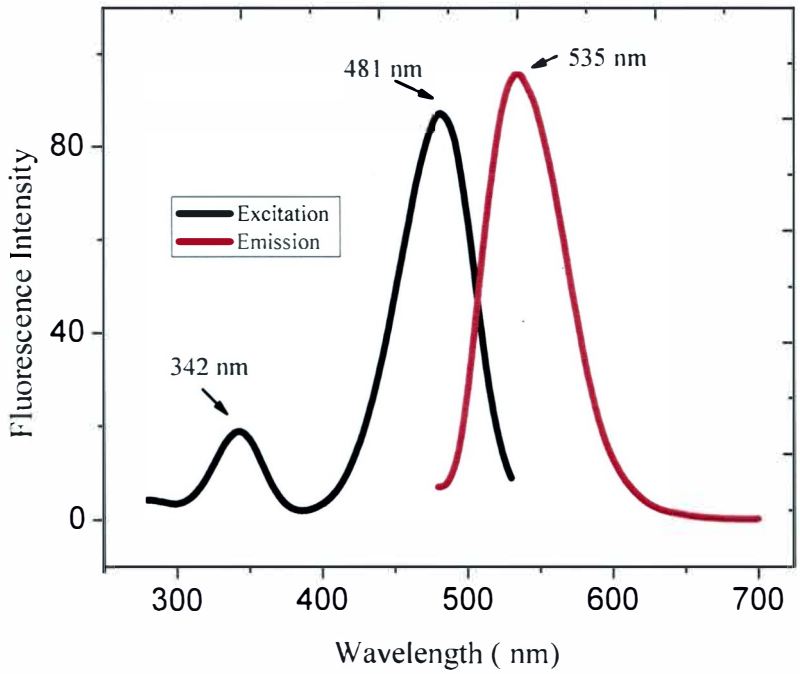

Figure 2.6. Fluorescence excitation and emission spectra of NBD PE in DMPC measured at 10 °C

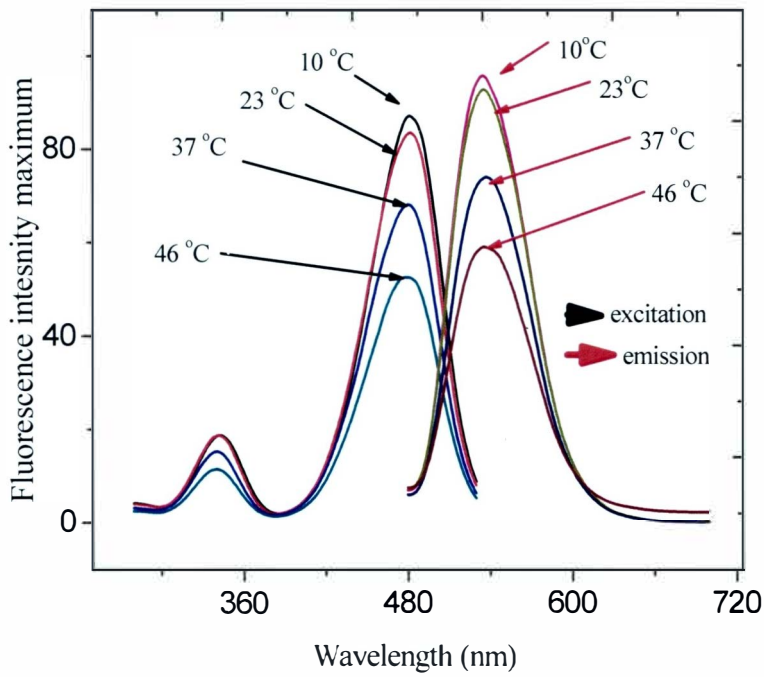

Figure 2.7. Fluorescence excitation and emission spectrum of NBD PE in DMPC at variable temperature condition

2.2.5 Shimadzu UV-VIS 1650PC Spectrophotometer

The UV-Vis spectral data of NBD fluorophore were collected from the Shimadzu UV-VIS1650PC spectrophotometer that employed a tungsten iodide lamp emitting visible wavelength range between 350 to 750 nm and an ultraviolet deuterium arc lamp source between 190 to 350 nm. The UV-Vis spectra of NBD were monitored at different analytical pure solvents and in vesicles made in 11 mM magnesium chloride. The data obtained was analyzed by UVProbe software that was re-plotted (Figure 2.8). In a typical sampling condition, absorbance was obtained from the software by calculating the difference of the reference sample cuvette and the sample cuvette. To determine the spectrum of the NBD PE in DMPC vesicles, a 300 ul of a 4mg/ml sample were diluted to 3ml using sodium

buffer pH 7.4 that was also used as a reference solution in the reference cuvette. The instrument was instructed to scan from 190 to 800 nm and the absorbance monitored for few minutes. A typical spectrum is shown in Figure 2.9.

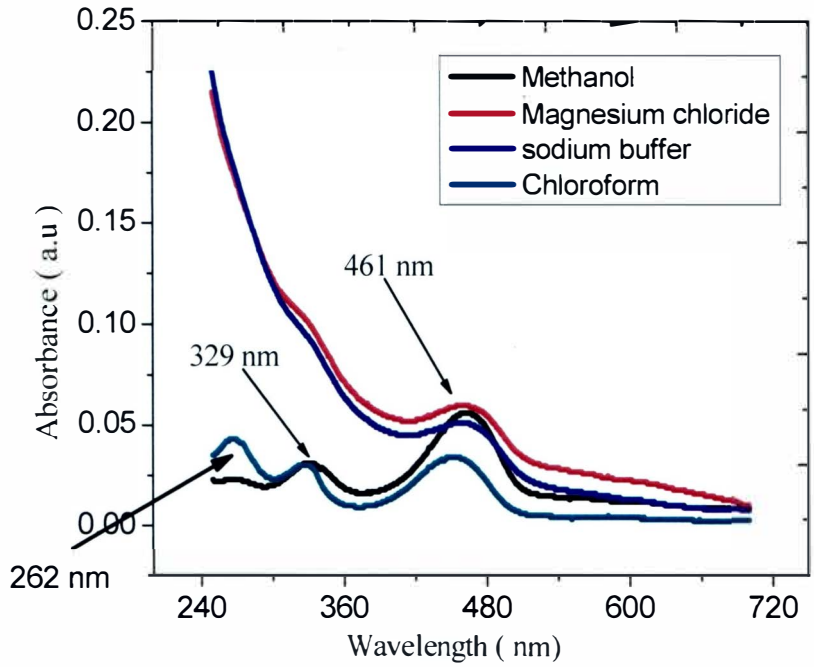

Figure 2.8. UV-Vis spectrum of NBD PE in different solvents.

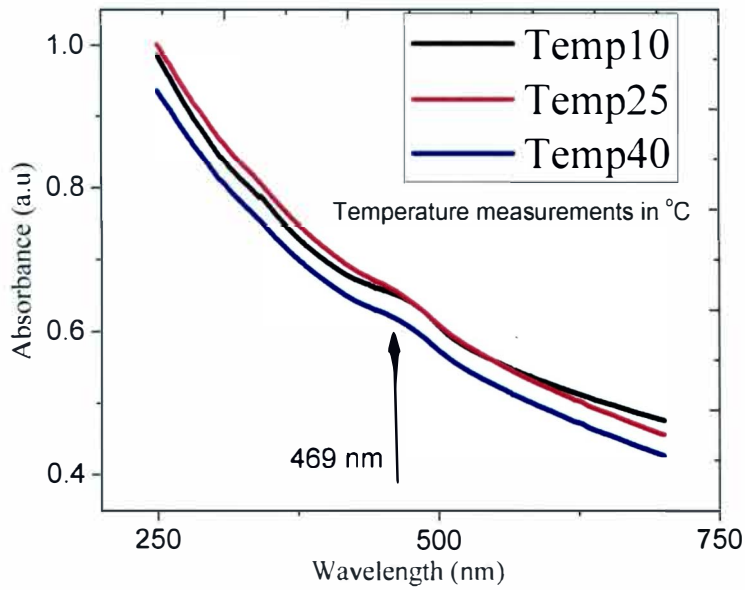

Figure 2.9. UV-vis spectrum in vesicles measured in regions corresponding to DMPC phases.

2.2.6 Fluorescence Lifetime and Time-Correlated Anisotropy

Temperature-dependent fluorescence lifetime and time-resolved anisotropy measurements were performed on a single vesicle in a custom-built time correlated single photon counting system (TCSPC) integrated with the inverted Nikon microscope as previously described. The temperature controller was used with a custom–built temperature stage consisting of a peltier thermoelectric device and a water circulator bath with a probe that could accurately measure 0.1 °C. The accessible temperature range for the sample was between 4 to 40 °C. Water condensation below 10 °C was reduced by blowing air through the sample slide. The temperature within the sample was measured using an external temperature probe to approximately 1 °C. The stage and the slide were equilibrated for at least 5 minutes before measurements were taken.

TCSPC is based on the detection of single photons from periodical light signals, measurements of the detection time of the individual photons within the signal period and finally the reconstruction of the waveform from the individual time measurements. Apart from measuring fluorescence intensities, TCSPC measures the fluorescence lifetime by using the pulsed laser excitation and correlating the photon detection times on nanosecond timescale with the pulse times of the laser (delay time of between the excitation and detection). In TCSPC, a given fluorescence event only one photon is captured and detected. For this photon the time that elapsed from the arrival of the excitation pulse at the sample until the photon is detected is measured. This recorded as one count in the x-axis and these steps are performed repeatedly (several million times) resulting in a curve that represent the intensity versus time as shown in Figure 2.10. The time-to-amplitude-converter (TAC), integrated in the computer software, transforms the arrival time between a start and a stop pulse into a voltage. Figure 2.11 illustrates the block diagram of the entire process that is further explained in the following reference (http://www.canberra.com/literature/1012.asp).

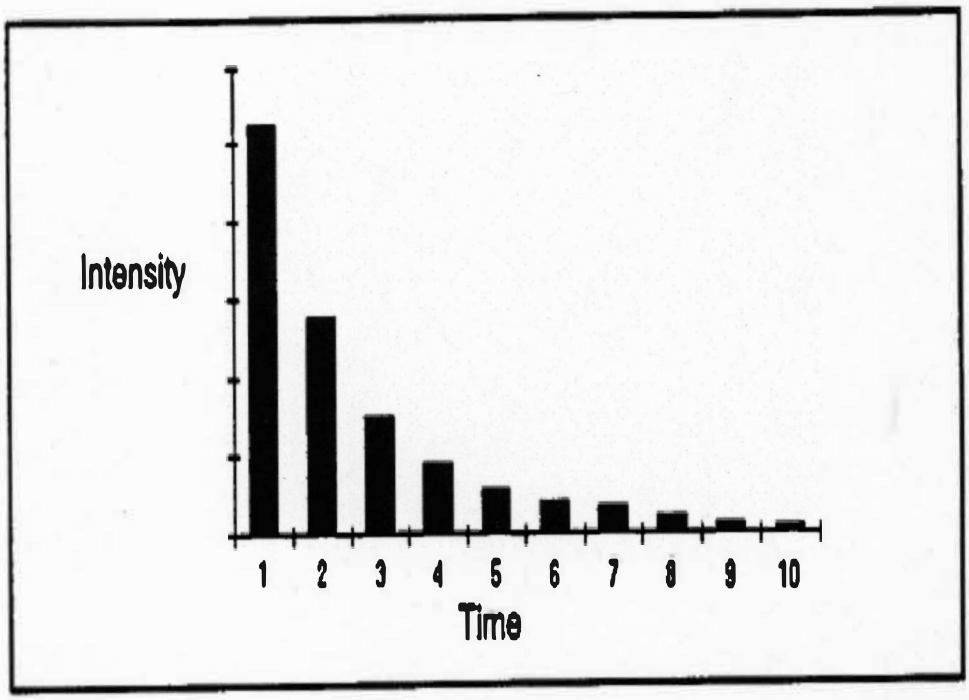

Figure 2.10. Profile of fluorescence decay as determined by TCSPC. http://www.canberra.com/literature/1012.asp)

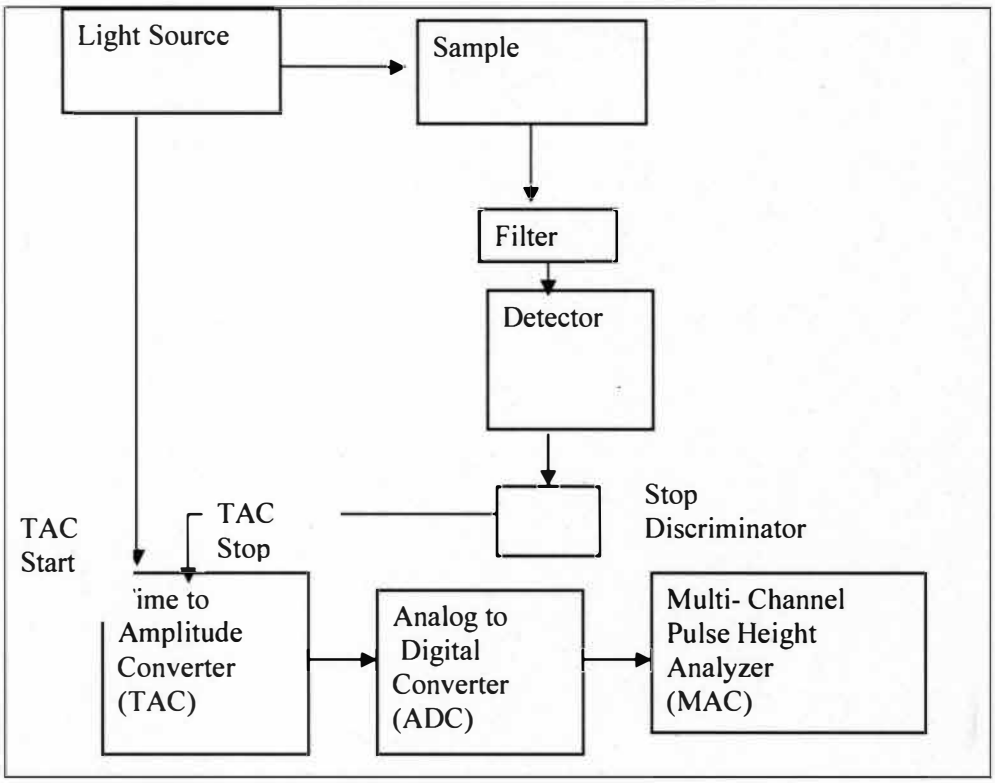

Figure 2.11. Schematic drawing of the time-correlated single photon counting technique used in fluorescence lifetime and time correlated anisotropy measurements and analysis. TAC, MAC, and ADC are incorporated in the computer software.

The sample was excited by a focused laser beam that induced fluorescence. The emission was collected by a high -aperture collection optics and then detected by a sensitive photomultiplier tube (PMT) as a sensitive photoelectric device. The experimental approach used in this study employed a 470 nm LED laser source (Picoquant) powered by PDL800- B laser driver and operating at 20 MHz with a rise time of 35 picoseconds. This was used to excite dyes incorporated in the vesicle preparations at relatively low concentrations. The LED laser was filtered using short pass filters that removed spurious larger wavelength emission. The fluorescence emission wavelength was selected with interference filters and

detected using photomultiplier tube. Light intensities at the detector were varied using adjustable iris and neutral density (ND). The Instrument Response Function (IRF) was obtained from non-fluorescent reflecting glass mirror attached to the oil immersion microscope 60 X objective lens. The timing electronics of this system is based on the TimeHarp 200 PC board operated in a Time-Tagged Time-Resolved (TTTR) mode (PicoQuant GmbH, Berlin, and Germany). The fluorescence signal obtained as a function of time was monitored at wavelength longer that 520 nm employing dichroic filter. The emitted photons were collected using a Becker and Hickl GmbH, Berlin Germany single photon photomultiplier. The experimental data for fluorescence decay and anisotropy measurements were processed and calculated on a PC by FluoroFit software. The software has the capacity to apply both Tail fitting as well as numerical reconvolution algorithm to account for the finite IRF that had time width less than the lifetime of the probes employed (Figure 2.12). The fitting limits were easily adjusted and the goodness of the fit was determined from the chi-square, weighted residual and autocorrelation trace (Figure 2.13).

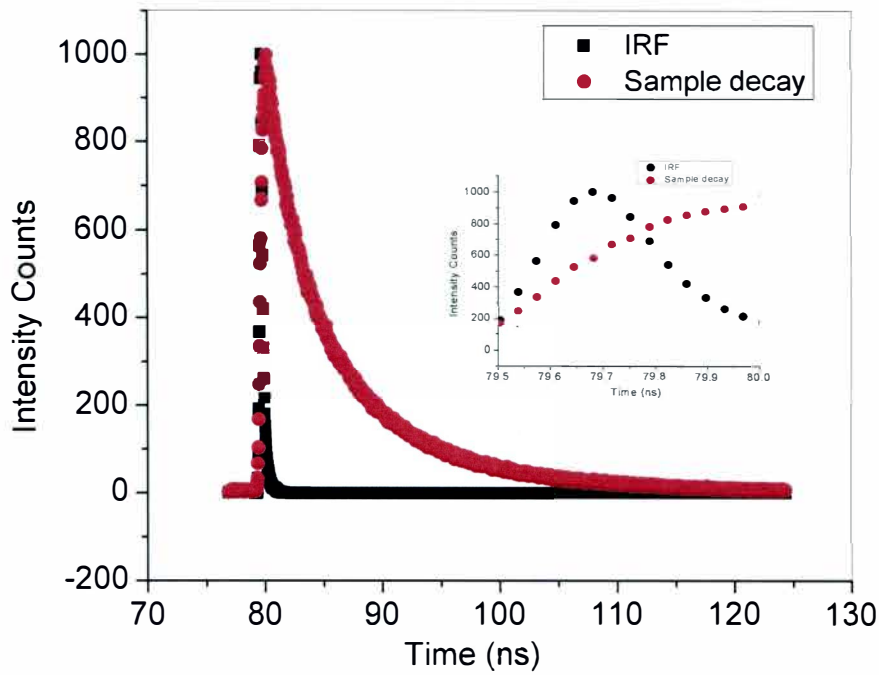

Figure 2.12. Fluorescence intensity decay profile for the sample and the IRF. The insert shows the width of IRF compared to the sample decay.

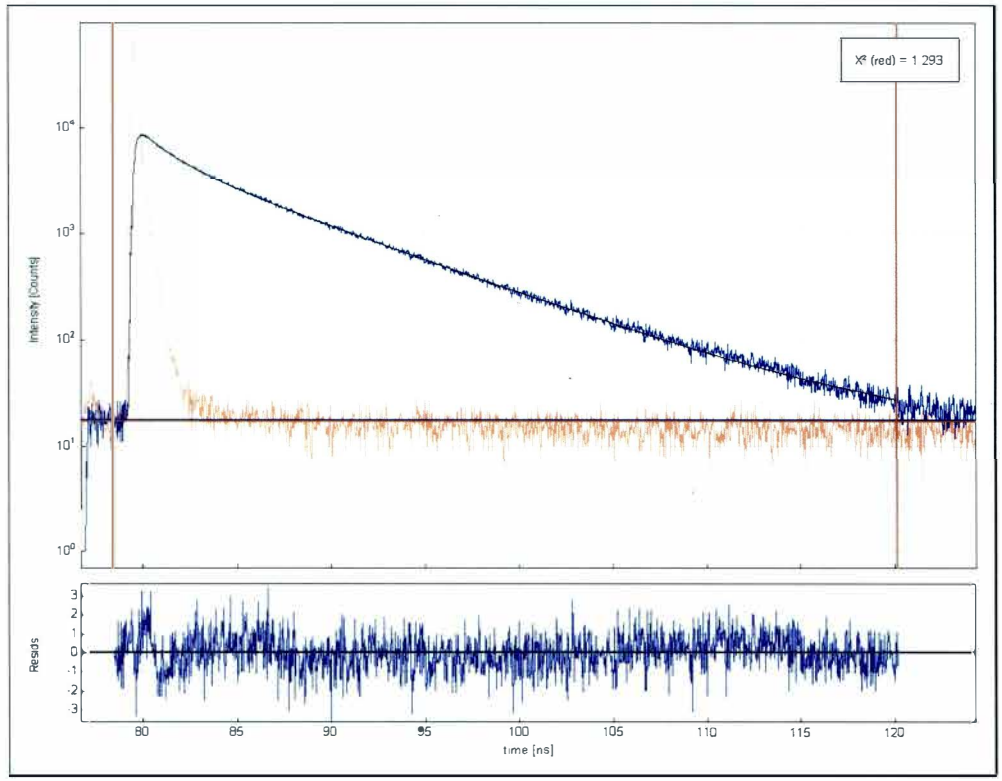

Figure 2.13. Analysis of the fluorescence decay by FluoroFit software. The orange line represents IRF and the blue line sample decay. The lower blue is the residuals that determine the best of the fit.

2.2.7 Fluorescence Time Correlated Anisotropy

Fluorescence time correlated anisotropy was investigated alongside the fluorescence lifetime and the procedure followed the same as mentioned in section 2.2.6. The anisotropy function (equation 2.0) was used to calculate the anisotropy at each temperature that was investigated.

$$A(t) = \frac{I_V(t) - I_H(t)}{I_V(t) + 2I_H(t)} \qquad (2.0)$$

The time-correlated anisotropy, A(t) measurement of NBD-labeled DMPC vesicles was performed at a fixed concentration of 0.5 % (w/w) NBD with respect to DMPC. The value was obtained electronically by calculating the difference between two fluorescence intensity decays $I_V(t)$, (parallel) and $I_H(t)$ (perpendicular) measured with an emission polarizer vertical and horizontal for the vertical orientation of the excitation polarizer. The anisotropy was measured in 11 mM magnesium chloride and the temperature was varied from 4 to 39 ˚C in a thermostated temperature controlled environment in the microscope stage. The instrumentation for the time-correlated anisotropy was designed to measure the anisotropy at the same time measuring lifetime conditions (see Figure 2.5).

In short the 470 nm laser beam was directed onto to the 50 µl sample that were labeled with either NBD PE or NBD PC probe as discussed in the previous section. The design incorporated a movable arm that controlled the movement of

the polarizer in or out of plane of the optics. The beam was directed to and from the microscope stage using a series of optics. The timing electronics of this system was based on the TimeHarp 200 PC board that worked in tandem with the lifetime measurements. The analysis of both perpendicular and parallel anisotropy orientations were performed using a PC by FluoroFit software based on the anisotropy reconvolution. The fitness of the data was assessed by the chi, square and the weighted residuals.

2.2.8 Edinburgh Instrument

The lifetimes of the NBD PE and NBD PC in DMPC vesicles were also determined from the bulk solution. This was done either in dilute or concentrated solution in Edinburgh instrument (Figure 2.14). The measurements were performed using a FLS920 Edinburgh instrument (Livingston, West Lothian, UK) (Figure 2.14) equipped with PCS900 card for single photon counting data acquisition, computer controlled wavelength collector and slit control and single photon counting stop photomultiplier. This instrument employed a 450 nm excitation laser and emission at 540 nm, operating at a frequency of 20 MHz. In this method, aluminum foil was employed to determine the IRF of instrument. The laser signal was initiated by the F900 software that has the capacity to control the operating parameters of the instrument. The lifetime data was acquired using F900 operating software and analysis of the kinetic traces by FAST software. A 4 mg/ml vesicle sample were diluted 20 times in sodium buffer pH 7.4

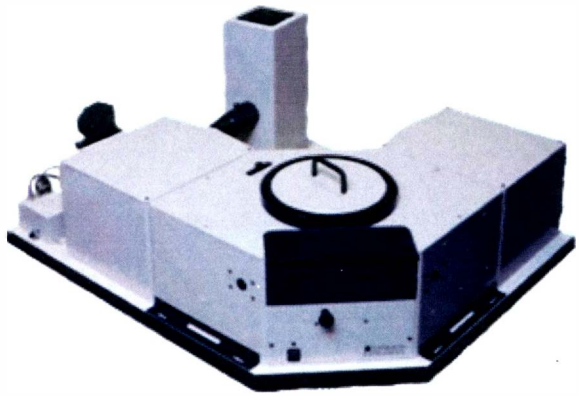

Figure 2.14. Edinburgh instrument.

2.2.9 Preparations of Vesicles of DMPC

The vesicles were prepared using modified rapid evaporation method based on the procedure reported by Moscho et al [103]. A total lipid concentration of 4 mg/ml with respect to DMPC lipid in $CHCl_3$ was transferred to a 50 ml round- bottomed flask that had been baked in an oven at 260°C. A mixture of chloroform and methanol in the ratio of 2:1 was used to disperse the lipid mixtures in the round bottomed flask. To the mixture, approximately 26 µl volume of 1 mg/ml of NBD-PE or NBD-PC was added to give a total of 0.5 mol % dye concentration with respect to DMPC lipids. The lipid dye ratio was therefore 200 to 1. The organic solvent content all added to a total volume of 1 ml including that from the lipid. A 1 ml of 11 mM magnesium chloride ($MgCl_2.6H_2O$) that had previously been filtered through a 0.2 µm polycarbonate membrane filter was gently added along the side of the volumetric flask onto the organic layer. The flask content was immersed in a water bath set at 65 ˚C and that had been previously equilibrated at the same temperature. A stream of nitrogen gas was gently passed through the

content to drive off completely the organic layer. This process typically took about 5 minutes. The flask and its content were left to cool slowly to room temperature in the water bath that had been switched off for a further 10 minutes. A greenish yellow cloudy fluid was obtained. The procedure yielded variety of vesicles sizes ranging from nanometer to tens of microns (Figure 2.15). The nanometer size distribution was characterized by light scattering while the micron sizes by the various microscopy technique as previously described.

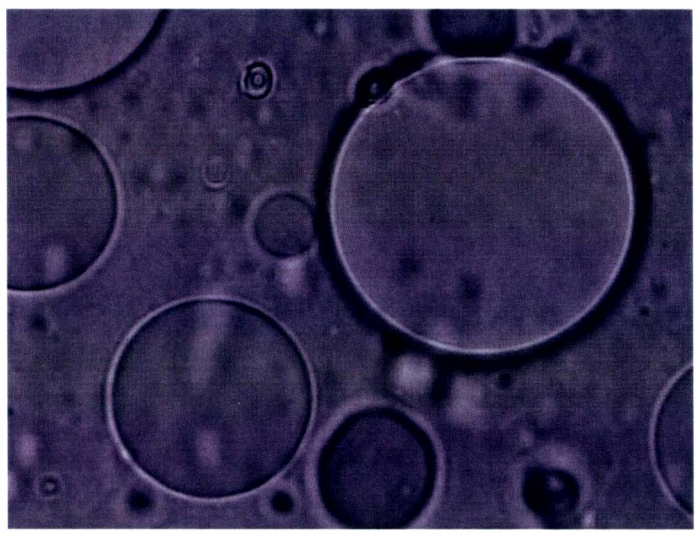

Figure 2.15. Bright field images of vesicles made from DMPC phospholipids The largest vesicle seen in this picture is 20 μm in size.

2.2.10 Lamellarity of Vesicles made from DMPC

Several methods were attempted in a bid to prepare giant unilamellar vesicles from DMPC phospholipids. Vesicles can be produced from a wide range of sizes and bilayers depending upon the technique used. We were interested in the preparation of giant unilamellar vesicles that could be manipulated using optical microscopy technique and that fall within the size range of normal eukaryotic cells. Eukaryotic cells have sizes ranging from 1 to 100 μm in diameter (http://micro.magnet.fsu.edu/cells/animalcell.html).

The sizes and lamellarity of giant unilamellar vesicles determine the quality of the final vesicle preparations. Temperature and presence of divalent ions have been shown to have a great influence on the size of vesicle formed from phospholipids. In this study, we determined lamellarity based on Gruber and Schindler method of external surface determinations resulting from the changes in fluorescence of N-(7-nitrobenz-2-oxa-1,3-diazol-4-yl) (NBD) residues in the lipid bilayer [102]. In this method, the fluorescence signal changes were monitored on addition of membrane impermeant sodium dithionite to vesicles that were labeled separately with small amounts of head and tail labeled lipophilic dyes, NBD PE and NBD PC respectively. NBD –lipid vesicles have a yellowish green fluorescence that can be reduced by sodium dithionite. When a known amount of dithionite is added to the vesicles labeled with NBD lipid derivative NBD PE or NBD PC, the exposed NBD-lipid will be quenched by dithionite resulting in a non fluorescent

moiety. Solubilization, using Triton X-100, of the vesicles results in exposure of the inner leaflets NBD to the excess dithionite and subsequent reduction. The number of bilayers can be deduced from the difference in fluorescence intensity before and after addition of sodium dithionite. The initial decrease in fluorescence intensity, I_1 is attributed to the reduction of the NBD residing in the outer leaflet that can be expressed as the percentage of the total, I_2 that include the inner leaflet NBD that are exposed upon addition of Triton X-100 The ratio I_1/I_2 is 0.5 for a perfect unilamellar vesicle (see Figure 2.16).

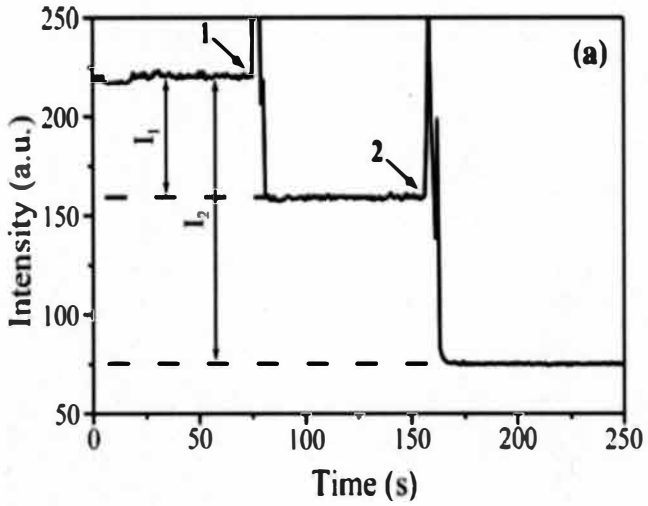

Figure 2.16. This is an illustration of the changes on the fluorescence of NBD upon addition of sodium dithionite(1) and a further addition of Triton X -100 (2) [104].

In this study, 150ul of 4mg/ml DMPC vesicles were added to 2.85 ml of sodium buffer pH 7.4 in a 1 cm quartz crystal cuvette containing a small bar magnet placed on the sample holder of the fluorimeter mentioned above. The temperature control bath circulator and magnetic stirrer were switched on and the sample

stirred gentle. The excitation and emission wavelength for NBD were set as previously explained and the baseline run for about 1 minute. This was followed by the quick addition of 30ul of 1 M sodium dithionite, freshly prepared. The changes in fluorescence were monitored for a further 9 minutes. A 150 ul 20 % w/v Triton X-100 was added to the solution to solubilize the vesicles and exposed the inner leaflets NBD. The procedure was carried out at different temperatures above and below the phase transition of DMPC.

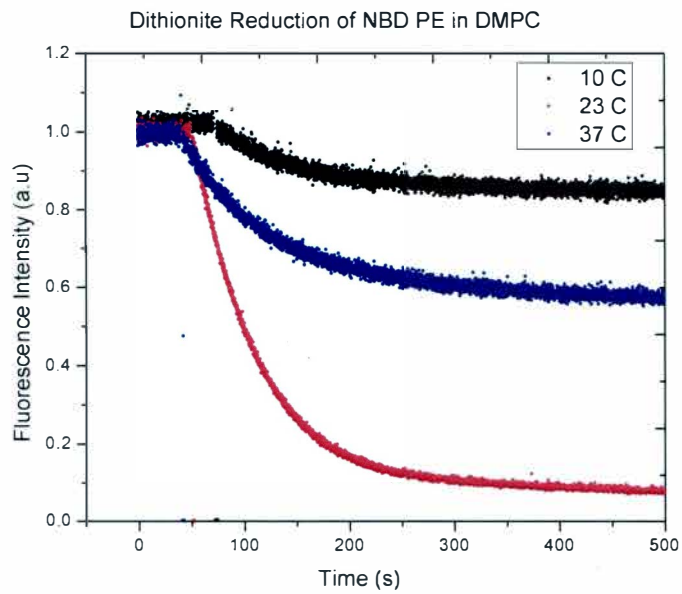

Figure 2.17. Fluorescence intensity changes of NBD PE in DMPC vesicles upon addition of sodium dithionite at different temperatures.

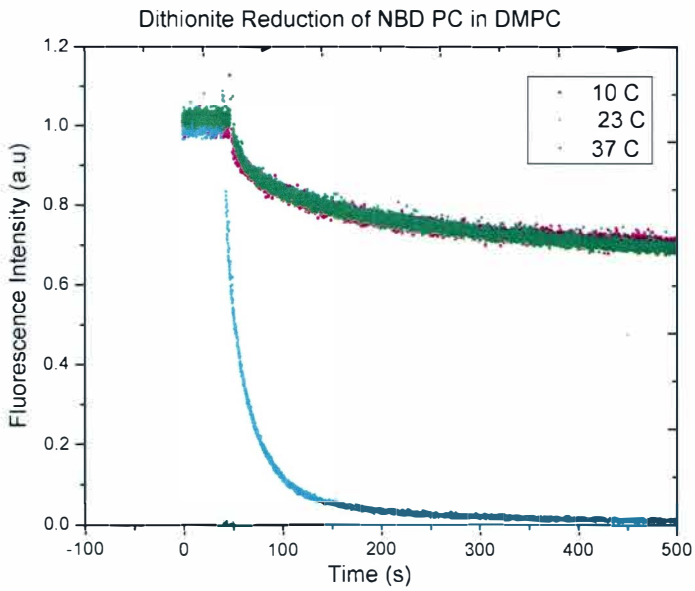

Figure 2.18. Fluorescence intensity changes of NBD PC in DMPC vesicles upon addition of sodium dithionite at different temperatures.

2.2.11 Fluorescence Quenching of NBD by Dithionite

Fluorescence quenching of NBD in the lipid vesicles by dithionite was performed based on Gruber and Schindler as previously mentioned. In summary, a 150 ul of the dye labeled vesicles was added to a 2.85 ml 'sodium buffer' pH 7.4 (100mM NaCl, 10 mm Hepes-NaOH) in a 3 ml fluorescent cuvette. The cuvette was placed in a temperature controlled Shimadzu fluorimeter RF 5301- PC spectrofluorometer was allowed to equilibrate with the set temperature for about 10 minutes. The temperature inside the cuvette was ascertained using a thermocouple immersion probe with a resolution of 0.1 °C. The specimen was continuously stirred using a magnetic stir bar placed inside the cuvette and that was externally controlled. A 30 µl from a 4 °C freshly prepared solution of 1 M sodium hypochlorite reagent (3.48 g $Na_2S_2O_4$ and 2.43 g Trizima base and

Millipore water added to give a final total weight of 21.4 g with automatic pH 10), (giving a final concentration of 0.01 M compared to 4.5 X 10^{-7} M for NBD PE and NBD PC) was accurately measured using a 150 ul glass syringe and immediately added to the mixture in the cuvette. The sample was irradiated with a 470 nm (5 nm slit) and fluorescence studies were followed at 540 nm (5 nm slit) for both NBD PE and NBD PC.

The spectral data obtained were analyzed by OriginLab 7.5 software a copyright of OriginLab Corporation (Northampton, MA, USA). The results demonstrated in Figure 2.19 showed two major components in the time course, the short and the longer component of which were further analyzed to give the corresponding rate constants for the reduction process. The rate constants for the reaction were obtained by fitting the fluorescence curve to a sum of two exponentials determined by equation 2.1. The fluorescence intensity S, was expressed as a sum of the fast step k_1 and the slow step k_2 with a_1 and a_2 corresponding to the contributions of each step.

$$S = a_1 e^{-k_1 t} + a_2 e^{-k_2 t} \qquad (2.1)$$

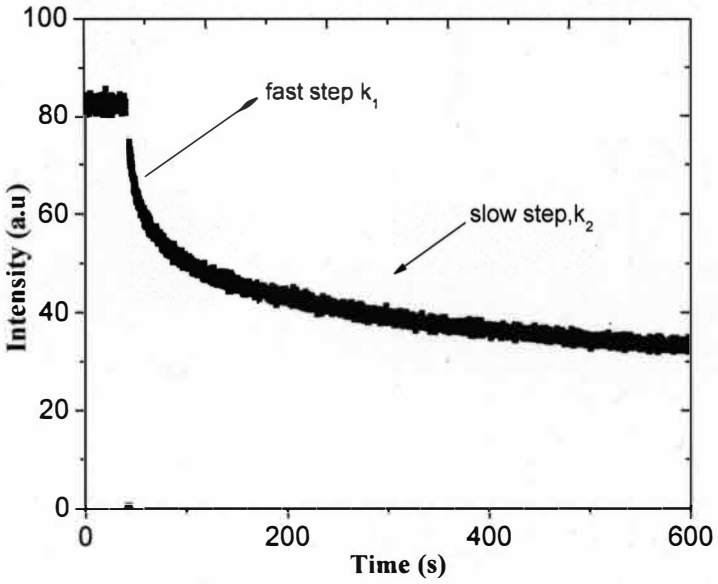

Figure 2.19. Dithionite induced reduction of NBD in DMPC vesicles showing the fats and the slow step upon addition of sodium dithionite.

2.2.12 Steady State Fluorescence Anisotropy

Temperature-dependence steady state fluorescence measurements were performed in the Shimadzu RF-5301 PC Spectrofluorophotometer with a detachable L-shaped polarizer accessories using 1 cm path length quartz cuvette. The excitation and emission slits were set at 5 nm for all measurements. The procedure was based on the dithionite measurements explained above. Fluorescence anisotropies <A>, were computed from the fluorescence intensities measured in directions parallel (I_{II}) and perpendicular ($I_{\perp}$) to the electric vector of the exciting light (using excitation and emission wavelengths of 460 nm and 540 nm, respectively) based upon equation 2.3

$$A = \frac{I_{\parallel} - GI_{\perp}}{I_{\parallel} - G2I_{\perp}} \qquad (2.3)$$

A refers to the anisotropy value and G is grating correction factor that is given by the ratio $I_{\perp}/I_{\parallel}$ which measures the instrument sensitivity or the detection efficiencies determined by that relationship.

2.2.13 Interaction of Dithionite and NBD in Bilayer Region

Fluorescence quenching of NBD PE or NBD PC in DMPC vesicles were investigated as a function of dithionite concentration below, at and above the phase transition of the DMPC. The study was performed in steady state mode in sodium buffer at pH 7.4. A 150 ul of a 4mg /ml DMPC labeled with 0.5 % w/w NBD PE or NBD PC in 11Mm magnesium chloride and the solution was further diluted to a 3 ml with sodium buffer at pH 7.4 and transferred to a fluorescence quartz crystal glass. The solution was mixed throughout the experiment using a thermostatted stirred cuvette.

The fluorescence spectroscopy measurements were achieved with the same settings using Shimadzu fluorimeter RF 5301- PC spectrofluorometer outlined in section 2.2.4. A 5 to 150 ul of a 4mg/ml volume sample of 1 M sodium dithionite corresponding to variable concentration of dithionite were investigated at fixed concentration of NBD.

The dithionite quenching was performed with an excitation wavelength 470 nm and emission wavelength 540 nm each set at operating slit width 5 nm. Each concentration of dithionite investigated resulted in the fluorescence intensity change that showed typical quenching decay curve (Figure 2.19) that was used to study the dependence of quenching of NBD and dithionite. The fluorescence intensity I_o which corresponds to intensity before dithionite addition and intensity I after addition were calculated after 30 seconds time in the time course of the experiment. A series of values of I_o / I corresponding to dithionite concentration were obtained. A double reciprocal plot of the ratios of the unquenched and quenched fluorescence intensity was plotted against dithionite taking into consideration the Stern –Volmer equation that yielded a regression line used to study the quenching efficiency of dithionite (equation 2.4).

$$I_O / I = 1 + K_{st}[Q] \qquad (2.4)$$

K_{st} refers to the Stern –Volmer quenching constant and [Q] in the concentration of the quenching for that case sodium dithionite.

2.2.14 Preparation of Asymmetrically Labeled Vesicles

Fluorescence intensity change was monitored in vesicles which were formed and labeled later in fluorimeter using either NBD PE or NBD PC. Fluorescence measurements were done in the Shimadzu RF-5301 spectrofluorometer equipped with temperature control as previous discussed. The measurements were taken at 10, 23 and 33 °C with continuous stirring of the cuvette. A 4 mg/ml of DMPC vesicles were prepared as in the previous section (see section 2.2.9). A 150 µl of the vesicle samples was transferred into a 2.85 ml of sodium buffer at pH 7.4 and was put under continuous stirring using a magnetic stir bar and then equilibrated with the set temperature for 5 minutes. The sample was irradiated with a 470 nm excitation wavelength and the fluorescence monitored at 540 nm with 5 nm slit width set for both cases. Fluorescence was initiated by adding NBD PE or NBD PC to the vesicles in the cuvette.

The probe was prepared by taking 10 ul of 1 mg/ml either NBD PE or NBD PC in chloroform into a 4 ml amber bottle. This sample was subjected to a stream of nitrogen to drive off the chloroform which was attained under 5 minutes. A 10 ul aliquot of methanol was added back to the amber bottle. The 10 ul of this concentration was added to the 150 µl of a 4mg/ml vesicle sample in a 2.85 ml in the cuvette and the fluorescence monitored as mentioned above.

2.2.15 DMPC Vesicles with Variable Dihydrocholesterol Content

The vesicles containing dihydrocholesterol were prepared by adding a calculated volume of DMPC lipids in chloroform to a mixture of chloroform and methanol in the ratio of 2:1. A 4 mg/ml DMPC sample was prepared by adding 59 ul of 0.1 M DMPC stock solution in chloroform to 50 ml volumetric flask that had been baked earlier to a 260 ˚C and cooled. The volume was dispersed in a total of 918 µl mixture containing chloroform and methanol in the ratio 2:1. A 0.5 % (mol/mol) with either NBD PE or NBD PC was added to the mixture. The amount of the dye was made relatively low in concentration resulting in 1 molecule of the dye to 200 molecules of DMPC phospholipids.

A 5 % (mol/mol) dihydrocholesterol content was prepared by adding 29.5 µl volume of 0.01 M dihydrocholesterol prepared in Millipore water that was equivalent to 2.95×10^{-7} moles in a 1 ml. A 1 ml solution of 1 lmM magnesium chloride that was previously filtered through a 200 nm polycarbonate membrane was gentle added along the side of the flask. The flask and its content were transferred to a water bath set at 65 ˚C and that had been previously equilibrated for about 30 minutes at the same temperature. A stream of nitrogen was passed through the solution through the content to drive off completely the organic layer. This process typically took about 5 minutes and then the solution was left to cool to room temperature. A range of dihydrocholesterol concentration between 0 to 60 % (mol/mol) was investigated for a fixed concentration of DMPC and the probe. Fluorescence anisotropy, quenching and microscopy techniques were

performed on the resulting vesicles. We plotted kinetics of dithionite reaction using Eyring model.

CHAPTER 3

RESULTS

3.1 Size Distribution of DMPC Vesicles

As discussed in the experimental section, we determined vesicle size and distribution using QELs scattering method. QELs is based on the determination of the average vesicle diffusion coefficient and relative dispersion in dilute suspensions which yields vesicle size and polydispersity from dilute polydisperse vesicle suspensions. The dynamic light scattering performed on the QELs light instrument on vesicles extruded through 100 nm polycarbonate membrane filters yielded polydisperse vesicles of hydrodynamic radius of about 50 nm size (Figure 3.0).

The procedure used to generate both labeled and unlabeled vesicles resulted in a polydisperse system ranging from a nanometer size to several microns. This was verified by both dynamic light scattering and light microscopy techniques. The latter showed vesicles that were widely distributed in size with 20 μm mean size range for DMPC phospholipid vesicles.

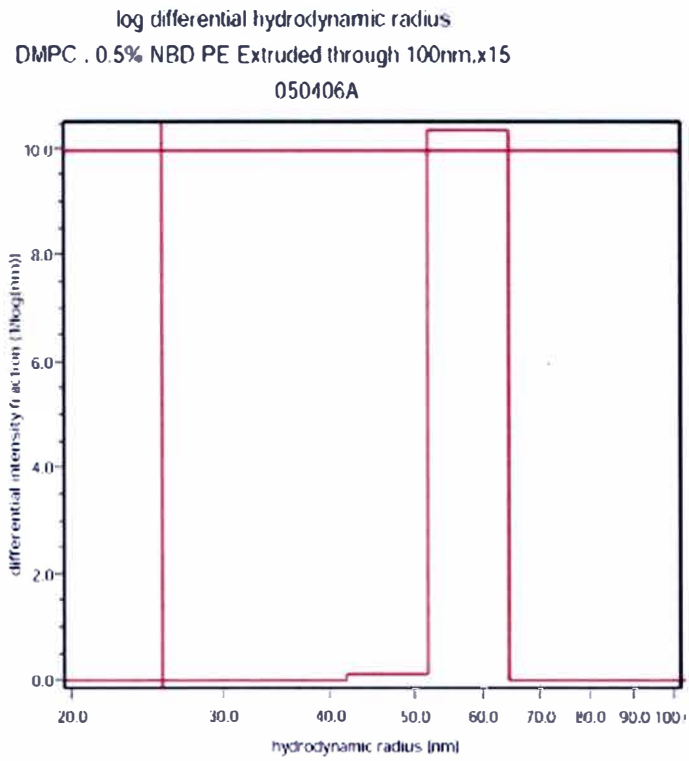

Figure 3.0. Size distribution of DMPC vesicles extruded through 1 μm and then finally through 100 nm size polycarbonate

The microscopy images, brightfield, phase contrast and epifluorescence from Nikon TE2000 inverted optical microscope, showed vesicles that were widely distributed in size. The DMPC vesicles showed average size distribution about 20 nm and were unilamellar under phase contrast (Figure 3.1).

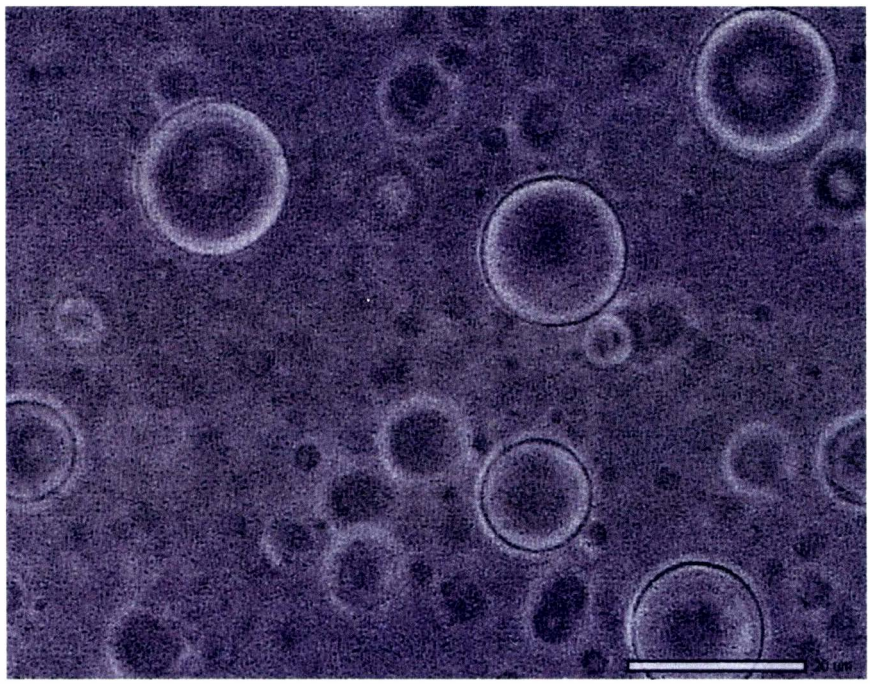

Figure 3.1. Phase contrast images of DMPC vesicles in 11mM magnesium chloride. The scale bar insert is 20 μm in length.

The emission from NBD fluorescent probes embedded in the DMPC bilayer, under fluorescence microscopy, showed the propensity of the dye to lipid bilayer region (Figure 3.2). The addition of 0.5 % (mol/mol) of the probe, relative to the DMPC phospholipids in a total lipid concentration of 4mg/ml, resulted in a strong fluorescence emission signal as captured by the CCD camera in epifluorescence mode of the optical microscope. The NBD moiety embedded in the lipid bilayer showed a UV-Vis signal at 469 nm irrespective of temperature (Figure 2.9). The UV-Vis spectrum measured in chloroform and methanol gave three absorption bands at 250, 329 and 461 nm. Similar experiment on DMPC vesicles made in sodium buffer at pH 7.4 and 11 mM magnesium chloride gave only two distinct

peaks (Figure 2.8). The emission spectra of the NBD PE in DMPC vesicles upon excitation at 470 nm yielded a strong signal at 535 nm (Figure 2.6).

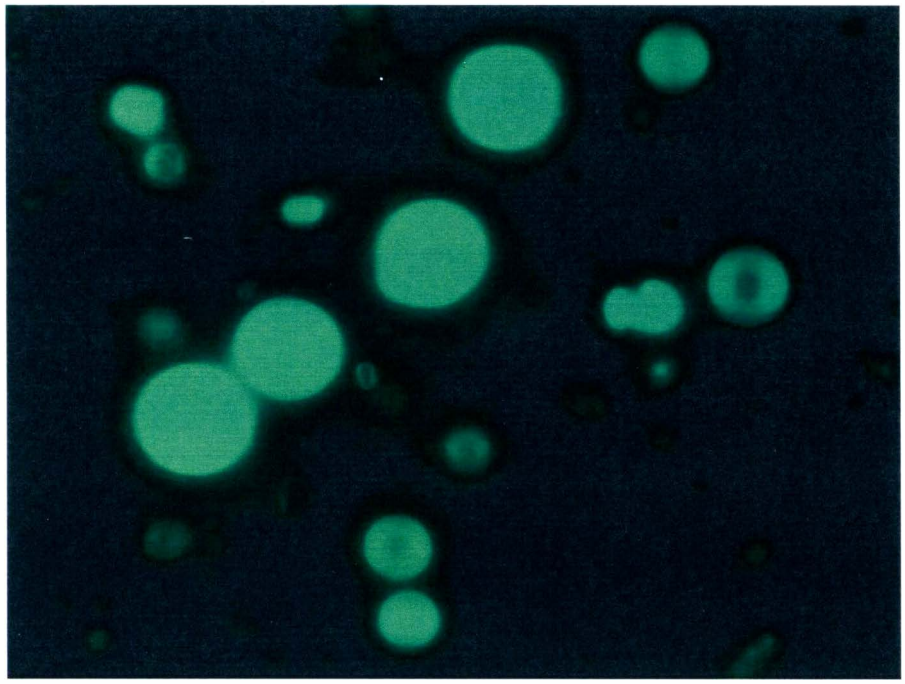

Figure 3.2. Epifluorescence images of DMPC vesicles. The fluorescence was due to the emission from NBD PE embedded in the bilayer region of the vesicles.

3.2 Percentage of NBD Quenched as a Function of Temperature

The dynamics of the membrane were monitored by fluorescence intensity changes occurring as a result of quenching of NBD induced by dithionite. The amount of the NBD PE or NBD PC incorporated in DMPC vesicles that were quenched by dithionite was calculated based on the lamellarity determination (section 2.210). The amount of NBD reduced upon addition of 30 ul of a 1 M sodium dithionite, performed at each temperature and across the phase profile of DMPC in a temperature range between 4 to 49 °C resulted in nearly 100 % quenching. This was true for NBD PE and NBD PC at the phase transition (Figure 3.3). A slight hump was observed below the phase transition while above the transition there is relatively small increment in the amount of NBD quenched.

We investigated fluorescence quenching of DMPC bilayer region at temperatures below, at and above the phase transition region. NBD PC in DMPC showed 100 % quenching at the phase transition (23 °C). In addition, NBD PC in DMPC below and above this temperature, the quenching remained similar in intensity (Figure 2.18). NBD PE showed a slight deviation from NBD PC above and below this temperature, while the phase transition had similar trend resulting in nearly 80 % quenching (Figure 2.17).

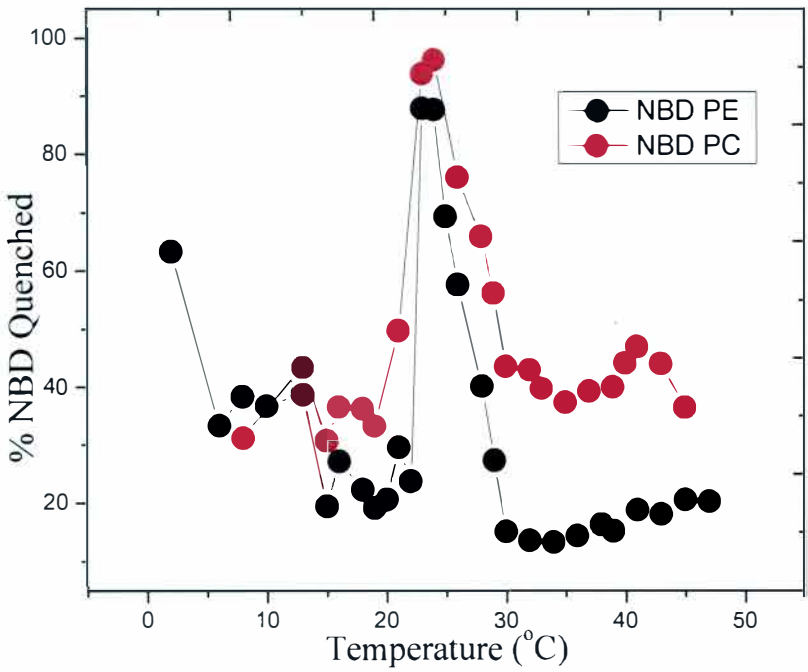

Figure 3.3. Percentage of NBD quenched as a function of temperature.

3.3 Asymmetrically Labeled DMPC Vesicles

To gain a deeper understanding of the behavior of NBD PE and NBD PC in DMPC, preformed vesicles were labeled by external addition method. Lipid-mixing was assayed by fluorescence method at 10, 23 and 33 ˚C in a cuvette in fluorimeter. The exponential growth of NBD in DMPC was observed with excited wavelength at 470 nm at 5 nm and the fluorescence monitored at 540 nm, 5 nm slit width. Figure 3.4 shows fluorescence intensity growth pattern at the three different temperatures. NBD PC gave relatively higher fluorescence intensity than NBD PE in the three different temperatures corresponding to gel, fluid and phase transition of DMPC. Above and below the transition temperature, NBD PC fluorescence intensity reached maximum after several seconds while the NBD PE

attained a plateau immediately. The dye incorporated in preformed vesicles at 23 ˚C showed significant increase with time for NBD PC, while NBD PE was less affected.

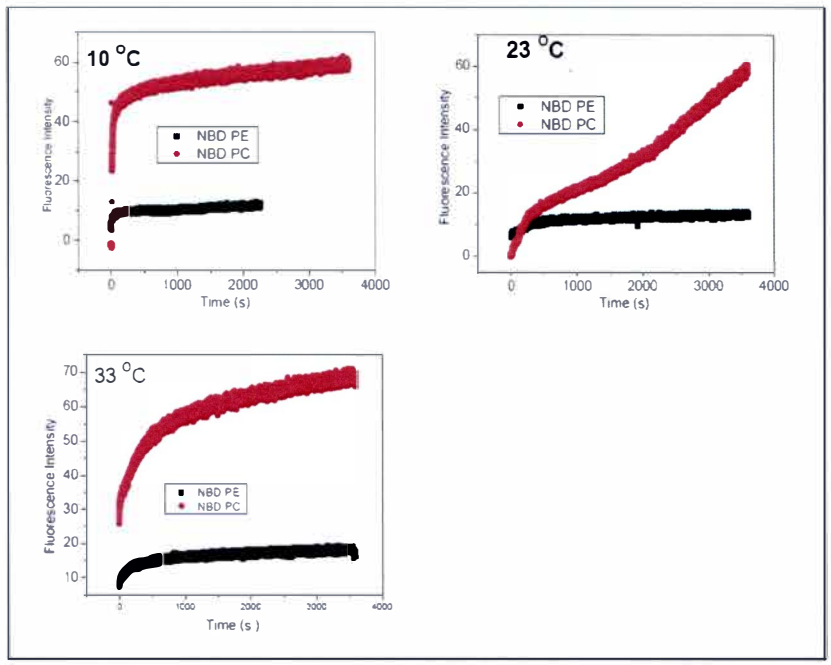

Figure 3.4. Addition of probes to preformed DMPC vesicles at phase states of the lipid

The time course events for dithionite quenching of the NBD PE and NBD PC in DMPC were investigated. This was done in the vesicles that had been pre-labeled with the probe at concentration of 0.5 % mol/mol. The sample time was run in hours to determine if there was significant deviation from the fluorescence decay. The result showed a diminishing trend with time with respect to the fluorescence decay curve. The trend showed an immediate quenching that was followed by a slow process that went for hours (Figure 3.5).

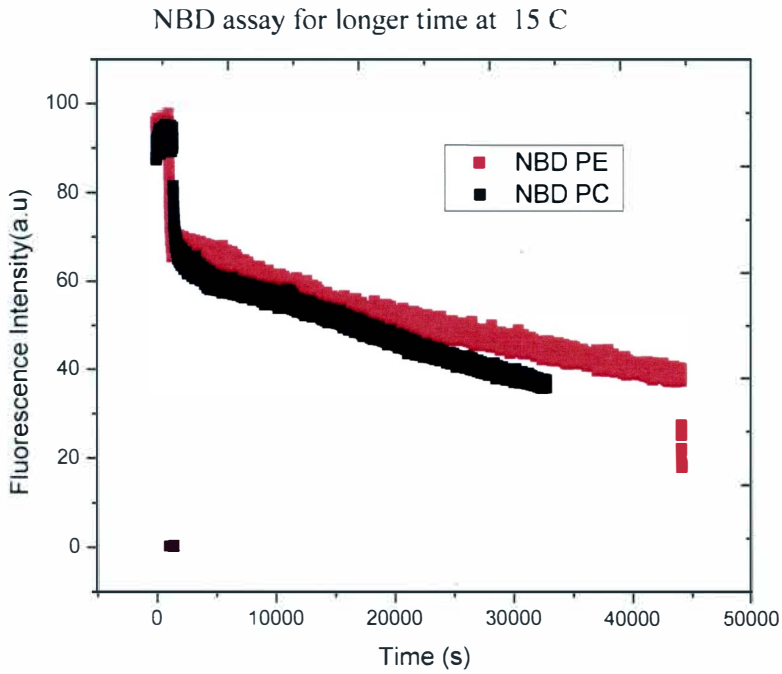

Figure 3.5. Fluorescence decay of NBD PE and NBD PC in DMPC for a longer period of time (hours).

3. 4 Steady State Fluorescence Anisotropy Measurements

The steady state fluorescence anisotropy studies conducted under equation 2.3 were performed for NBD PE and NBD PC in a series of temperatures occurring in the region between 10 and 46 ˚C. These measurements were initiated in order to study the microviscosity of the bilayer around the fluorophore. This constitutes the property of the entire bilayer fluidity and membrane organization. The plot of the anisotropy as a function of temperature showed anisotropy decreases with increasing temperature for both NBD PE and NBD PC labeled vesicles. The NBD PE and NBD PC exhibited a reduction in fluorescence anisotropy in the gel-to-fluid (Figure 3.6).

The temperature-dependence anisotropy of the two probes in DMPC indicate that the fluorescence lifetime of the NBD moiety decreases with increasing temperature as a result of the decrease in fluorescence intensity. A derivate plot of the anisotropy measurements (Figure 3.7) showed a dip at the region around the phase transition temperature. The decrease in anisotropy of the NBD PE in the temperature range between 10 and 46 ˚C is larger (0.1) than for NBD PC (0.06).

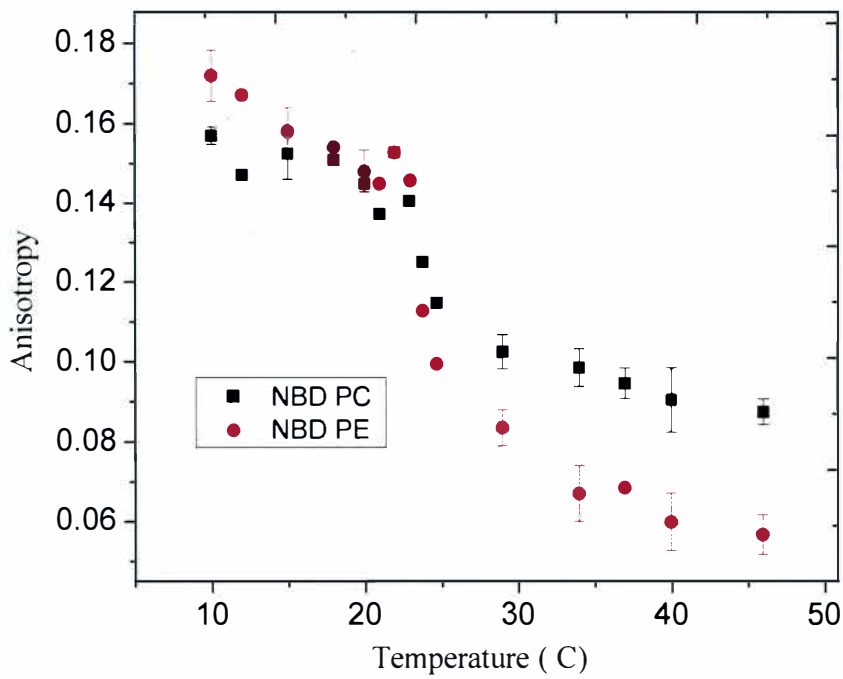

Figure 3.6. Temperature-dependence steady state fluorescence anisotropy of NBD PE and NBD PC in DMPC.

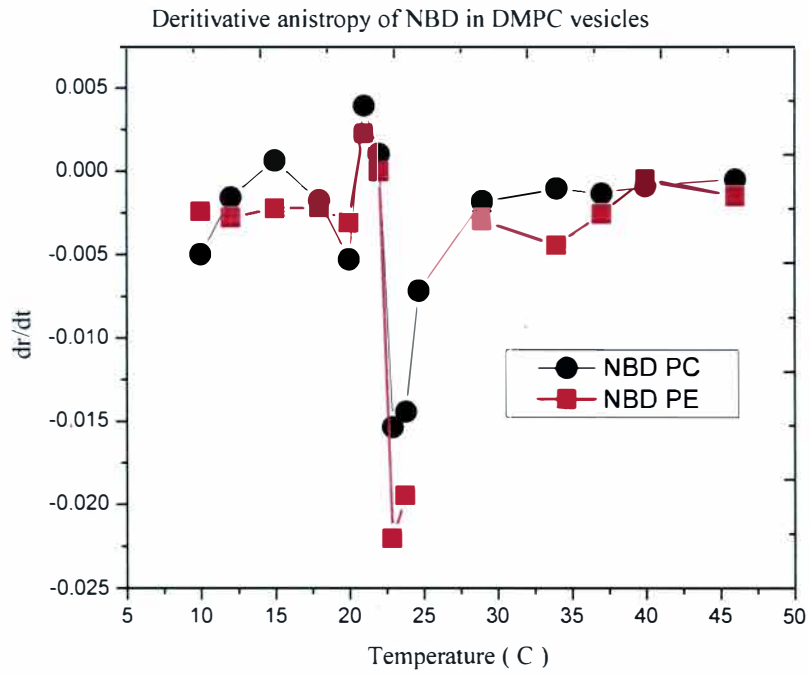

Figure 3.7 Derivative plot for the steady state fluorescence anisotropy of NBD PE and NBD PC in DMPC vesicles.

3.5 Dithionite Quenching of NBD in the Bilayer

Sodium dithionite is a strong reducing agent. In our study, dithionite was used to qualify and quantify the rate of quenching of NBD-labeled phospholipids vesicles. Dithionite reduces the nitro group in NBD to a nonfluorescent amine group, ABD (Figure 1.5). The readily accessible NBD residing in the outer leaflets are reduced first before the inner leaflets NBD. As a result of the concentration gradient initiated by the immediate reduction of the outer leaflets NBD, there is a tendency of the inner leaflet NBD translocate to the outer leaflet to be reduced by dithionite. Figure 2.19 shows a kinetic trace of sodium dithionite induced reduction of NBD labeled DMPC phospholipid vesicles. The addition of dithionite in excess was followed by loss of fluorescence intensity over time. This

is characteristic of a pseudo-first order reaction. The immediate quenching was shown by the fast step that was determined by rate constant k_1 while the slow process that could be attributed to the translocation, as previously mentioned, was analyzed and the rate constant given by k_2. The vesicle was ruptured by the addition of 150 µl of 20 % (w/v) Triton X-100. Thus, allowing the complete reduction of the NBD by excess dithionite.

The rate constant was analyzed using OriginLab 7.5 software. The exponential decay curve fitted well to double exponential function. The representative rate constants at some temperatures corresponding to the phases of DMPC for the slow and the fast steps are tabulated (see Table 4). The reduction of NBD PC in DMPC was faster than NBD PE for both the slow and the fast steps.

The rate constants for the fast and the slow steps at the phase transition (23 ˚C) were about two orders of magnitude greater for NBD PC than NBD PE. Both the probes exhibited the slow and the fasts steps and the differences arising from the rate constants was an indication of the differences in their orientation in the bilayer region of DMPC.

Table 1. Fluorescence lifetime of NBD PE and NBD PC in single vesicles of DMPC in 11 mM Magnesium chloride at 25 °C without the polarizer in place for the anisotropy measurements.

DMPC	Fast		Slow	
	τ1, ns	Contribution (%)	τ2, ns	Contribution (%)
NBD PE	9.7 ± 0.4	67	2.4 ± 0.4	33
NBD PC	6.9 ± 0.5	64	2.3 ± 0.2	36

3.6 Kinetics of Dithionite Quenching of NBD PE and NBD PC in DMPC

We used the kinetics and thermodynamics of dithionite and NBD interactions in the bilayer region to determine the dynamic properties as well as the physical properties of the DMPC lipid bilayer. The approach used to study these properties involved the use of NBD attached to the head (NBD PE) that probed the interfacial regions of the bilayer and the tail labeled NBD PC for the hydrocarbon region. DMPC was also important in the investigation of these properties as it exhibited the gel and fluid phase transition at room temperature.

Dithionite quenching resulted in two kinetically distinct processes that were represented by rate constants k_1 and k_2. The faster step was immediate and occurred in few minutes while the slow process extended for several hours (Figure 3.5). The first ten minutes or below were used to determine the rate constants. The slow and fast steps were studied further by fitting the temperature-

dependence rate constant to the Eyring model (equation 3.0). The model was used to determine the entropy ($\Delta S^{\ddagger}$) and enthalpy ($\Delta H^{\ddagger}$) of activation. The enthalpy was obtained from the slope of the lines and the entropy from the y-intercept of the same y-axis plots.

The kinetics of the fluorescence quenching of NBD by dithionite was determined under excess of dithionite giving a pseudo-first order reaction with respect to NBD concentration. Furthermore, dithionite quenching experiments were initiated for temperatures 10, 23 and 37 ˚C with dithionite concentrations ranging from 1-50 mM. A double reciprocal plot of the observed rate constant and dithionite concentrations from the quenching kinetics at 10, 23 and 37 ˚C for both NBD PC and NBD PC in DMPC yielded the inverse of the pre-equilibrium constant from the slope. These were used to recalculate the pre-equilibrium constants as summarized in Table 2.

Table 2. Pre-equilibrium constant for the association of dithionite NBD PE and NBD PC inserted in DMPC vesicles at different temperature

Temp. (°C)	NBD PE		NBD PC	
	K_1, M^{-1}	K_2,M^{-1}	K_1, M^{-1}	K_2, M^{-1}
10	152.23± 15.12	98.22 ± 5.31	437.43 ± 22.32	404.52 ± 22.12
23	219.61± 39.22	150.32 ± 8.03	527.44 ± 27.12	503.13 ± 25.64
37	427.72 ± 20.12	300.03 ± 14.22	680.62 ± 36.23	549.83 ± 30.12

A plot of pre- equilibrium constant verses 1/T yielded thermodynamic parameters ΔH given by slope and ΔS by y-intercept (Table 3). The ΔH is positive indicating that the pre-equilibrium step of dithionite associating with NBD in the DMPC bilayer is endothermic. In general, the values were approximately three times greater in NBD PE than NBD PC. The ΔS values are also positive reflecting on increasing in entropy. A sum of the activation and thermodynamic parameters was used to determine the kinetics of the overall process (Table 5).

Table 3. Thermodynamic parameters associated with the pre-equilibrium constants for NBD PE and NBD PC in DMPC vesicles

	NBD PE		NBD PC	
	K1	K2	K1	K2
ΔH (kcal/mol)	6.65±1.12	7.22 ± 1.02	2.85 ± 0.26	1.98 ± 0.04
ΔS (cal/mol/K)	33.42 ± 3.83	34.43 ± 3.04	22.15 ± 0.82	18.98 ± 1.62

$$\ln\left(\frac{k}{T}\right)=\frac{-\Delta H^{\ddagger}}{RT}+\ln\left(\frac{kr}{h}\right)+\frac{\Delta S^{\ddagger}}{R} \qquad (3.0)$$

where is k is the rate constant, kr is the Boltzmann's constant, T is the absolute temperature (degrees K) , h is the Planck's constant and R is the universal gas constant ,$\Delta H\ddagger$,enthalpy of activation ($Jmol^{-1}$) and $\Delta S^{\ddagger}$, entropy of activation ($Jmol^{-1}K^{-1}$)

Figure 5 shows enthalpies and the entropies of activation. The slow and fast step, for the NBD PE and NBD PC look similar. In both cases, a small positive value for the enthalpy and a large negative value for the entropy are observed. The enthalpies of activation for the fast steps for NBD PE and NBD PC are similar and the same was true for the slow steps. The overall change for the reduction process for the reactants moving to the activated complex showed values that are a factor of two larger for NBD PE compared to NBD PC.

Table 4. Quenching rate constants for the reduction of NBD PE and NBD PC by dithionite in DMPC vesicles

Temp. (°C)	NBD PE		NBD PC	
	k_1 x10^2, s^{-1}	k_2 x 10^4, s^{-1}	k_1 x 10^2, s^{-1}	k_2 x 10^4, s^{-1}
10	2.73± 0.22	1.24 ± 0.12	3.42 ± 0.13	1.83 ± 0.12
23	3.34 ± 0.08	18.3 ± 1.24	6.92 ± 0.23	39.95± 6.32
37	2.82 ± 0.12	2.65 ± 0.12	3.5 ± 0.12	3.20 ± 0.52

The activation barriers for the overall curve were calculated and tabulated (Table 6). The regions around the phase transition (phase 1 and phase 2) and the slow step for both the NBD PE and NBD PC are anomalous (Table 6) and are difficult to understand and interpret, especially on the basis of the negative enthalpy barriers that violate the Eyring transition theory.

Table 5. Activation parameters for the reduction by dithionite of NBD PE and NBD PC in DMPC without considering the phase transition region. $\Delta H^{\ddagger}$ and $\Delta S^{\ddagger}$are enthalpy and entropy of activation respectively.

t

NBD PE				NBD PC			
k_1		k_2		k_1		k_2	
$\Delta H^{\ddagger}$ (kcal/mol)	$\Delta S^{\ddagger}$ (kcal/mol)	$\Delta H^{\ddagger}$ (kcal/mol)	$\Delta S^{\ddagger}$ (kcal/mol)	$\Delta H^{\ddagger}$ (kcal/mol)	$\Delta S^{\ddagger}$ (kcal/mol)	$\Delta H^{\ddagger}$ (kcal/mol)	$\Delta S^{\ddagger}$ (kcal/mol)
2.84	-52.13	2.95	-65.85	2.28	-57.80	3.02	-64.14
$\Delta H + H^{\ddagger}$	$\Delta S + S^{\ddagger}$	$\Delta H + H^{\ddagger}$	$\Delta S + S^{\ddagger}$	$\Delta H + H^{\ddagger}$	$\Delta S + S^{\ddagger}$	$\Delta H + H^{\ddagger}$	$\Delta S + S^{\ddagger}$
9.49	-18.71	10.17	-31.42	5.13	-35.65	5.00	-45.16

The Eyring model plot yielded typical curves that showed differences in NBD PE and NBD PC for the fast and the slow steps. The curves for the phase transition for the rate constants k_1 and k_2 for NBD PE (Figure 3.8 and 3.9) and for NBD PC (Figure 3.10 and 3.11) respectively showed anomalous behavior around the phase transition temperature. The Eyring plot of NBD PE showed an anomalous behavior around 26 °C close to the phase transition of DMPC.

The quenching rate constants k_1 and k_2 were determined in the temperature range between 2 to 45 °C for NBD PE and 10 to 45 °C for NBD PC by taking temperature after every 2 °C in the gel and fluid phases. Measurements were taken at 1 °C intervals for the region around the phase transition. To ascertain the reproducibility of the kinetic procedure, studies were conducted in the same temperature range by increasing and decreasing the temperature.

The rate constants were shown to increase with temperature with anomalous increase around the phase transition. The rate constant k_2 for the slow step was two orders of magnitude slower than the fast step k_1.

The Eyring plot for the slow and the fast step were reconstructed by considering only the gel and the fluid phases. This demonstrated a linear dependence indicated by the solid blue lines. The rate constant for the fast step for NBD PE around the phase transition showed a negative deviation from the blue line while the rate constant for the slow step for NBD PE (see Figure 3.8) and that of the fast and slow steps for NBD PC exhibited a positive behavior from the blue line. The activation parameters derived from the linear plots were calculated as represented in Table 5.

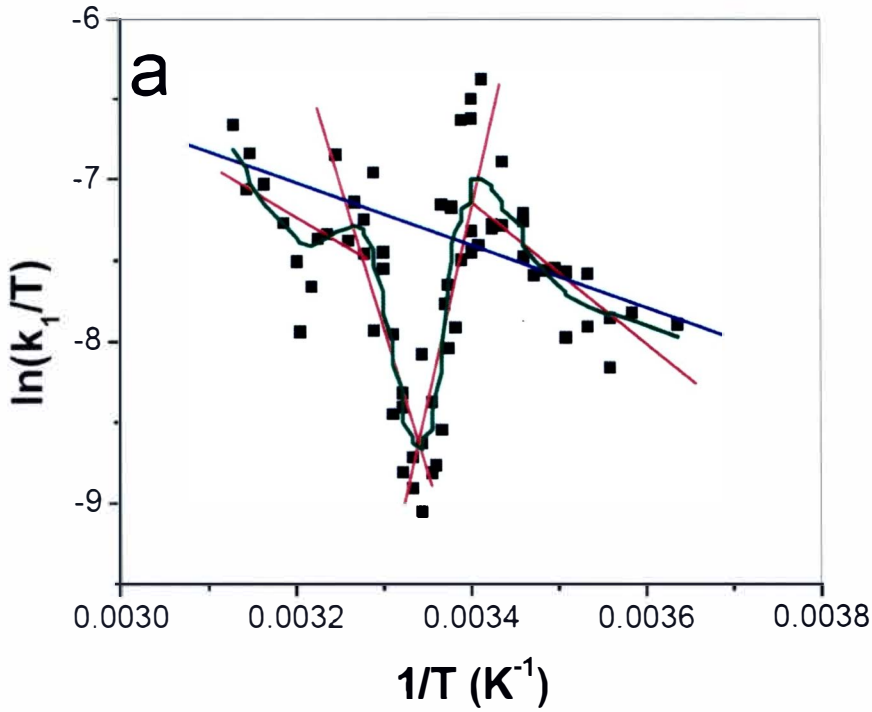

Figure 3.8 Eyring plot for dithionite fluorescence quenching of NBD-PE in DMPC vesicles for fast step.

Note:

Green line represents the overall trend,

Blue line Eyring plot without considering the rate constants in the phase transition

temperature range

Red lines Eyring plots for Gel, Phase 1, Phase 2, and fluid regions.

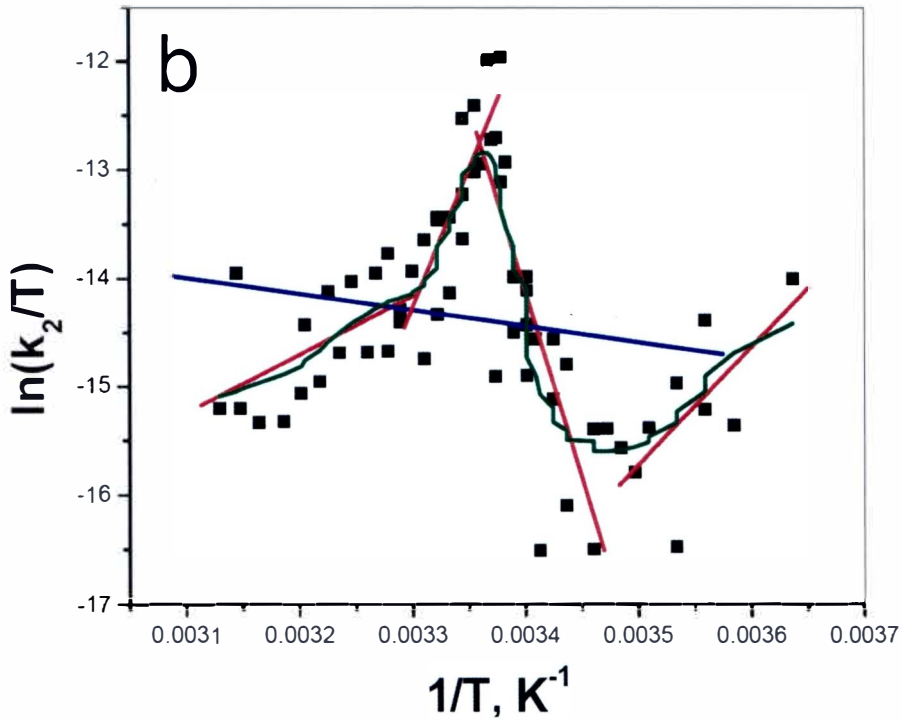

Figure 3.9. Eyring plot for dithionite fluorescence quenching of NBD-PE in DMPC vesicles for slow step.

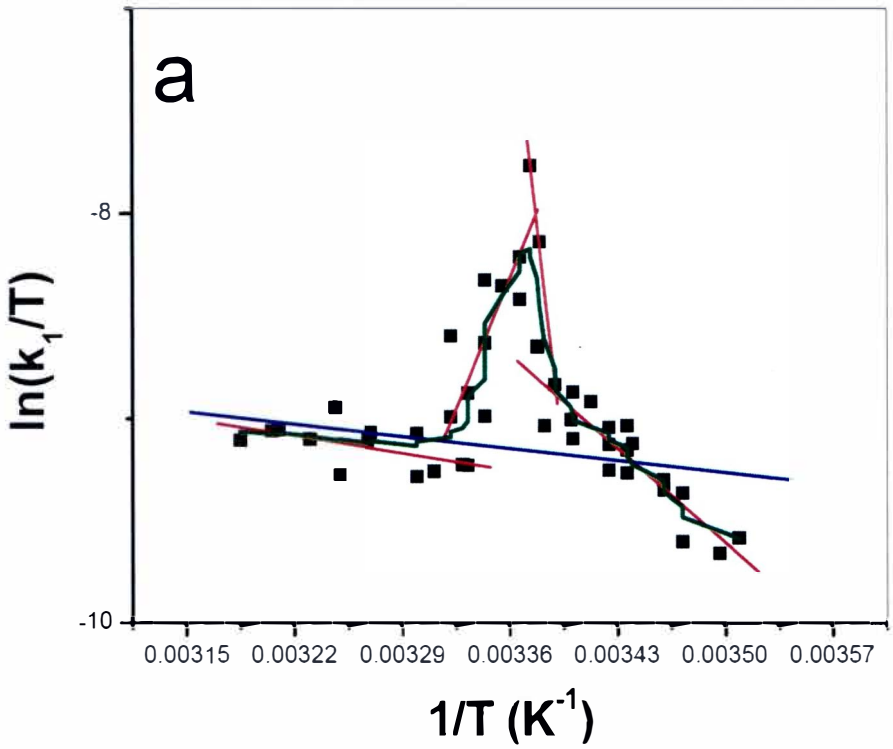

Figure 3.10. Eyring plot for dithionite fluorescence quenching of NBD-PC in DMPC vesicles for fast step.

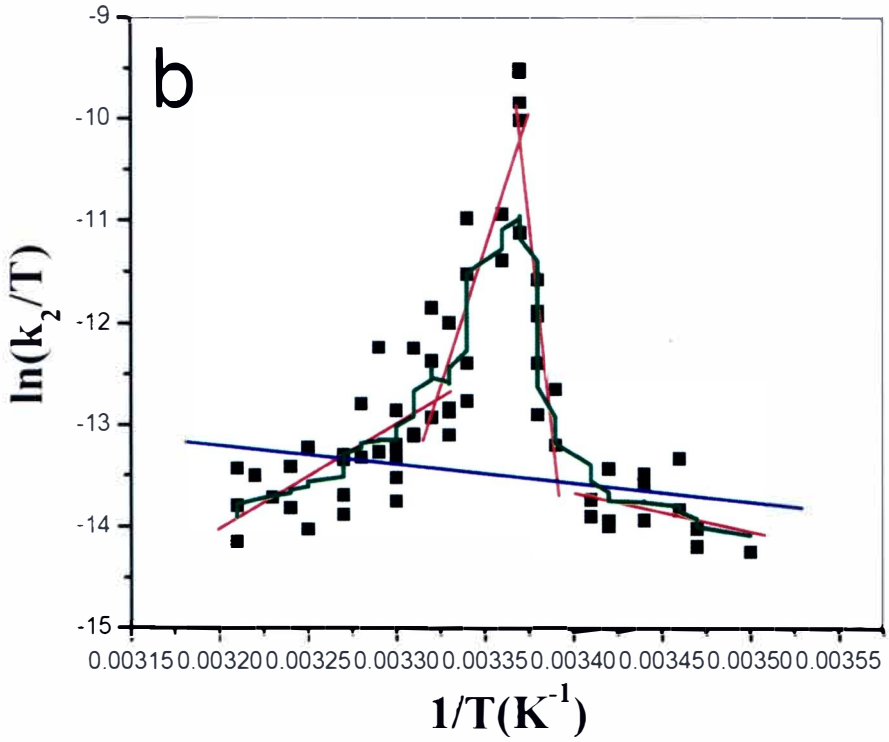

Figure 3.11. Eyring plot for dithionite fluorescence quenching of NBD-PC in DMPC vesicles for slow step.

3.7 Fluorescence Intensity and Dithionite Quenching of NBD

Dithionite quenching was followed by monitoring changes in fluorescence intensity on addition of dithionite to NBD-labeled vesicle suspensions. NBD in the outer leaflet of the vesicles that were accessible to dithionite, were converted to a nonfluorescent amino moiety as described earlier. The distribution of NBD in the bilayer region was used to determine the fraction of NBD exposed to the outer leaflet membranes.

Experiments were initiated on dithionite quenching of NBD PE and NBD PC in the gel, fluid and phase transition temperature. This experiment was used to determine the influence of temperature on fluorescence intensity as dithionite-reduced NBD moiety in the bilayer (Figure 2.17 and 2.18). In the gel phase (17 ˚C) and fluid (37 ˚C) phases for NBD PC and NBD PE, the fluorescence emission of NBD was partially quenched. By contrast, it was totally quenched at the phase transition temperature (23 ˚C) (Figure 2.17 and 2.18).

3.8 Fluorescence Lifetime Measurements

Fluorescence lifetime was used as an indicator of the local environment at which the fluorophore resides. The fluorescence lifetimes of NBD in NBD-PE and NBD-PC incorporated in the DMPC vesicles were determined on single vesicles of diameter 5 μm or larger. The lifetime measurements were made as a function of temperature in the custom-built Nikon inverted microscope system employing the time-correlated single photon counting technique. The NBD was excited at 470 nm and emitted at wavelength emission near 540 nm as described in section 2.2.6. Fluorescence lifetimes were determined from the fluorescence decays using a photon counting technology custom-built lifetime instrument (Arryx, Chicago) in the time-correlated single photon counting mode.

The NBD-PE and NBD-PE molecules were excited by directing the laser beam on to a single vesicle through the microscope objective (Figure 3.12) and the emitted photons also collected through the objective with both photons passing through a filter cube for isolation of wavelengths. A typical fluorescence decay curve for NBD-PE fitted well to a biexponential equation. The results of the decay and the associated statistical parameters used to check the goodness of the fit is illustrated in Figure 2.13. Fluorescence decays with biexponential fit equation resulted in both the short and the long lifetime components in NBD-PE and NBD-PC (Table 1).

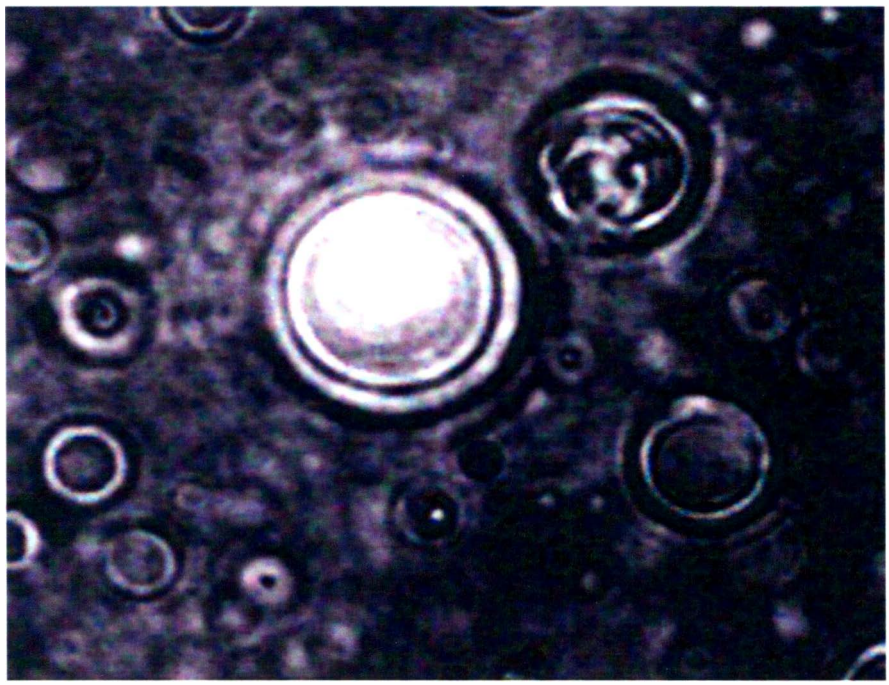

Figure 3.12. Laser beam directed on a single vesicle under microscope.

The lifetime of NBD PE at room temperature without the polarizer in place was found to be 9.71 ns for the long component that formed 67 % while the shorter component was 2.3 ns and contributed about 33 % (Table 1). Similar studies were conducted with the polarizer in place either in parallel or perpendicular position and showed long and short lifetimes of 11.4 ± 0.7 and 2.8 ± 0.2 ns. The corresponding contributions were 36 % and 63 % respectively. The measurements in the perpendicular position had only the longer component of 9.3 ± 0.1 ns.

Studies conducted with NBD PC embedded in DMPC under similar conditions, with the polarizer out of place, yielded a longer lifetime of 6.9 ± 0.5 ns and a shorter lifetime of 2.3 ± 0.2 ns and the contributions were 64 % and 36 % respectively. Experiments with the polarizer in the parallel position resulted in a value of 6.6 ± 0.5 ns and shorter component of 1.8 ± 0.3 ns with corresponding contributions of 54 % and 45 % respectively. The perpendicular position fitted well to a single exponential resulting in 7.1 ± 0.2 ns.

Table 6. Activation parameters for the dithionite reduction of NBD moiety in DMPC considering the phase transition range

Probe	Activation Parameters For the fast step			Activation Parameters For the slow step		
	Temp. range (°C)	$\Delta H^{\ddagger}$ (Kcal/mol)	$\Delta S^{\ddagger}$ (Kcal/mol)	Temp. range (°C)	$\Delta H^{\ddagger}$ (Kcal/mol)	$\Delta S^{\ddagger}$ (Kcal/mol)
NBD PE gel	0.2-21	8.7± 1.6	-31.6 ± 6.3	1-14.4	-27.6 ± 8.0	173.8 ± 50.2
NBD PE fluid	38.5-47.5	6.4 ± 4.2	41.0 ± 26.9	29.1-48.5	-10.7 ± 4.2	110.7 ± 43.4
NBD PC gel	11.1-23.7	13.0 ± 1.3	-20.6±2.6	11.9-21.1	7.6 ± 5.6	-48.4±35.6
NBD PC fluid	25.5-42.5	2.4±1.1	-57.5±27.5	27.3-39.5	-20.5±4.6	140.7±31.4
NBD PE phase 1	18.5-28.2	-47.0±7.3	221.4±32.0	15.2-24.6	68.3±12.1	157.0±27
NBD PE phase 2	24.6-36.6	35.7±5.2	54.9±7.8	22.9-30.9	50.7±10.2	-242.8±48.9
NBD PC phase 1	22-23.7	132.7±6.1	384.0±20.7	22-23.7	317.0±51.3	999.9±160
NBD PC phase 2	22.9-28.2	-36.1±6.0	185.2±31.1	23.7-28.2	106.0±16.3	424.7±65.8

The temperature-dependence studies for the two probes without the polarizer in place showed a decrease in fluorescence lifetime with increasing temperature. The temperature range for NBD PC was from 8 to 36 °C while NBD PE range was from 7 to 39 °C (Tables 7 and 8.). The fitting was deemed acceptable with a minimum chi-square value of 1.40.

Table 7. Lifetimes of NBD PC in DMPC in a series of temperatures (Polarizer out of position)

Temp. (°C)	τ1	Contrib. (%)	τ2	Contrib. (%)	χ2
8	8.4	71	2.7	29	1.11
15	7.8	58	2.6	42	1.36
19	7.5	63	2.6	37	1.28
23	7.1	62	2.3	38	1.32
28	6.5	63	2.1	37	1.25
32	5.9	62	1.9	38	1.31
36	5.4	68	1.7	32	1.20
38	5.2	70	1.7	30	1.20

Table 8. Lifetimes of NBD PE in DMPC in a series of temperatures (Polarizer out of position)

Temp. (˚C)	τ1	Contrib. (%)	τ2	Contrib. (%)	χ2
7	10.9	67	3.2	33	1.11
14	10.7	65	3.2	35	1.11
19	10.5	60	3.1	40	1.21
23	10.1	64	2.6	36	1.19
27	9.3	64	2.3	36	1.20
30	8.5	64	2	36	1.24
36	8	68	1.8	32	1.12
39	7.4	65	1.9	35	1.30

The temperature-dependent fluorescence lifetimes in a single vesicle done under microscopy conditions showed a linear dependence for both NBD PE and NBD PC. Similar studies conducted in ensemble dilute conditions under Edinburgh instruments followed a similar trend (Figure 3.13 and 3.14.) Under Edinburgh instruments conditions, in the gel and around the phase transition of DMPC, the diluted sample showed a relatively higher lifetime values than the undiluted vesicles. Edinburgh instrument data was successful with a single exponential. A similar decrease in fluorescence lifetimes with increasing temperatures was observed.

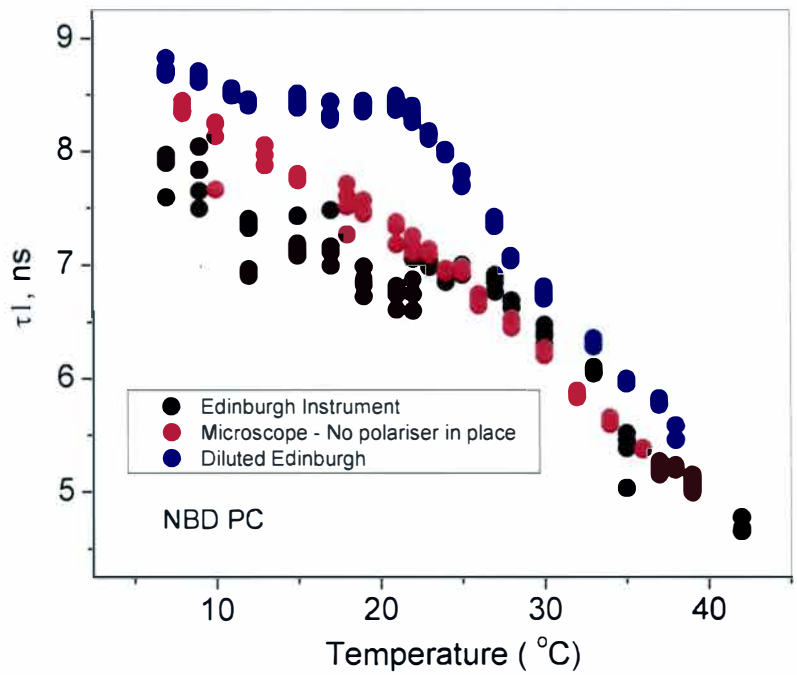

Figure 3.13. Fluorescence lifetime of NBD PC determined in microscope and Edinburgh conditions in DMPC in a series of temperatures..

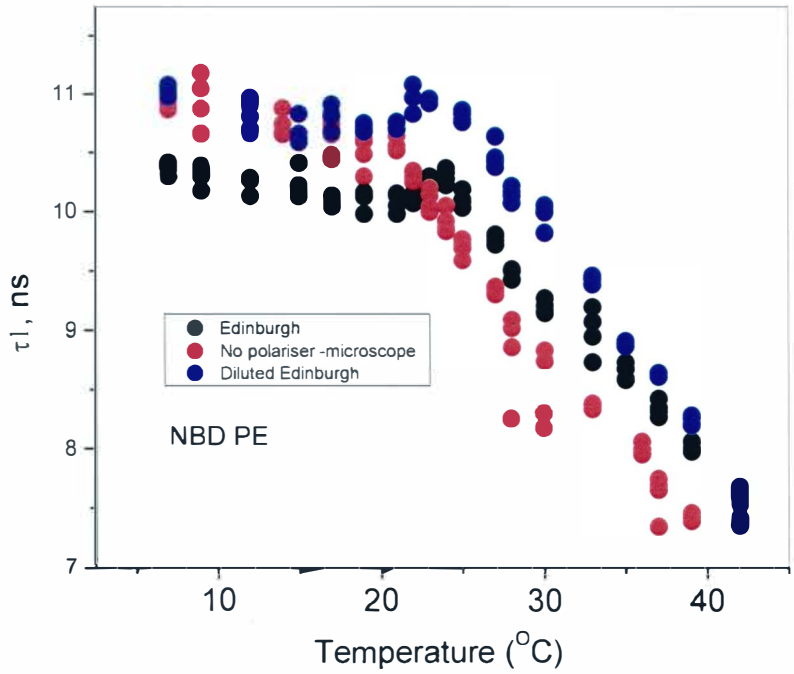

Figure 3.14. Fluorescence lifetime of NBD PE determined in microscope and Edinburgh conditions in DMPC in a series of temperatures..

3.9 Fluorescence Time-Correlated Anisotropy

The fluorescence anisotropy decays were measured with the single photon counting technique. The decay of the anisotropy was assumed to be single exponential. Decay of polarized fluorescent light of the fluorescent probes, NBD PE and NBD PC was measured at various temperatures. The anisotropy measurements under time-resolved mode showed a linear relationship with temperature. The anisotropy data was determined by fixing the values of the lifetime that were obtained without the polarizer in position. Table 9 shows a summary of anisotropy with the values of lifetime obtained at 25 °C. The anisotropy for NBD PC is almost twice in magnitude compared to NBD PE in

DMPC vesicles. The anisotropy decreased with increase in temperature as expected. NBD PE in DMPC showed a distinct transition around the phase transition of DMPC. On the other hand, the anisotropy values for NBD PC in the same region gave a linear temperature-dependence (Figures 3.15 and 3.16). NBD PE anisotropy values were less sensitive to increases in temperature beyond the phase transition of DMPC vesicles. The anisotropy values for NBD PE in the temperature range between 7 and 37 °C were from 4.6 to 1.5 ns respectively. NBD PC in the temperature range between 5 to 38 °C showed anisotropy value between 4.2 and 1.8 ns. The change in NBD PC was larger than in NBD PE over the temperature range compared.

Table 9. Fluorescence lifetime (τ) and anisotropy with corresponding fitting parameters. Measurements were taken at 25 ˚C with polarizer in position. Φ is time-correlated anisotropy and G-factor is the correction for sensitivity of measurement for perpendicular and parallel position.

Temp. (˚C)	τ1	Contrib. (%)	τ2	Contrib. (%)	ϕ	G-factor
NBD PE	9.7 ± 0.1	70	2.3 ± 0.1	30	1.6 ± 0.3	1.1 ± 0.1
NBD PC	6.9 ± 0.1	48	2.2 ± 0.1	52	2.9 ± 0.1	1.0 ± 0.1

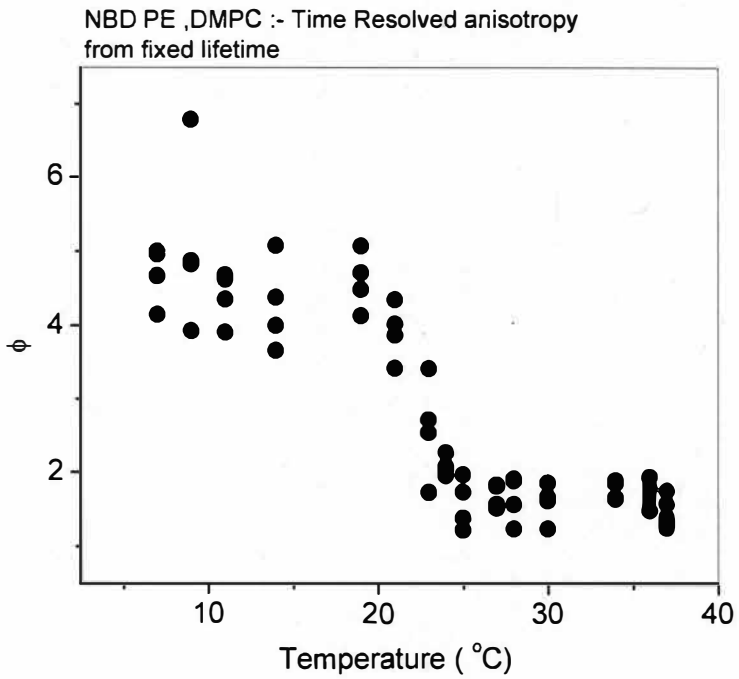

Figure 3.15. Fluorescence time correlated anisotropy of NBD PE measured in a series of temperatures. The anisotropy was recalculated with fixed lifetimes.

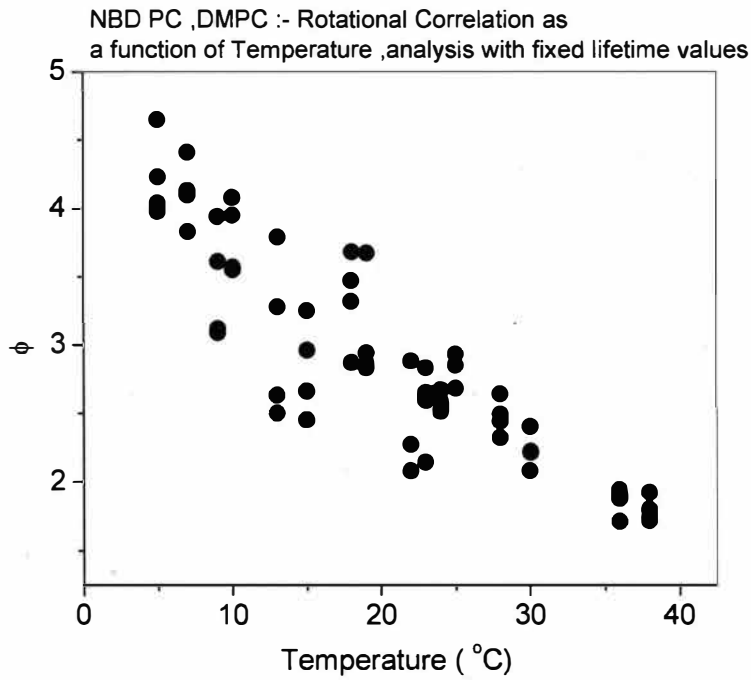

Figure 3.16. Fluorescence time correlated anisotropy of NBD PC measured in a series of temperatures. The anisotropy was recalculated with fixed lifetimes.

3. 10 Stern-Volmer Plots

The change in accessibility of the NBD and to dithionite quencher was investigated by fluorescence emission measurements at fixed wavelength in the absence and presence of dithionite quencher. The degree of quenching was analyzed using the Stern-Volmer law that describes the steady-state collision quenching (Equation 2.4) [81]. The bimolecular rate constant K_Q determines the accessibility of the fluorophore to the quencher. The nature of bimolecular interactions was used to determine the dynamic properties of the DMPC vesicles. Analysis of state emission can be used to determine information on the

permeability of the lipid water interface to the quencher. In Stern Volmer plots the quenching efficiency can be related to the quencher concentration.

The Stern-Volmer plots for the steady state fluorescence quenching study showed a linear dependence of quenching on concentration of dithionite at low concentrations (Figure 3.17 (a) and (b)). In contrast, a deviation from linear dependence was observed at higher concentration of dithionite. A double reciprocal plot of change in intensity and dithionite concentration was linear relationship (Figures 3.18 (a) and (b)).

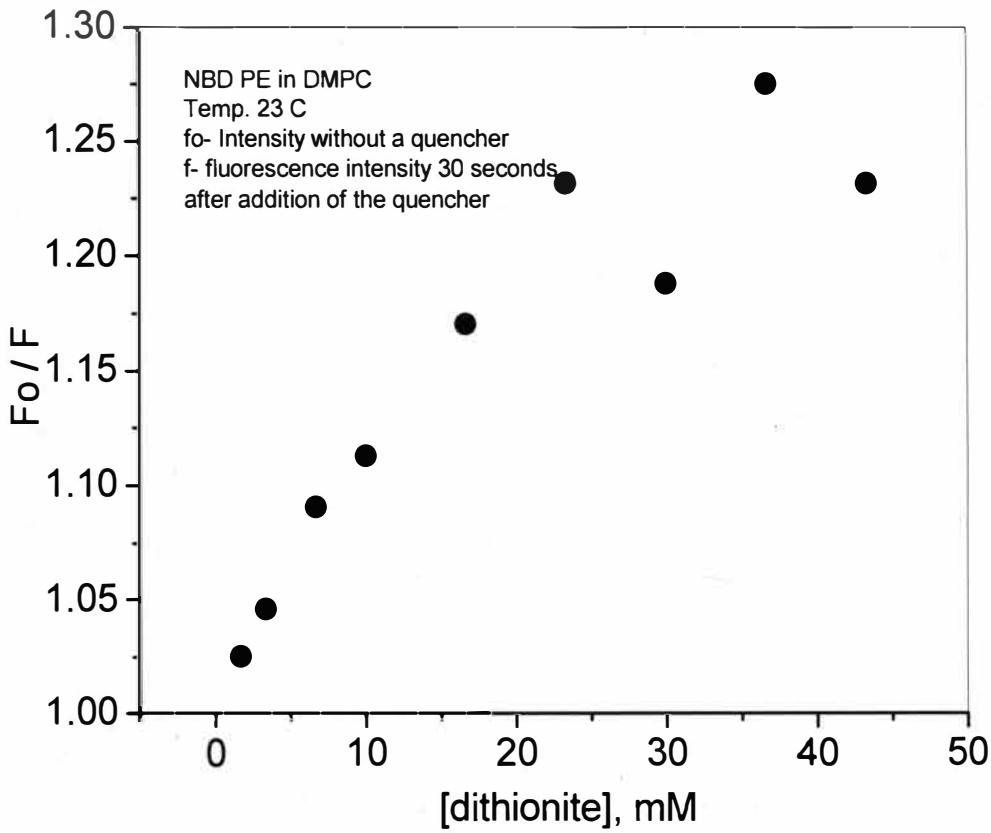

Figure 3.17(a). Direct Stern-Volmer plot for dithionite reduction of NBD PE.

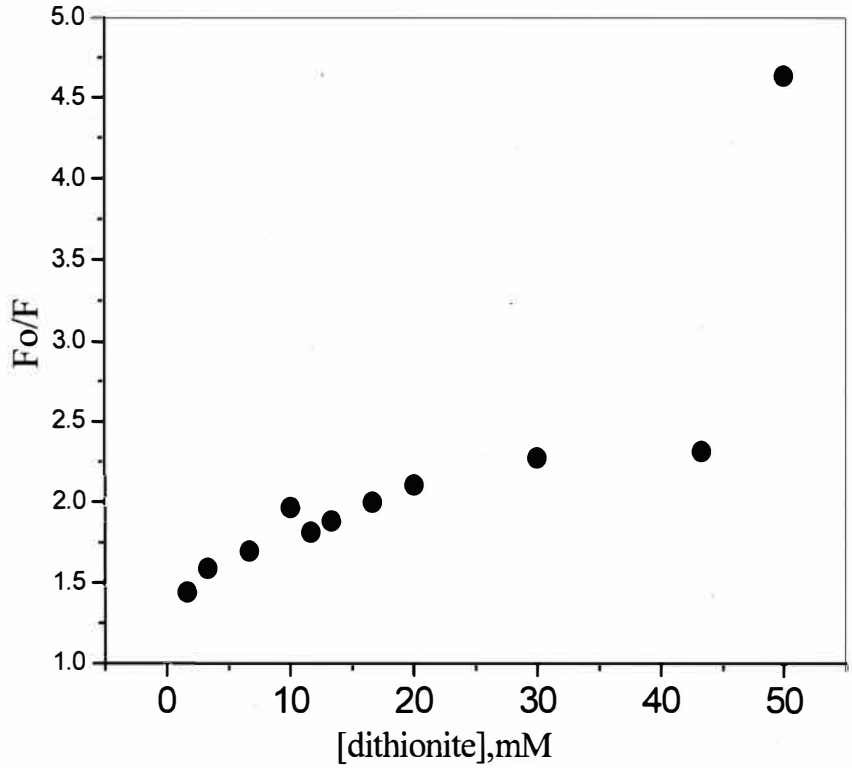

Figure 3.17 (b). Direct Stern-Volmer plot for dithionite reduction NBD PC in DMPC.

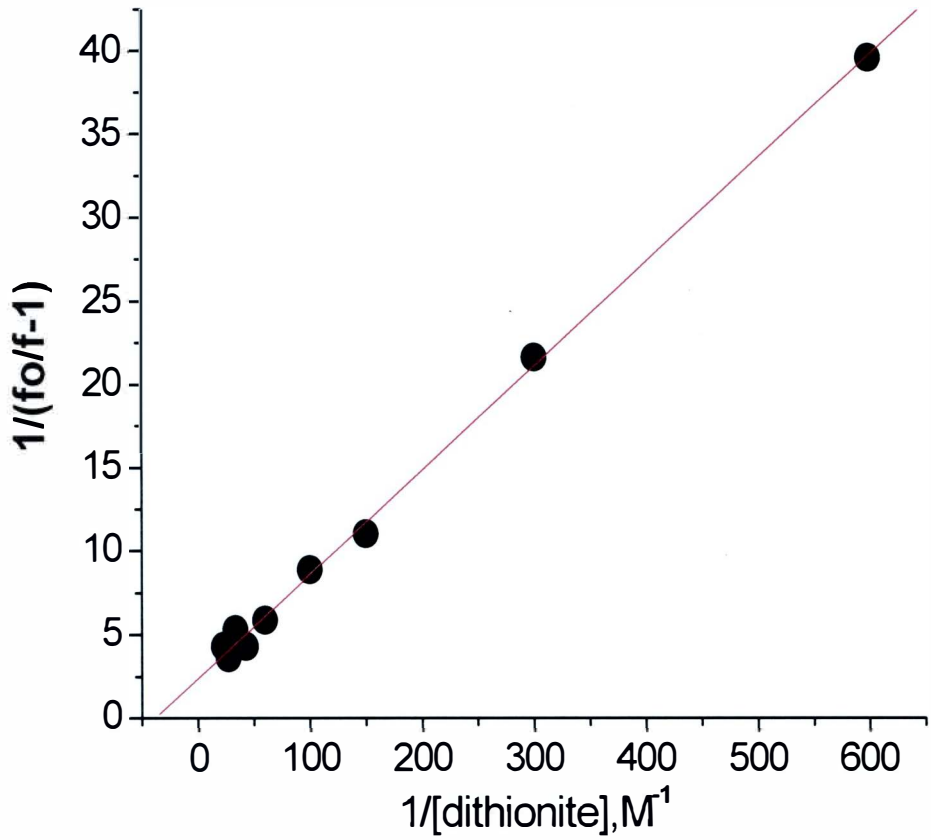

Figure 3.18(a). Modified Stern-Volmer plot for dithionite reduction of NBD PE at 23 °C.

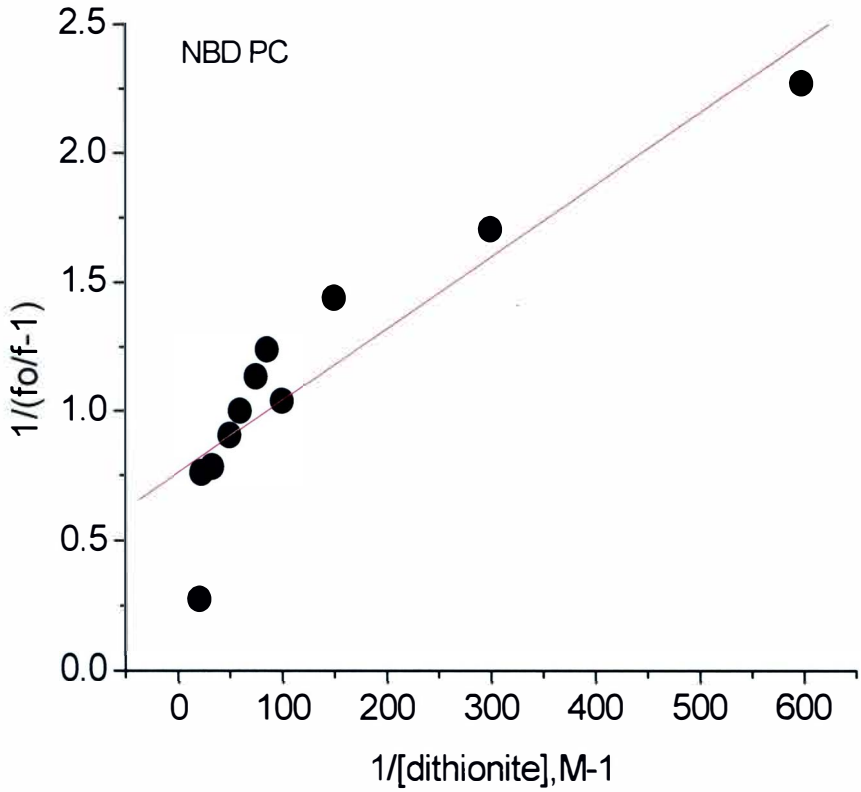

Figure 3.18 (b). Modified Stern-Volmer plot for dithionite reduction of NBD PC at 23 °C.

The Stern-Volmer plots deviation from linearity can be attributed to complex formation. A typical quenching process goes through complex formation in which there is an inaccessible population of fluorophores. The linear dependence in a double reciprocal plot is characteristic of a static quenching mechanism that is related to binding.

3.11 Dihydrocholesterol in DMPC Bilayer

We included dihydrocholesterol to investigate DMPC bilayer in the presence of a sterol. The behavior of NBD PE and NBD PC in DMPC bilayer was investigated in the presence of dihydrocholesterol of varied concentrations. The dynamics of the DMPC bilayer was studied by varying the dihydrocholesterol content and monitoring changes using fluorescence steady-state anisotropy, dithionite quenching and microscopy techniques.

Dihydrocholesterol has three well defined regions: a small polar hydroxyl group, a rigid plate like steroid ring and an alkyl chain 'tail' (Figure 2.3). It has a tendency to influence membrane permeability of small molecules. The influence of the probes on the DMPC bilayer, in the presence of dihydrocholesterol, was determined using temperature-dependent studies of steady-state fluorescence anisotropy and dithionite quenching kinetics.

Dihydrocholesterol was added at concentrations ranging between 0 and 60 % (mol/mol) in the DMPC bilayer at a fixed total lipid concentration of 4 mg/ml in 11 mM magnesium chloride. This was studied in a series of temperatures. The dihydrocholesterol structure is well compatible with the phosphatidylcholines since it has both the hydrophilic head group formed by the hydroxyl moiety and a tail consisting of the short acyl chain attached to the steroid ring. The exact location of cholesterol in the membrane is well established and the steroid

structure is not expelled from the membrane during the gel to fluid phase transition [105].

Dihydrocholesterol is a hydrogenated form of cholesterol (see Figure 2.3). It was preferred to pure cholesterol since it is less prone to air and photo-oxidation. Therefore, presents fewer artifacts that can possibly add to the results. Dihydrocholesterol has little effect on the phase behavior of the lipid in which it is embedded. A typical curve for percentage quenching was reported for NBD PC (Figure 3.19). It is clear from the plot that the percentage of NBD quenched in the presence of dihydrocholesterol was higher around the phase transition. In this plot, the amount of NBD quenched remains nearly constant with temperature with increasing dihydrocholesterol concentration. A relatively sharp transition was observed for dihydrocholesterol content below 10 %. Meanwhile at 25 % dihydrocholesterol the amount of NBD reduced remained nearly independent of temperature which changes dramatically with 30 % dihydrocholesterol. This could be attributed to changes in the environment of the probe as a result of dihydrocholesterol concentration.

The steady state fluorescence anisotropy (Figure 3.21) showed that the sharpness of transition is diminished beyond 10 % dihydrocholesterol for NBD PC and 30 % for NBD PE.

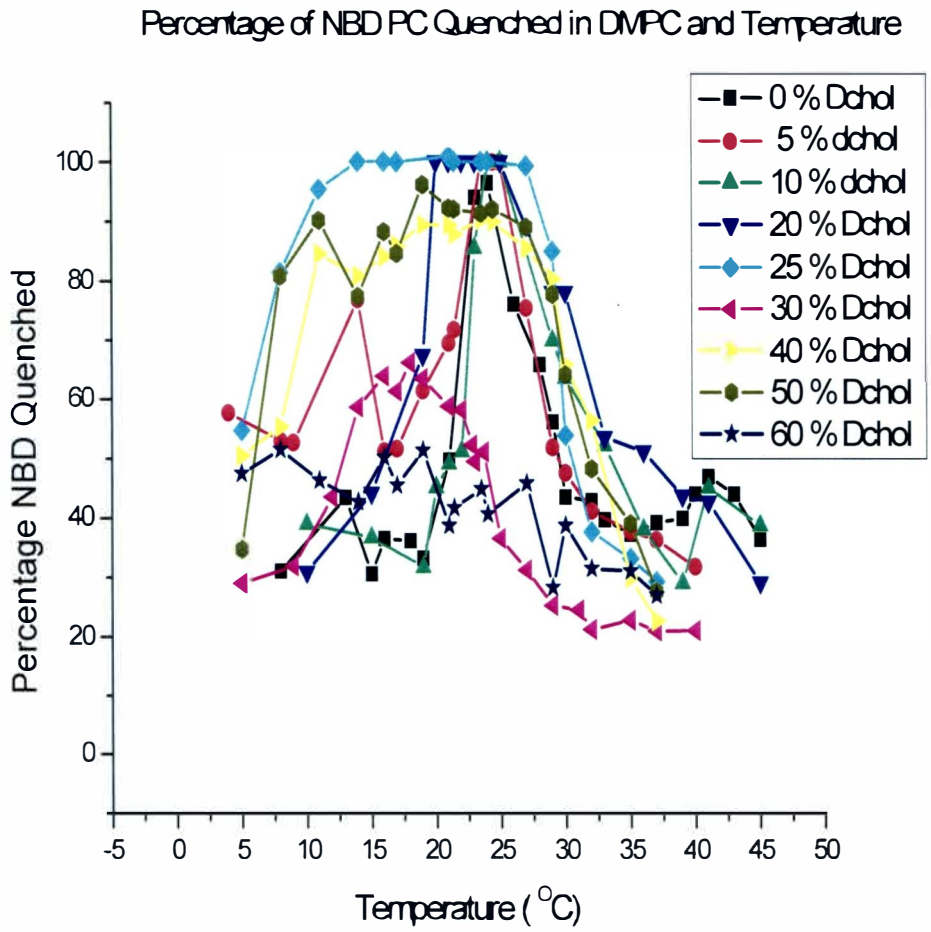

Figure 3.19. Percentage of NBD PC quenched in DMPC with variable dihydrocholesterol content.

Figures 3.20(a) and (b)) show display Eyring plot of some selected dihydrocholesterol concentrations. 5 % dihydrocholesterol content for NBD PC was relatively well defined. A strong peak develops around the phase transition for 5 % dihydrocholesterol concentration and below. The effect was more pronounced in NBD PC that NBD PE. With increasing dihydrocholesterol content, the peak becomes broader. It is established that low cholesterol

concentrations decreases the surface tension between the gel and fluid domains, thus promoting domain formation and decreasing the cooperativity of the transition [106].

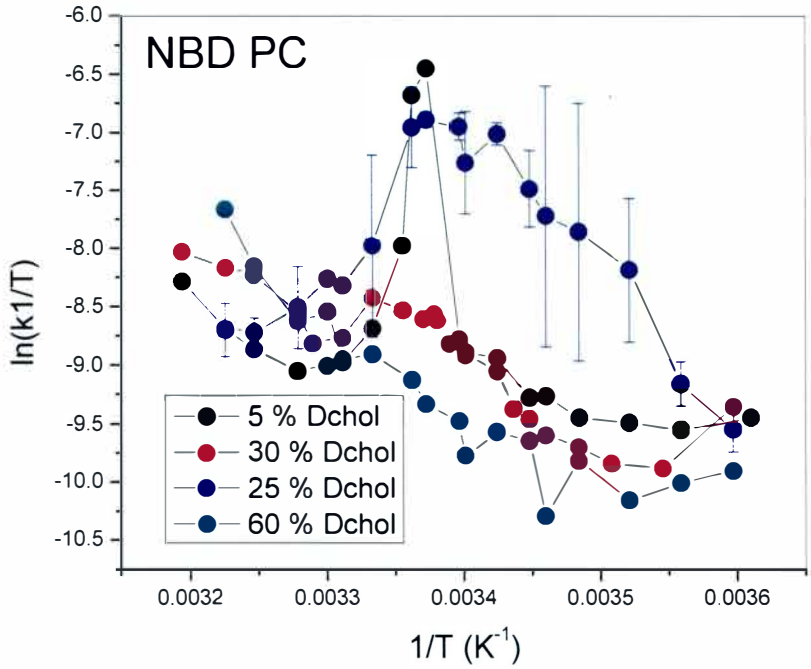

Figure 3.20 (a). Eyring plot for dithionite quenching of NBD PC in DMPC with variable dihydrocholesterol concentration.

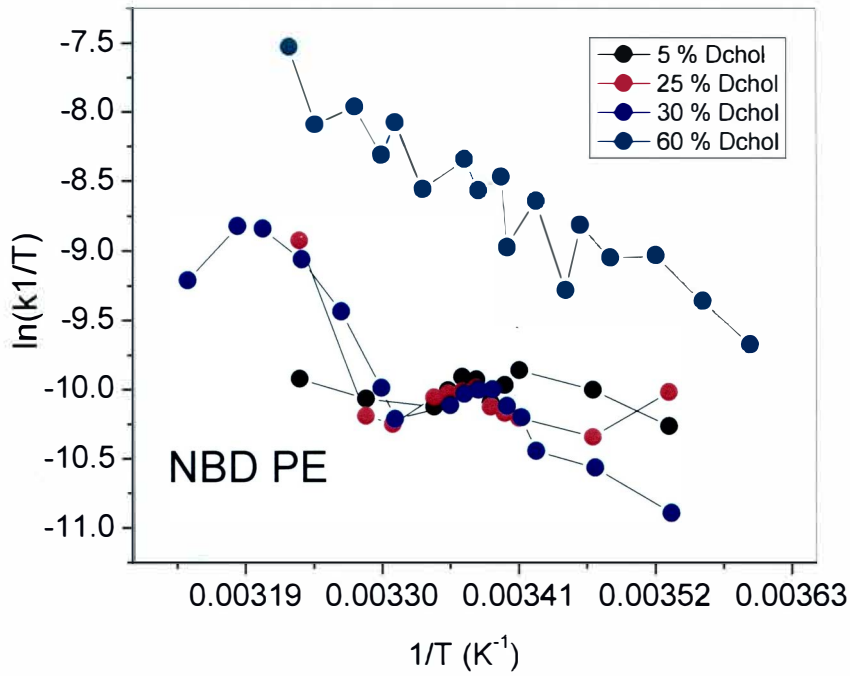

Figure 3.20 (b). Eyring plot for dithionite quenching of NBD PE in DMPC with variable dihyocholesterol concentration.

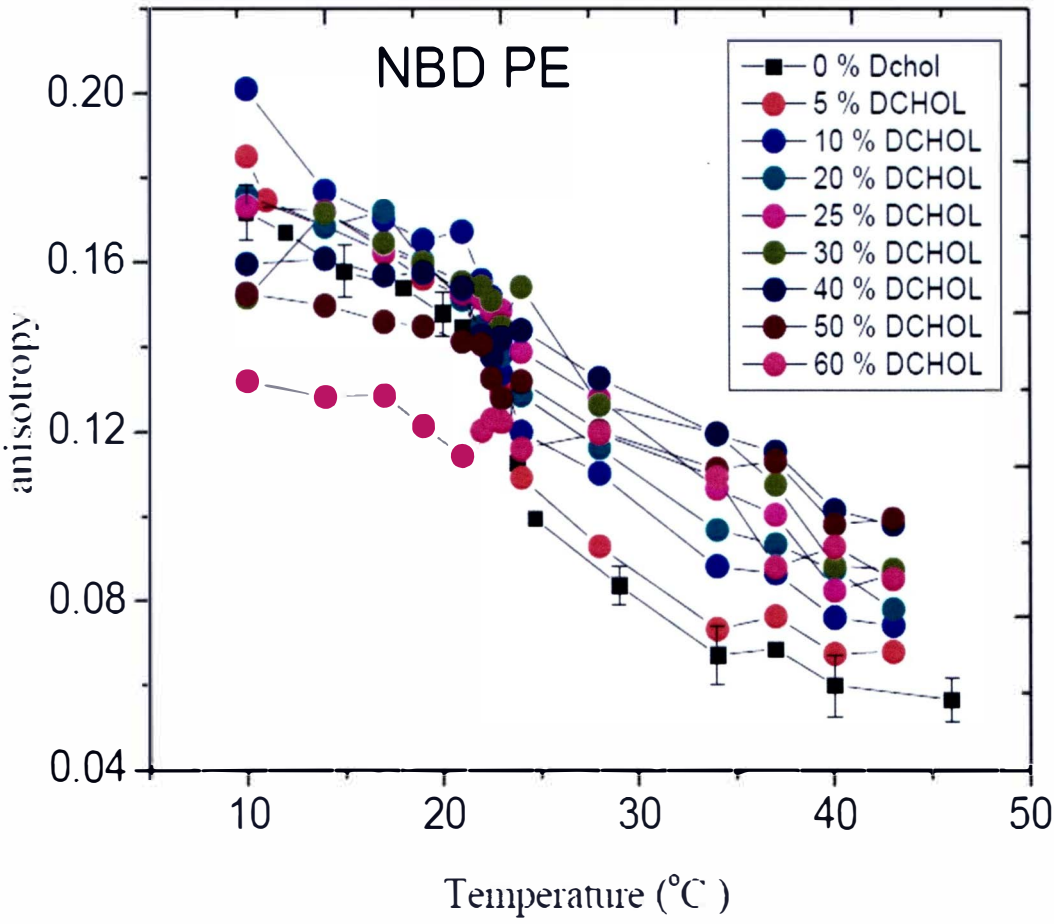

Figure 3.21(a) Fluorescence steady state anisotropy of NBD PE in DMPC with dihydrocholesterol.

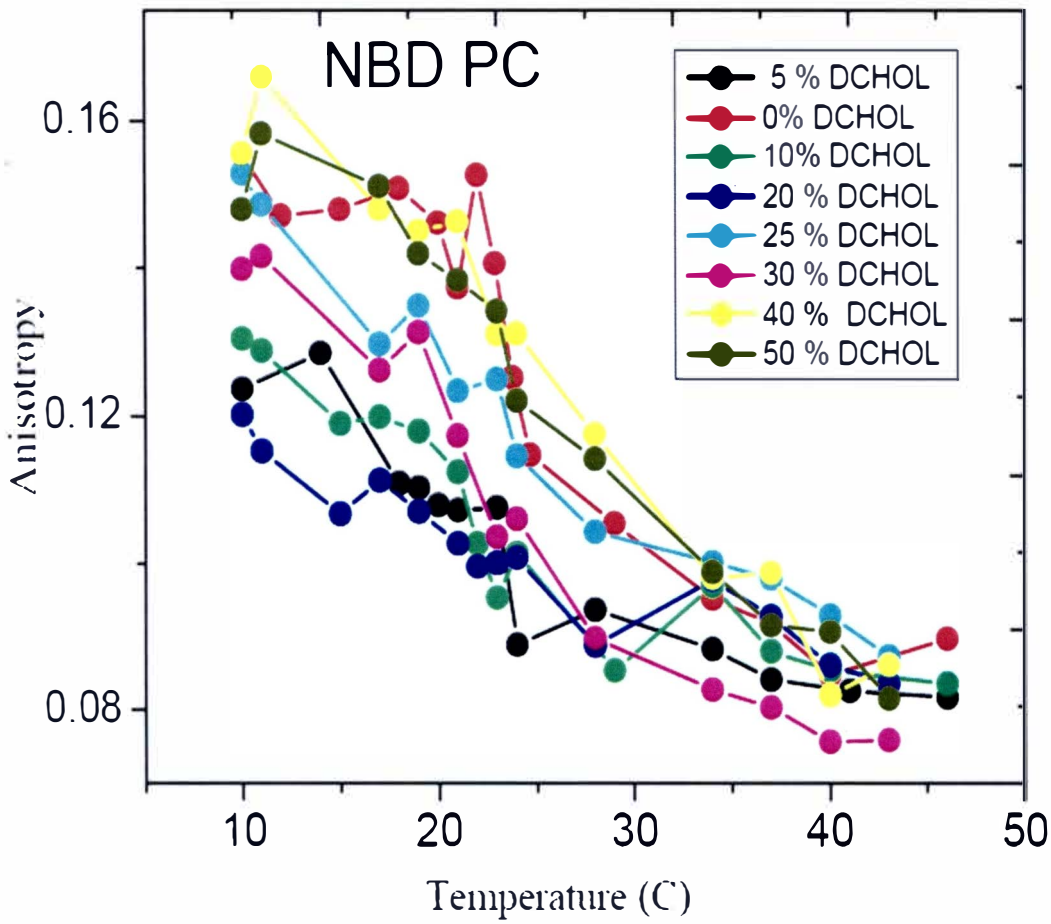

Figure 3.21(b). Fluorescence steady state anisotropy of NBD PC in DMPC with dihydrocholesterol.

Figures 3.21(a) and (b) show steady state anisotropy of NBD PE and NBD PC respectively. The anisotropy was plotted as a function of temperature over the range of concentration employed that varied from 0 to 60 % (mol/mol.) The figures show decreasing anisotropy with increasing temperature. Fluorescence

anisotropy can be correlated to the rotational diffusion rate of probes embedded in the lipid bilayer, which are sensitive to the packing of the fatty acyl chain and sterol. The decreasing anisotropy therefore means that the bilayer region becomes disordered with increase in temperature. Figure 3.22 shows a plot of anisotropy as a function of dihydrocholesterol concentration. There is relatively large increase in anisotropy up to 40 % dihydrocholesterol at the phase transition of DMPC and fluid phase. However the gel phase (10 °C) showed a large decrease in fluorescence anisotropy for NBD PE probe embedded in DMPC bilayer. NBD PC was inconsistent over range of concentrations of dihydrocholesterol used (Figure 3.22). Here, the general trend obtained from the plot is that the anisotropy increases over range of the temperature measured.

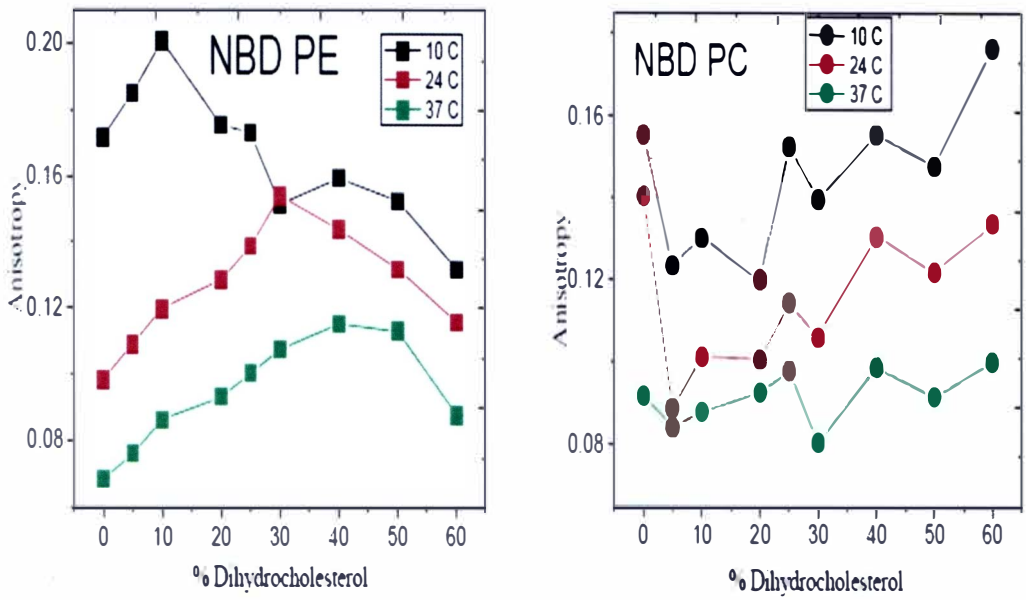

Figure 3.22. Steady state fluorescence anisotropy of NBD PE and NBD PC in DMPC with variable dihydrocholesterol concentration.

CHAPTER 4

DISCUSSIONS

4. 1 DMPC Vesicles Formed From Modified Rapid Evaporation Method

To facilitate proper understanding of the bilayer region of DMPC vesicles, NBD PE and NBD PC probes were used to study the interface and the hydrocarbon region respectively via microscopy, steady state and time-resolved fluorescence. To begin the procedure, the DMPC phospholipids that display phase transition at room temperature were determined, such that the gel and fluid phases could be investigated in one single lipid as opposed to binary or ternary mixtures.

Single lipid components such as DMPC, in the presence of high water content exist in the gel, ripple and liquid crystalline (fluid) phases, driven by temperature. The gel and fluid phases have characteristic lipid acyl chain configuration [39]. The phases can be altered dramatically by cholesterol-phospholipid mixture and thus we require new definition based upon order of the membrane. We investigated this behavior by adding variable concentrations of dihydrocholesterol to DMPC lipid bilayer.

Perturbation of the lipid bilayer in the presence of membrane embedded probes can influence the fluorescence emission intensity. To gain further insights into this effect, we assessed the dynamical behavior of NBD PE and NBD PC on

DMPC by external addition of the probes to preformed vesicles. Both probes were easily incorporated into the DMPC bilayer at all temperatures used in the experiment (Figure 3.4). The NBD PE was less affected by temperature and by analog-dependent perturbation of the lipid bilayer organization. Growth in fluorescence intensity for NBD PE showed that this probe is less incorporated in the bilayer than NBD PC. The rapid increase in fluorescence in NBD PC over the entire range of the temperature employed is an indication the fluorescent analog is well incorporated in the bilayer. Since the NBD is located in the fatty acyl chain of the lipid, the lipid bilayer is more likely to be perturbed as a result of locating a more polar group in the nonpolar environment. Indeed, this was reflected at temperature corresponding to the phase transition of DMPC which had a remarkable distinction from the rest of the temperatures. Membrane perturbations by fluorescent analogs were investigated by Muller et al [93]. They reported the location and dynamics of NBD covalently attached to short (C6) or long (C12) acyl chain of phosphatidylcholine molecule using ^{2}H NMR and fluorescence spectroscopy. The long acyl chain had NBD preferentially located in the lipid-water interface and attributed to looping back of the acyl chain as first reported by Chattopadhyay [107].

Mechanisms of vesicle formation have been proposed and factors affecting the stability of such processes established. The quality of vesicle preparation is judged by the size distribution and lamellarity. Lipids self- assemble in water or

in buffer solution which can result in small, large or giant unilamellar vesicles and variable distribution.

To explore the structure of the bilayer, first a procedure was developed that resulted in a rapid and efficient means of producing giant unilamellar vesicles. Rapid evaporation method is usually efficient and quick methods that generate vesicles within a short time to allow encapsulation of labile materials such as proteins [103, 104]. Vesicles formation occurs in dilute concentration of lipids dissolved in chloroform and methanol mixture to solubilize lipids that come in chloroform.

A 4 mg/ml total lipid in 11 mM magnesium chloride was used to generate vesicles from DMPC lipids that were dissolved in chloroform and methanol mixture in the ratio of 2:1. The concentration was optimized after a series of trials and giant vesicles were produced from DMPC. The rapid evaporation method yielded giant vesicles of DMPC that were observed under optical microscope. Figure 2.15 showed generation of giant unilamellar vesicles of variable sizes from DMPC phospholipids, using 11 mM magnesium chloride solution as an aqueous medium.

The application of that technique generated vesicles ranging from a nanometer to microns in diameter. Nanometer sizes were analyzed by dynamic light scattering studies on QELs and were found to be more polydisperse (Figure 3.0). Furthermore, the micron sizes were characterized in optical microscope based on

brightfield, fluorescence and phase contrast modes of microscopy techniques. The resulting fluorescence images showed the presence of NBD dye in the bilayer region, causing an intense fluorescence due to its high quantum yield in lipids vesicles (Figure 3.2). Phase contrast screening showed that the vesicles were unilamellar (Figure 3.1). The 11 mM Magnesium chloride solution was expected to produce giant vesicles since this concentration was normal, as warranted by physiological conditions. The role of divalent metals in lipid vesicle formation has been established. Divalent metal cations promote vesicle formation from electrically neutral phosphatidylcholines [108]. The Mg^{2+} introduced net positive charge which leads to the repulsion of individual vesicles formed and spontaneous fusion of vesicles.

In our procedure, vesicles were formed at 65 ˚C above the phase transition of DMPC and gradually cooled to room temperature and thereafter measurements were made. The vesicles exhibited a dynamic behavior that could be influenced by temperature. Previous studies have shown that the effect of temperature on the kinetic rate constant of aggregation and fusion of phosphotidylserine were directly correlated [109]. They showed that the rate constant of aggregation had a direct relationship with temperature. Temperature has been proved to provide the force required to drive the vesicle assembly that occurs successfully above the phase transition temperature.

4. 2 Probes Embedded in DMPC Bilayer

To provide a deeper understanding of dynamical properties of the DMPC bilayer, lipophilic fluorescent probes were incorporated to the bilayer in extremely low concentrations (1 dye molecule to 200 molecules of DMPC) to avoid the introduction of artifacts in the main lipid by these probes. We determine the spectrum of NBD in organic solvent, 11 mM magnesium chloride and in vesicles. The result gave fluorescent intensity that was dependent on the dielectric constant value of the medium under investigation. The properties of NBD PE are known. Shaw and his group reported a direct relationship between the fluorescence emission and dielectric constant or the micro environment of the fluorophore. It was noted that the polar head groups, NBD, being in proximity, existed in unstable configuration re-orientated towards the solvent as the solvent dielectric constant was increased [110].

NBD is widely used as a fluorescent probe in biological systems [92]. The UV-Vis spectrum (Figure 2.8) showed three strong absorption maxima peaks at 250, 340 and 470 nm measured in both chloroform and methanol. The NBD embedded in DMPC in 11 mM magnesium chloride exhibited two signal maximum at 340 nm and 470 nm. The shorter wavelength band at 340 nm is attributed to the π- π^* transition while the longer wavelength band absorption peak at 470 nm is as a result of a charge-transfer transition. The excitation and emission wavelengths measured with the dye embedded in DMPC bilayer, employing a 5 nm slit widths, for both cases, showed strong signals at 481 and 535 nm respectively (Figure 2.6).

Fluorescence emission intensity diminished with the increase in temperature (Figure 2.7) as a result of increased nonradiative processes.

4. 3 Steady State Fluorescence Anisotropy

The studies conducted on fluorescence anisotropy and quenching were performed with all size ranges of vesicles that were made from the procedure as described earlier. Steady-state fluorescence anisotropy of vesicles labeled with either NBD PE or NBD PC was studied as a function of temperature and anisotropy value calculated using equation 2.3. The plot of anisotropy as a function of temperature for NBD PE and NBD PC are displayed in Figure 3.6.

The decrease in anisotropy for both NBD PE and NBD PC can be attributed to the changes in orientation that becomes more random with increasing temperature. In DMPC, as the temperature was increased from 10 to 45 ˚C, the lipid bilayer underwent a transition from the gel to the fluid phase in a well defined phase transition temperature region of 23 to 24^{o}C. This phase transition temperature region in DMPC was clearly demonstrated by NBD PE and NBD PC. A derivative plot displayed in Figure 3.7 indicates a sharp dip at this phase transition temperature region. The decrease in the anisotropy for NBD-PE in the temperature range between 10 to 46 ˚C was larger (0.1) than for NBD-PC (0.06). We can rationalize the differences based on the recent report by Chattopadhyay and his group [111]. The higher values of change in anisotropy in the case of the NBD PE could be due to the exact location of the probe in the DMPC bilayer so

that the change is reflective of change in membrane packing induced by the phase transition. The small change for the NBD PC case could be attributed to the change in location (looping up) when DMPC undergoes a phase transition. In other words the change in membrane packing as a result of the phase transition would be counteracted by the change in anisotropy induced by the looping up of the acyl chain.

The NBD of NBD-PE is be expected to have a greater rotational degree of freedom compared to that of NBD-PC, as NBD-PE is present at the bilayer-aqueous interface in the outer and inner leaflets while NBD-PC resides hydrocarbon region of the bilayer. The greater rotational degree of freedom for NBD-PE compared to NBD-PC leads to a change of almost a factor of two in its fluorescence anisotropy with temperature compared to NBD-PC. The sudden drop in fluorescence anisotropy at the phase transition temperature maybe explained on the basis of sudden increase in bilayer polarity as a result of gel fluid coexistence [112].

4. 4 Kinetics of Quenching of NBD-PE and NBD-PC with Dithionite

A detailed investigation of the quenching of the fluorescence of NBD-PE and NBD-PC by dithionite at various temperatures was conducted as detailed in section 2.2.11. Typical examples of the quenching of NBD-PE and NBD-PC in the gel (10°C) and fluid (37°C) phases and the transition (23°C) temperature are displayed in Figure 2.17 and 2.18 respectively. The fluorescence of the NBD

moiety is only partially quenched at 10°C and 37°C. However, this becomes totally quenched at the phase transition of DMPC (23°C). The complete quenching of the fluorescence of NBD in NBD-PE and NBD-PC at the phase transition temperature is similar to the large decrease in fluorescence anisotropy of NBD at this temperature (Figure 3.6). The percentage of NBD in NBD-PE and NBD-PC quenched as a function of temperature is displayed in Figure 3.3. A similar pattern is exhibited in the extent of its quenching, which increases near the phase transition temperature, reaching a maximum at the transition temperature. The dithionite quenches the readily accessible NBD groups on the surface of the vesicle in NBD-PE, while in NBD PC those groups bent towards the outer leaflet become easily accessible and hence get reduced first.

Dithionite quenching was a two step reaction displayed as shown in Figure 2.19. The rapid step is due to the immediate quenching of readily accessible NBD as explained above. The slow step in the quenching kinetics corresponds to the transmembrane migration of the NBD lipids in the inner leaflets that migrate to the outer leaflet due to the concentration gradient resulting from the reduction of the NBD moiety in the outer leaflet. The transmembrane migration rate increases by a factor of 10 at the phase transition temperature 23°C which accounts for the almost complete quenching of the fluorescence at this temperature. The kinetic of these two processes was treated as a sum of two exponentials displayed in equation 2.1.

The kinetics of the fluorescence quenching of NBD by dithionite was studied under excess dithionite such that the reactions were pseudo first-order in NBD concentration. The fluorescence quenching of NBD by dithionite proceeds through a rapid pre-equilibrium association of dithionite with NBD followed by electron transfer in the slow step. The mechanism of fluorescence quenching was proposed and treated according to equation 4.0. The kinetic rate constants were obtained from the double-exponential fit of the decay curve shown in Figure 2.19 and treated as pseudo first-order rate constant k with NBD being the limiting reagent.

$$NBD + N_2S_2O_4 \overset{K}{\rightleftharpoons} [NBD.....S_2O_4^{2-}] \rightarrow ABD \qquad (4.0)$$

$$\frac{d[ABD]}{dt} = \left\{ \frac{kK[S_2O_4^{2-}]}{1+K[S_2O_4^{2-}]} \right\} [NBD] \qquad (4.1)$$

The double-exponential kinetic treatment resulted in two pseudo first-order rate constants, the fast step k_1 and the slow step by k_2 which corresponded to the immediate quenching and the migration of the inner leaflet NBD respectively. The observed pseudo first-order rate constants had two limiting values Kk $[SO_4^{2-}]$ at low dithionite concentrations and k at higher dithionite concentration as predicted in equation 4.1.

To gain a deeper understanding of the quenching kinetics of NBD embedded in the DMPC bilayer, concentration dependent studies were initiated at different temperatures that correspond to the phases of DMPC lipids. Typical results were shown as Stern-Volmer plots displayed in Figure 3.13. The study confirmed a linear relationship between quenching and dithionite concentration at low concentrations, which is characteristic of binding processes in biochemical reactions.

4. 4.1 Pre-equilibrium Constant

The experimental pseudo first-order rate constant given in equation 2 contains the pre-equilibrium constant K and the reduction rate constant k. The pseudo first-order rate constants were determined in the dithionite concentration range between 1 to 50 mM at the temperatures 10°C, 23°C, and 37°C for the fast and slow steps in the kinetics. The pre-equilibrium constants K_1 and K_2 for NBD-PE and NBD-PC are listed in Table 2. The values obtained were approximately a factor of two larger for NBD-PC than for NBD-PE. The thermodynamic parameters ΔH and ΔS associated with the pre-equilibrium constants are listed in Table 3.

The ΔH values are positive indicating the pre-equilibrium association to be endothermic with the values for NBD-PE being about three times the values of NBD-PC. The difference can be attributed to the differences in the location of NBD moiety within the bilayer region. In short, NBD PE is present at the bilayer-

aqueous interface while NBD-PC is present in the hydrocarbon region. The NBD moiety in NBD-PE is located in a more polar environment (bilayer-aqueous interface) than in the NBD-PC (bilayer region). The solvation of the NBD moiety by water in the two regions will be different, contributing not only to the enthalpy change but also the entropy change.

Surprisingly the ΔS values for the association of dithionite with NBD-PE and NBD-PC are positive opposite of what might be expected for association equilibrium. This could be interpreted as reorganization of the bilayer region where the NBD moiety is present following the association with dithionite. Thus it leads to an overall increase in entropy even though the association of dithionite with NBD by itself should result in a decrease in entropy. This reorganization must be substantial as indicated by the magnitude of the ΔS values. It is interesting to note that the ΔS values for NBD-PE are larger than for NBD-PC indicating that the reorganization is larger in the former than the latter.

The NBD moiety in NBD-PE is present at the outer and inner leaflets at the lipid bilayer-aqueous interface and in NBD-PC is present in the hydrophobic interior of the bilayer region. Previous studies based on the fluorescence of NBD-PC have concluded that the NBD at the tail of hydrocarbon chain in NBD-PC orients itself towards the polar aqueous phase through a bent conformation of the hydrocarbon chain as this group prefers a more hydrophilic environment [107, 111]. The ΔS values suggest that due to the bending of the hydrocarbon chain, the NBD moiety

in NBD-PC is present in a more disordered environment in the bilayer region while in NBD-PE it is present in a more ordered environment at the bilayer-aqueous interface. As a result the reorganization in the vesicle bilayer, NBD PE is more extensive than in NBD-PC following the association of dithionite with NBD..

The pre-equilibrium constants were calculated using the thermodynamic parameters at the various temperatures of kinetic studies except at those where they were experimentally determined. Representative values of rate constants at 10, 23, and 37°C are given in Table 1 to illustrate the difference between the k_1 and k_2 values and the anomalous behavior at 23 °C. Both the rate constants increase with temperature but show an abnormal increase in the phase transition temperature range. The rate constant k_2 for the slow step is two orders of magnitude smaller than rate constant k_1 for the fast step. The k_2 value is similar to transmembrane migration rates for NBD-PE and NBD-PC reported by Vaz [100].

This indicates that the experimentally determined rate constant for the slow quenching step actually represents the transmembrane migration rate of the lipid tagged with the dye molecule. The migration is the rate limiting step which is followed by the reduction with dithionite with the rate constant k_1 determined in the fast initial step of the fluorescence quenching reaction. The fluidity of the lipid bilayer region in the phase transition temperature range likely results in abnormally large quenching (k_1) and transmembrane migration (k_2) rate constants.

4. 4.2 Eyring Model

The rate constants k_1 and k_2 determined in the temperature range between 2 to 45 °C for NBD-PE and between 10 to 45 °C for NBD-PC were analyzed based on Eyring's transition state model of reaction kinetics. Previous studies of the temperature dependent studies of NBD fluorescence quenching by dithionite in various vesicle systems had employed the Arrhenius model. While the two models provide the activation energy (enthalpy) barrier for a given reaction, Eyring's transition state model also provides the entropic barrier.

As discussed below, Eyring's model is especially useful and important to understand the kinetic behavior at and near the phase transition temperature. The Eyring plots of ln k vs. 1/T for the fast and slow kinetic steps for NBD-PE are displayed in Figures 3.8 and 3.9 and for NBD-PC in Figures 3.10 and 3.11 respectively. It is evident that the Eyring plot is complex near and at the phase transition temperature but has the expected shape in the gel and fluid phases.

The Eyring plots for the rate constants k_1 and k_2 were constructed considering only the values in the gel and fluid phases which provided a reasonable linear dependence for ln (k/T) with 1/T for the fast and slow steps. Such linear plots are shown as solid blue lines in Figures 3.8 and 3.9 for NBD-PE and NBD-PC 3.10 and 3.11. The rate constants for the fast step, k_1 as seen in Figure 3.8 for NBD-PE exhibits a negative deviation from the blue line while the rate constants for the slow step for NBD-PE as seen in Figure 3.9 and the rate constants for the fast and slow steps for NBD-PC exhibit a positive deviation from the blue line.

The activation parameters derived from the linear plots (blue lines) are listed in Table 5. The enthalpies and entropies of activation for the fast and slow steps for NBD-PE and NBD-PC are similar to the small positive value for the enthalpy of activation and a large negative value for the entropy of activation. It is evident from this table that the main barrier for the reduction of NBD by dithionite is entropic and not enthalpic in nature. In other words the reduction of NBD to ABD by dithionite proceeds through a transition state which requires a much greater order in the bilayer region where the dye molecules are present. This is in contrast to the positive entropy change accompanying the pre-equilibrium association of dithionite with NBD resulting in reorganization of the vesicle bilayer region where NBD is present.

The order is required for the two electron transfer between the dithionite and NBD. In the bilayer region the reduction of NBD by dithionite initially requires reorganization (disorder) due to association of dithionite with NBD in the pre-equilibrium step and organization (order) for the electron transfer in the reduction step. The entropy decrease in the electron transfer step is much larger than the entropy increase in the pre-equilibrium step such that the overall entropy change ($\Delta S+\Delta S^{\ddagger}$) for the reduction of NBD to ABD is a negative value. The formation of the activated complex leading to the reduction is accompanied by a reduction in entropy for the fast and slow steps for NBD-PE and NBD-PC as indicated by the sum of entropy values in Table 4.

The enthalpies of activation for NBD-PE and NBD-PC for the fast steps are similar as are the values for the slow steps (Table 4). The entropy increase for the pre-equilibrium step for the reduction of NBD-PE is larger than for NBD-PC. This results in a smaller overall entropy reduction for NBD-PE than NBD-PC going from the reactants to activated complex as indicated in Table 4.

This could be attributed as previously discussed to difference in the locations of the NBD moiety of NBD-PE and NBD-PC in the vesicle bilayer region. The enthalpies of activation for the fast and slow steps in the reduction of NBD moiety in NBD-PE and NBD-PC as seen from Table 4 are similar. The overall changes in enthalpy in going from the reactants to the activated complex are given in Table 4. This value is about a factor of two larger for NBD-PE than NBD-PC and the difference primarily stems from the difference in the enthalpy change accompanying the pre-equilibrium step.

As discussed above the difference in the location of the NBD moiety in NBD-PE and NBD-PC contributes to the difference in the enthalpy change for the pre-equilibrium step and the overall enthalpy change in going from the reactants to the activated complex.

The Eyring plots for NBD PE (Figures 3.8 and 3.9) and NBD PC (Figures 3.10 and 3.11), considering the phase transition clearly indicates that the plots over the entire range of temperatures are more complex than the model that omits the transition region. A curve passing through all the data points resemble the ones

obtained from fluorescence intensity change and fluorescence anisotropy change, in Figures 3.4 and 3.6 respectively. The Eyring plots indicate that the transitions from gel to fluid phase with rising temperature. There is a similar range of phase transition temperatures as fluorescence anisotropy and intensity changes. With the exception of Figure 3.8 for the fast kinetic step for NBD-PE, all plots exhibit a positive deviation in the temperature range of phase transition.

Eyring plots indicate regions of linearity identified as gel, phase 1, phase 2, and fluid, from which the corresponding activation parameters were calculated. These values are given in Table 6 which gives the temperature ranges over which the activation parameters for the different phases were calculated. Table 5 shows the temperature range for the gel, phase 1, phase 2 and fluid regions for the fast and slow reduction steps for NBD-PE and NBD-PC. We interpret phase 1 and phase 2 regions as region of mixed gel and fluid phases spanning about 10 °C.

Presumably phase 1 is richer in gel and phase 2 is richer in the fluid. The Eyring plots indicate that the activated complex is more sensitive to the environment of the NBD moiety than fluorescence anisotropy and intensity. The transition from the gel to fluid phase of the bilayer, and *vice versa*, appears to be a complex cooperative phenomenon of the self-assembled lipid molecules. The Eyring plots in Figures 3.8, 3.9,, 3.10 and 3.11 exhibit three breaks in the regions of linearity which could be considered as three transition temperatures. The Eyring plots were obtained with the average values of these rate constants. Kinnunen [98]

reported a similar but much less complex behavior employing the Arrhenius kinetic model for the reduction of DPPN and NBD-PC in DPPC vesicles, which were extruded through 100 nm membranes. This provided small unilamellar vesicles with a narrow size distribution. Plots of ln k vs. 1/T, following the Arrhenius model, resemble the Eyring plots.

We determined the steady state and time-resolved anisotropy, the lifetimes and the quenching kinetics from a wide range of size distributions. Heimburg *et. al* [53, 113] reported the phase transition characteristic of DPPC vesicles of variable sizes. They showed that the phase transition is sharper in MLV, broader for LUV and even broader in SUV.

The complex behavior seen in these studies may be attributed to a mixture of sizes of DMPC vesicles. This mixed system is normally obtained by the various methods of preparation of vesicles from phospholipids and it is useful to understand the bilayer region in such systems. This complexity was not observed in steady-state anisotropy as previously mentioned, since anisotropy measurements are not as sensitive to the mixed vesicle system as are the activation parameters.

The 11 mM $MgCl_2$ solution accounts for 63 to 98 % of the total vesicle volume in the diameter range between 50 to 1000 nm and contributes significantly to the results. Complete miscibility liquid and solid phases of lipids can also occur at the

phase transition temperature [114]. The presence of NBD-PE and NBD-PC in the bilayer region at a ratio of 1 dye to 200 DMPC molecules can contribute to the complex phenomenon at the phase transition.

The activation parameters that can be understood from the Eyring model are those for the fast kinetic steps for NBD-PE and NBD-PC in the gel and fluid phases. These values are clearly different from the values obtained from Eyring plots in which the transition region is ignored. In particular the gel and fluid phases for DMPC vesicles with NBD-PE and NBD-PC are characterized by positive enthalpies of activation and negative entropies of activation. The enthalpies of activation in the gel phase are higher than those in the fluid phase with the values for NBD-PC exhibiting a much larger difference than for NBD-PE.

Similarly the entropies of activation for NBD-PE in the gel and fluid phases are closer than the values for NBD-PC in these two phases. These differences need to be considered in light of the various regions of the vesicle in which NBD-PE and NBD-PC reside. Others factors that must be considered are their stabilizing effect on the bilayer region, the nature of the mixed vesicle system, and the presence of $MgCl_2$. These factors can limit a detailed explanation of the activation parameters obtained in the current report.

A detailed analysis on the activation enthalpies obtained in this study and those analyzed using Kinnunen's Arrhenius activation energies for the reduction of

NBD-PE and NBD-PC by dithionite in 100 nm DPPC extruded vesicles in the absence of magnesium chloride; reveal differences arising from the analytical approach that was followed in the current report. According to Kinnunen the activation energies from DPPC for NBD-PE below and above the phase transition temperature (41°C) are 5.25 and 19.1 kcal/mole respectively. The activation enthalpies for NBD-PE from this report (see Table 6) below and above the phase transition temperature (23°C) are 8.73 and 6.42 kcal/mole respectively and are not comparable to the values for DPPC. The activation energies below and above the phase transition temperature for the reduction of NBD-PC in DPPC are 14.1 kcal/mole and 15.53 kcal/mole, which are similar to the ones reported here. These values in DMPC as given in Table 6 are quite different, namely 13.1 Kcal/mole and 2.4 Kcal/mole respectively. The results obtained in both cases indicate that the activation energies for the reduction of NBD-PE and NBD-PC are sensitive to the phase of the bilayer region and the nature of the vesicle.

The activation parameters for the phase 1 and phase 2 regions and the slow kinetic step are even more difficult to rationalize as some values of enthalpy of activation are negative, in violation of the prediction by Eyring's model. Additionally some unrealistically large positive and negative values are difficult to interpret given the experimental conditions. The rate constant for the slow kinetic step for NBD-PE corresponds to the transmembrane migration, while it can be attributed to flip-flop for NBD-PC case. The migration and flip-flop in the bilayer region are

complex cooperative phenomena for which the Eyring model has no physical reality.

A possible explanation for the deviations from Eyring model for the fast kinetic step in the range of phase transition temperatures and for the transmembrane migration and flip-flop of the dye labeled lipids stems from the chemical potentials of NBD and ABD as defined by their free energies not being constant. Eyring theory considers reactant and product of a well defined chemical potential. The activation barrier and the activated complex are also well defined with reference to these chemical potentials. Considering the chemical potentials ($\mu = \mu^0$ + RTln a) for NBD and ABD in the range of phase transition temperatures and during the transmembrane and flip-flop processes, defining a standard chemical potential μ^0, is difficult as a standard state for NBD and ABD cannot be properly defined. Additionally the activity coefficient and hence the activity a, of NBD and ABD also will not be constant during these processes.

In the phase transition regime the membrane bilayer is not as uniform as the gel and fluid phases. Slight variations in temperature result in large variations in the bilayer region at phase transition temperature region. The lipid molecules are in a high state of flux which makes it impossible to define the oxidized (NBD) and reduced (ABD) forms of the dye with characteristic chemical potentials. The constant state of flux also leads to anomalously high permeability for various ions and neutral molecules as observed by Mouritsen [18].

The permeability of dithionite ions in the phase transition temperature range can also be expected to be higher where the bilayer exists in the gel or fluid phase. Langner and Hui [96] found a dithionite permeability maximum at the phase transition temperature of DMPC and they attributed this to packing defects enhanced at the phase separation in the transition region. The fluorescence intensity change upon quenching, and the anisotropy of NBD also exhibits anomalous values in the range of phase transition temperatures. The same group also determined the influence of free fatty acids on the permeability of DMPC bilayer that was higher at the phase transition region [115].

The transmembrane migration and flip-flop of NBD-PE and NBD-PC respectively can be expected to generate disorder in the region of the bilayer, creating a situation similar to the disorder in the phase transition temperature range. The transmembrane rate constant for the NBD PE and NBD PC was higher at the phase transition than the gel or fluid phase. The rate for NBD PC was even higher than NBD PE. The local disorder during the transmembrane migration and flip-flop occurs at all temperatures in the gel and fluid phases. This phase transition regime can produce unrealistic values for the activation parameters for these processes not only in the phase transition regime but also in the gel and fluid phases.

4. 5 Fluorescence Lifetime Measurements

Fluorescence lifetime is the time a fluorescent probe remains in the excited state. The lifetime with polarizer in place fitted well to a biexponential function (chi square less than 1.40). Both NBD PE and NBD PC resulted in a short and long lifetime of nanoseconds. Table 8 shows measurements done at 25 ˚C for long and short lifetimes and also time-correlated anisotropy with the all the statistical parameters used to gauge the goodness of the fit. The NBD PE yielded longer lifetimes in DMPC compared to NBD PC. The lifetimes of the NBD PE were found to be 9.71 and 2.3 ns for the long and short lifetimes respectively. NBD PC showed 6.95 and 2.25 ns for the long and short lifetimes respectively. The lifetimes obtained for NBD PE were compared to those reported previously [116, 117]. The reported lifetimes of NBD PE in DOPC vesicles were 8.4 ns for the long and 3.6 ns for the short lifetime. On the other hand NBD PC gave 4.9 and 7.5 ns for the short and long lifetimes respectively.

DOPC phospholipids exist in fluid phase at room temperature while DMPC displays both the gel and fluid phase at the same temperature. The longer lifetime of NBD PC was comparable while that of the NBD PE was higher in DMPC case that was reported. The short lifetime in NBD PC was higher and comparable to that of Chattopadhyay. Johnson et al [118] used NBD PE to investigate the perfingolysin conformation in cell membranes. The results in aqueous solution gave the NBD PE lifetimes of 0.9 ns (20 %) and 9 ns (80 %). The short lifetime was attributed to the probe existing in a hydrophilic environment while the longer

one was due to the existence in the hydrophobic environment. The long lifetime in the NBD PE contributed about 70 % intensity and the short one 30 %. This could be rationalized based on the results of Johnson et al. A 70 % of the NBD PE exist in the hydrophobic region of the bilayer while 30 % in the hydrophilic environment. NBD PC is almost equally distributed in the hydrophobic (52% for the short lifetime) and hydrophilic (48 % for the long lifetime). The NBD group of the acyl chain loops back as a result of its polarity as previously mentioned. NBD moiety in NBD PE is uncharged at a neutral pH [119] and therefore ensures that the NBD does not project into the external aqueous environment. Therefore the results obtained from this study indicates that NBD in NBD PE in 11mm $MgCl_2$ does resides in the hydrophobic region, while NBD of NBD PC exists in equal distribution in the hydrocarbon and the hydrophilic environment.

There is a continuous decrease of lifetime with increasing temperatures in single vesicles and ensembles for both NBD PC and NBD PE (Figures 3.10 (a) and (b) respectively. The long lifetime of the NBD PE in DMPC decreased from 10.9 to 7.4 ns within a temperature range of 7 to 39 ˚C resulting in a difference of 3.5. The short lifetime decreased from 3.3 to 1.9 ns resulting in a change of 1.4 ns within the same temperature range. The long lifetime in NBD PC decreased from 8.4 to 5.2 ns with a change equal to 3.2 ns, while the short lifetime decreased from 2.7 to 1.7 resulting in a change of 1nanosecond.

The decrease in fluorescence lifetimes of the NBD PE and NBD PC with increasing temperature indicates a change in membrane polarity around the

excited state of the NBD group in DMPC. The change in polarity is as a result of water penetration in the bilayer induced by the phase transition from gel to fluid phase. Hydrogen bond formation can occur between the fluorophore and the water molecules which can be accompanied by reduction in the lifetime of the excited state as a result of increase in nonradiative decay [87, 120]. The change in the long lifetime in the NBD PE is slightly higher than NBD PC that can be attributed to the orientation of NBD moieties in these probes. The fluorescence lifetime of NBD in NBD PC is less sensitive to changes in temperature. This can be attributed to the vertical distributions of the fluorophore in the bilayer at different temperatures while undergoing phase transition.

The diluted sample for the ensemble measurements in the Edinburgh instrument gave relatively longer lifetimes than the single vesicle under microscope condition. The undiluted sample had relatively shorter lifetime compared to the dilute and the microscope measurements. This could be attributed to concentration quenching that lead to increase in the nonradiative processes of energy transfer.

4.6 Time Correlated Anisotropy

The measurement of lifetime and excited state lifetime of a fluorophore can be used to determine the rotational correlation time which in return reflects the re-orientational correlation time of the acyl chain in the membrane. Fluorescence anisotropy measures rotation freedom within the time range of the excited state. In time-correlated anisotropy, the molecular rotation is recorded as a function of time that can be used to investigate the dynamics and structure of lipid bilayer. The time dependent parallel and perpendicular emissions components relative to the polarizing beam measure fluorescence anisotropy which decays exponentially according to equation 8.

$$r(t) = r_o e^{-t/\theta} \qquad (4.2)$$

where r_o is the anisotropy at t = 0, and Θ is the rotational correlation time of the fluorophore considered as a sphere.

In this study the time correlated anisotropy of the NBD PE and NBD PC gave single correlation time ϕ (see Table 8). The observed anisotropy decay reflected mainly the motion of long-lived fluorophores. The time-correlated anisotropy measured at 25 °C was relatively longer in NBD PC compared to NBD PE resulting in 2.78 ns and 1.58 ns respectively. Rotational time is used to determine rotational mobility of a fluorophore which in turn is sensitive to the acyl chain packing in membranes. NBD located in the acyl chain is likely to experience more changes in membrane organization than the head labeled moiety. In addition, the consequences of looping back for NBD in NBD PC and the fact that this polar

group is located in the non-polar region could account for the relatively higher value in NBD PC than the NBD PE. The decay of polarized fluorescent light from the NBD PE and NBD PC was determined at various temperatures. Figures 3.11 showed time-correlated anisotropy of the NBD PE as a function of temperature. There is a rapid decrease in anisotropy with increase in temperature in the gel phase. There is a sudden decrease at the phase transition of DMPC followed by a constant phase that could be attributed to restricted motion within the bilayer. As the rotational diffusion increases with rising temperature, there is a corresponding decrease of anisotropy.

4. 7 Influence of Dihydrocholesterol in DMPC Bilayer

The DMPC lipid bilayer region was investigated further in the presence of dihydrocholesterol. We used variable dihydrocholesterol concentration in the bilayer region and determined behavior of the fluorescent probes using steady state anisotropy and dithionite quenching kinetics of the NBD PE and NBD PC embedded in DMPC bilayer. The gel to fluid transition peak, of DMPC bilayer with 30 % dihydrocholesterol concentration and above, is broadened significantly. This is demonstrated by steady state anisotropy and the kinetics of dithionite quenching. The percent quenching was used to gauge the extent of reduction of the NBD PE or NBD PC in DMPC. A typical plot is seen in Figure 3.19 for NBD PC. At 25 % dihydrocholesterol the amount of NBD reduced remain the same over a wide range of temperature.

The anisotropy data clearly indicate that the order in the lipid bilayer packing is affected by dihydrocholesterol. The fluorescence anisotropy measurements showed that as the amount of dihydrocholesterol increases, the anisotropy increases to a maximum 40 % at temperature above the phase transition (Figure 3.22). As mentioned earlier, the anisotropy can be correlated to the diffusion rate of the probes embedded in the bilayer region. This is sensitive to the packing of fatty acyl chain and sterols. As dihydrocholesterol concentration increases the fatty acyl chain become ordered (rigid) and tightly packed, and shield the nonpolar cholesterol from the unfavorable contact with water. This action is promoted by the lipid polar head group. There is a limit to this behavior. This explains the decrease in anisotropy with increasing dihydrocholesterol above 40 %. This behavior is clearer in the NBD PE case than NBD PC.

Previous studies on lipid membrane have indicated that the addition of cholesterol to the membrane can strongly be correlated with membrane fluidity. Cholesterol shifts the phase transition temperature in membrane and prevents crystallization of hydrocarbon with the result that it introduces disorder in the gel phase while introduces order in the fluid phase [121]. On the other hand, cholesterol has a tendency to decrease order of phospholipid bilayers in the crystalline phase by perturbing the order of the hexagonal packing of lipids. The opposite is true in the fluid state because of the rigid ring structure of cholesterol limiting the *cis-trans* isomerization of the neighboring lipids [122]. Davis *et al* [123] reported on the changes in optical density of a phospholipid bilayer membrane at the phase

transition temperature. These changes in optical density are as result of the amount of light scattered by the vesicles. The study reports that the optical density of the bilayer increased linearly with increasing cholesterol content and that the absolute change occurring at the phase transition was reduced with a resulting broadened transition. They also report a growing hysteresis effects with increasing cholesterol content and that samples with 19.5 % cholesterol showed an extreme hysteresis in the temperature- turbidity relationship. These reports can provide an explanation for the observation made with 25 % dihydrocholesterol in our case. The steady state fluorescence anisotropy and kinetics, displayed by 25 % dihydrocholesterol in DMPC, showed a bilayer region that represents a region of the partial phase diagram where pure DMPC and DMPC-Cholesterol domains coexist (liquid-ordered and disordered phase).

CHAPTER 5

CONCLUSIONS AND FUTURE DIRECTIONS

As discussed in chapter 4, a detailed investigated of bilayer regions of DMPC vesicles of mixed sizes gave the kinetics and thermodynamics of the quenching of the NBD-PE and NBD-PC induced by sodium dithionite. In addition, steady state and time-resolved anisotropy measurements on NBD moiety attached to the tail and head of phospholipids are presented. The bilayer region was characterized by the enthalpies and entropies of activation based on Eyring model. As a result of the orientation of NBD moiety in the lipids, NBD-PE probed the hydrophilic region while NBD-PC monitored the hydrophobic regions of the bilayer.

The data obtained here attest to the nature of dithionite quenching of the NBD moiety in lipid bilayers as was previously discussed in the literature. The quenching of NBD by dithionite involves a two step reaction, the reduction of readily accessible NBD moieties resulting in a rapid step, followed by transbilayer migration of the inner leaflets NBD which are finally reduced in the slow step. We report the general quenching mechanisms of the NBD moiety by dithionite. It was found to proceed through a pre-association of dithionite with NBD, followed by its reduction to ABD.

In the immediate quenching step, the equilibrium constants for the pre-equilibrium was higher for NBD-PC than for NBD-PE possibly due to the nonpolar region of the bilayer in which the NBD resides in the former compared to the polar region for the latter. The enthalpies and entropies associated with the pre-equilibrium step are positive indicating the process to be endothermic and leading to disorder in the bilayer region of the dye molecule. The subsequent reduction of the NBD by dithionite has complex temperature dependence especially in the range where the reversible transition of the gel to fluid phase occurs.

The enthalpies and entropies of activation for the gel and fluid phases for NBD-PE are closer relative to the values for NBD-PC. The differences could be attributed to the location of NBD either in the polar region for NBD PE or in the nonpolar in the case of NBD PC. The entropies of activation are negative for both cases in the gel and fluid phases indicating that the activated complex resides in an ordered environment. This is a return to order in the bilayer region for the activated complex following the initial association of the dithionite with the NBD moiety. In particular the enthalpy of activation for NBD-PC in the gel phase is six times larger in the gel phase, while the entropy of activation is a factor of three more negative in the fluid phase compared to the gel phase. Thus, the activation barrier is mainly enthalpic in the gel phase and entropic in the fluid phase. The activation parameters in the range of temperatures corresponding to the reversible transition from gel to fluid phase are anomalously large with even negative

enthalpies of activation. Such values do not have a physical reality and indicate that the Eyring model of activated complex fails in this region possibly due to the inability to define the standard states, standard chemical potentials, and activity coefficients for NBD and ABD in the phase transition region where varying amounts of gel and fluid phases co-exist. The anomalous behavior in the phase transition region is also observed in the fluorescence anisotropy and fluorescence intensity change upon quenching.

The quenching kinetics for the slow step corresponding to the reduction of NBD moieties following transmembrane migration and flip-flop can be treated with the same kinetic model as the rapid step. The pre-equilibrium association constants for NBD-PC are higher than for NBD-PE as for the rapid kinetic step. The enthalpies and entropies associated with these pre-equilibrium follow the same trend as the rapid kinetic step. However, the enthalpies and entropies of activation for the slow kinetic step in the gel and fluid phases and in the phase transition region are difficult to interpret as many of the enthalpies and entropies of activation have large positive and negative values. Negative enthalpies of activation are not realistic in the Eyring model. This most likely result from the inability to define the chemical potentials for NBD and ABD in the activated complex during the transmembrane migration and flip-flop processes.

Further evidence on the location of the probes was analyzed by time-resolved anisotropy and lifetime measurements. The values of lifetime of the NBD PE

were relatively higher compared to NBD PC. This is attributed to changes in vertical distribution of the NBD moiety in NBD PC as result of attaching the polar group into a more hydrophobic environment. This may be explained on the basis of chain reversal or looping back of the acyl chain that becomes more accommodated in the interfacial region. This becomes more random with increasing temperature. The NBD PE has a greater rotational freedom in the bilayer that gives a change in a factor of two in fluorescence anisotropy with temperature compared to NBD PC. At the phase transition, there is a very sharp drop in anisotropy that can possibly be explained on sudden increase in polarity at gel-fluid phase coexistence. The anisotropy values presented are relatively higher compared to literature. We rationalize this partly on the basis of size distribution used to perform the experiments and partly on the gel-fluid phase coexistence that is displayed by DMPC at room temperature.

We succeeded in generating giant vesicles from pure DMPC and DMPC with dihydrocholesterol content to a maximum 60 % (mol/mol). The steady state anisotropy of DMPC with dihydrocholesterol demonstrated influence of low and high dihydrocholesterol in fluidity and rigidity of the bilayer region. The values obtained are relatively higher in NBD PE than NBD PC, similar to DMPC without dihydrocholesterol. Anisotropy measured close to phase transition and above this temperature was positively correlated with dihydrocholesterol concentration to about 40 % for NBD PE. In the gel phase, values decreased with increasing dihydrocholesterol concentrations, as result of condensing effect of

cholesterol that dissociate endothermically above the phase transition. We have also conducted kinetic studies for DMPC with varying concentrations of dihydrocholesterol in the bilayer region. There is a significant broadening of the gel to fluid phase transition in the region of 30 % dihydrocholesterol content and above. In addition, NBD PC with 25 % dihydrocholesterol displayed unusual broadening effect. We attributed this behavior to maximum partitioning of dihydrocholesterol-phospholipid in the liquid-ordered and liquid-disordered phases formed in bilayer region.

5.1 Future Directions of the Project

In summary, we have observed the DMPC lipid bilayer as a simple model system that displays both the gel and fluid phases close to the standard room temperature. The kinetics and thermodynamics parameters presented here can provide a basis for future studies involving single vesicles studies under the microscope. The data obtained from lifetime on single and ensemble measurements is unique. It is known that ensemble behavior give average parameters of the bulk as opposed to a single entity. Our study on single vesicle can provide an advantage in depicted molecular processes occurring in a single vesicle. Dithionite quenching experiment can be pursued further on a single vesicle experiment in an optical microscope. Here, the NBD present in the bilayer region can be excited with a laser which can provide a fundamental understanding of the nature of ground and excited state reactions in a single vesicle with well defined characteristics. The results can be useful in understanding cell membrane dynamics.

REFERENCES

1. Nichols, B., *Lipid Rafts and Caveolae: From Membrane Biophysics to cell Biology Edited by Christopher J. Fielding.* Nature Cell Biology, 2006. **8**(7): p. 644.

2. Luo, L.; Eisenberg, A., *Thermodynamic Size Control of Block Copolymer Vesicles in Solution.* Langmuir, 2001. **17**: p. 6804-6811.

3. Singer, S.J. and G.L. Nicolson, *The fluid mosaic model of the structure of cell membranes.* Science, 1972. **175**(23): p. 720-31.

4. Devaux, P.F., *Static and dynamic lipid asymmetry in cell membranes.* Biochemistry, 1991. **30**(5): p. 1163-73.

5. Yeagle, P.L., W.C. Hutton, and R.B. Martin, *Transmembrane asymmetry of vesicle lipids.* J Biol Chem, 1976. **251**(7): p. 2110-12.

6. Virtanen, J.A., K.H. Cheng, and P. Somerharju, *Phospholipid composition of the mammalian red cell membrane can be rationalized by a superlattice model.* Proc Natl Acad Sci U S A, 1998. **95**(9): p. 4964-9.

7. Raudino, A. and D. Mauzerall, *Dielectric properties of the polar head group region of zwitterionic lipid bilayers.* Biophys J, 1986. **50**(3): p. 441-9.

8. Gradzielski, M., *Vesicles and vesicle gels-structure and dynamics of formation.* Journal of Physics: Condensed Matter, 2003. **15**(19): p. R655-R697.

9. Walde, P. and S. Ichikawa, *Enzymes inside lipid vesicles: preparation, reactivity and applications.* Biomol Eng, 2001. **18**(4): p. 143-77.

10. Monnard, P.A., A. Luptak, and D.W. Deamer, *Models of primitive cellular life: polymerases and templates in liposomes.* Philosophical translocations of Royal Society of London. Series B, Biological sciences, 2007. **362**(1486): p. 1741-50.

11. Kulin, S.; Kishore, R.; Helmerson, K.; Locascio, L., *Optical manipulation and fusion of liposomes as microreactors.* Langmuir, 2003. **19**(20): p. 8206-8210.

12. McGloin, D., *Optical tweezers: 20 years on.* Philosophical transactions. Series A, Mathematics, physical, and engineering sciences, 2006. **364**(1849): p. 3521-37.

13. Ashkin, A.; Dziedzic, J. M.; Bjorkholm, J.E.; Chu, S., *Observation of a single-beam gradient force optical trap for dielectric particles.* Optical Letters, 1986. **11**(5): p. 288-90.

14. Helfrich, M.R., et al., *Aqueous phase separation in giant vesicles.* J Am Chem Soc, 2002. **124**(45): p. 13374-5.

15. Long, M.S., et al., *Dynamic microcompartmentation in synthetic cells.* Proc Natl Acad Sci U S A, 2005. **102**(17): p. 5920-5.

16. Ulrich, A.S., *Biophysical aspects of using liposomes as delivery vehicles.* Bioscience Reports, 2002. **22**(2): p. 129-50.

17. Ropert, C., *Liposomes as a gene delivery system.* Brazilian Journal of Medical and Biological Research, 1999. **32**(2): p. 163-9.

18. Mouritsen, O.G.; Editor., *Life -As a Matter of Fat: The Emerging Science of Lipidomics.* 2005.: p. 276 pp.

19. Bear, R.S.; Palmer, K. J.; Schmitt, F. O., *X-ray diffraction studies of nerve lipides.* Journal of Cellular and Comparative Physiology, 1941. **17**: p. 355-67.

20. Small, D.M., *Phase equilibria and structure of dry and hydrated egg lecithin.* J Lipid Res, 1967. **8**(6): p. 551-7.

21. Andelman, D.; Kawakatsu, T.; Kawasaki, K., *Equilbrium shape of two - component unilamellar membranes and vesicles.* Europhysics Letters, 1992. **19**(1): p. 57-62.

22. Pencer, J.;Nieh, M. P.;Harroun, T. A.;Krueger, S.,Adams, C.,Katsaras, J., *Bilayer thickness and thermal response of dimyristoylphosphatidylcholine unilamellar vesicles containing cholesterol, ergosterol and lanosterol: a small-angle neutron scattering study.* Biochim Biophys Acta, 2005. **1720**(1-2): p. 84-91E.

23. Zemlyanaya, E.V.; Kiselev, M.A.; Zbytovska, J.; Almasy, L.; Aswal, V.K.; Strunz, P.; Wartewig, S.; Neubert, R., *Structure of unilamellar vesicles: numerical analysis based on small-angle neutron scattering data.* Crystallography Reports, 2006. **51**(Suppl. 1): p. S22-S26.

24. Kiselev, M.A.; Zemlyanaya, E. V.; Aswal, V. K.; Neubert, R. H., *What can we learn about the lipid vesicle structure from the small-angle neutron scattering experiment?* Eur Biophys J, 2006. **35**(6): p. 477-93.

25. Brown, M.F., A.A. Ribeiro, and G.D. Williams, *New view of lipid bilayer dynamics from 2H and 13C NMR relaxation time measurements.* Proc Natl Acad Sci U S A, 1983. **80**(14): p. 4325-9.

26. Akashi, K.; Kinosita, K.; Miyata, H.; Itoh, H., *Observation of a variety of giant vesicles under optical microscope.* Perspectives in Supramolecular Chemistry, 2000. **6**(Giant Vesicles): p. 45-48.

27. Davis, S.S., *Giant Vesicles, edited by P.L. Luisi and P. Walde.* Journal of Controlled Release, 2000. **68**(1): p. 135-136.

28. Luisi, P.L.; Walde, P., *Giant Vesicles.* Wiley, Chinchester, 2000.

29. Betzig, E.; Chichester, R. J., *Single molecules observed by near-field scanning optical microscopy.* Science (Washington, DC, United States), 1993. **262**(5138): p. 1422-5.

30. Peterman, E.J., H. Sosa, and W.E. Moerner, *Single-molecule fluorescence spectroscopy and microscopy of biomolecular motors.* Annu Rev Phys Chem, 2004. **55**: p. 79-96.

31. Korlach, J., et al., *Characterization of lipid bilayer phases by confocal microscopy and fluorescence correlation spectroscopy.* Proc Natl Acad Sci U S A, 1999. **96**(15): p. 8461-6.

32. Edidin, M., *The state of lipid rafts:From model membranes to cells.* Annual Review of Biophysics and Biomolecular Structure, 2003. **32**: p. 257-283.

33. Liu, J.; Qi,S.; Groves, J.T.; Chakraborty,A.K., *Phase segregation on Different Length Scales in a Model Cell Membrane System.* Journal of Physical Chemistry B, 2005. **109**(42): p. 19960-19969.

34. Lisette, L.; Andrew, F.G. Q., *Supramolecular complex formation in a cell signalling and disease: an update a reccurrent theme in cell life and death.* Biol Res, 2004. **37**: p. 29-43.

35. Nathaniel, C.; Denis, G., *Virus Entry, Assembly,Budding and Membrane Rafts.* Microbiology and Molecular Biology Reviews, 2003. **67**(2): p. 226-237.

36. Scherfeld, D., N. Kahya, and P. Schwille, *Lipid dynamics and domain formation in model membranes composed of ternary mixtures of unsaturated and saturated phosphatidylcholines and cholesterol.* Biophys J, 2003. **85**(6): p. 3758-68.

37. Brown, D.A. and E. London, *Structure and function of sphingolipid- and cholesterol-rich membrane rafts.* Journal of Biological Chemistry, 2000. **275**(23): p. 17221-4.

38. Horton, M.R., J. Radler, and A.P. Gast, *Phase behavior and the partitioning of caveolin-1 scaffolding domain peptides in model lipid bilayers.* Journal of Colloidal and Interface Science, 2006. **304**(1): p. 67-76.

39. Koynova, R.; Caffrey, M., *Phases and phase transitions of the phosphatidylcholines.* Biochim Biophys Acta, 1998. **1376**(1): p. 91-145.

40. Choucair, A.A.; Kycia, A. H.; Eisenberg A., *Kinetics of Fusion of Polystyrene-b-poly(acrylic acid) Vesicles in Solution.* Langmuir, 2003. **19**: p. 1001-1008.

41. Leng, J.; Egelhaaf, S.U.; Cates, M.E., *Kinetic pathway of spontaneous vesicle formation.* Europhys. Lett., 2002. **59**(2): p. 311.

42. Lasic, D.D., *The mechanism of vesicle formation.* Biochemical Journal, 1988. **256**(1): p. 1-11.

43. Angelova, M.; Dimitrov, D., *Liposome electroformation.* Faraday Discussions of the Chemical Society, 1986. **81**(1): p. 303-11.

44. Pereira-Lachataignerais, J., et al., *Study and formation of vesicle systems with low polydispersity index by ultrasound method.* Chem Phys Lipids, 2006. **140**(1-2): p. 88-97.

45. Akashi, K.; Miyata, H.; Itoh, H.; Kinosita, K., Jr., *Preparation of giant liposomes in physiological conditions and their characterization under optical microscope.* Biophys J, 1996. **71**: p. 3242-3250.

46. Janiak, M.J., D.M. Small, and G.G. Shipley, *Nature of the Thermal pretransition of synthetic phospholipids: dimyristolyl- and dipalmitoyllecithin.* Biochemistry, 1976. **15**(21): p. 4575-80.

47. Kucerka, N.; Kiselev, M.A.; Balgavy, P., *Determination of bilayer thickness and lipid surface area in unilamellar dimyristoylphosphatidylcholine vesicles from small-angle neutron scattering curves: a comparison of evaluation methods.* European Biophysics Journal, 2004. **33**(4): p. 328-34.

48. Nagle, J.F. and S. Tristram-Nagle, *Structure of lipid bilayers.* Biochim Biophys Acta, 2000. **1469**(3): p. 159-95.

49. Sheetz, M.P. and S.I. Chan, *Effect of sonication on the structure of lecithin bilayers.* Biochemistry, 1972. **11**(24): p. 4573-81.

50. Sakanishi, A., S. Mitaku, and A. Ikegami, *Stabilizing effect of cholesterol on phosphatidylcholine vesicles observed by ultrasonic velocity measurement.* Biochemistry, 1979. **18**(12): p. 2636-42.

51. Nagle, J.F. and D.A. Wilkinson, *Lecithin bilayers. Density measurement and molecular interactions.* Biophys J, 1978. **23**(2): p. 159-75.

52. Chapman, D.; Williams, R. M.; Ladbrooke, B. D., *Physical studies of phospholipids. VI. Thermotropic and lyotropic mesomorphism of some 1,2-diacylphosphatidycholines (lecithins).* Chem Phys Lipids, 1967. **1**(5): p. 445-75.

53. Heimburg, T., *Coupling of chain melting and bilayer structure: domains, rafts, elasticity and fusion.* Membrane Science and Technology Series, 2003. **7**((Planar Lipid BiLayers (BLM) and Their Applications)): p. 269-293.

54. Tilcock, C.P.; and P.R. Cullis, *Lipid polymorphism.* Annals of the New York of Sciences, 1987. **492**: p. 88-102.

55. Luzzati, V., *Biological significance of lipid polymorphism: the cubic phases.* Current Opinion in Structural Biology, (1997). **7**(5): p. 661-8.

56. Tarahovsky, Y.S., et al., *Electrostatic control of phospholipid polymorphism.* Biophys J, 2000. **79**(6): p. 3193-200.

57. Huang, C. and S. Li, *Calorimetric and molecular mechanics studies of the thermotropic phase behavior of membrane phospholipids.* Biochim Biophys Acta, 1999. **1422**(3): p. 273-307.

58. Bacia, K., P. Schwille, and T. Kurzchalia, *Sterol structure determines the separation of phases and the curvature of the liquid-ordered phase in model membranes.* Proc Natl Acad Sci U S A, 2005. **102**(9): p. 3272-7.

59. Kahya, N., et al., *Probing lipid mobility of raft-exhibiting model membranes by fluorescence correlation spectroscopy.* J Biol Chem, 2003. **278**(30): p. 28109-15.

60. Radhakrishnan, A., T.G. Anderson, and H.M. McConnell, *Condensed complexes, rafts, and the chemical activity of cholesterol in membranes.* Proc Natl Acad Sci U S A, 2000. **97**(23): p. 12422-7.

61. Radhakrishnan, A. and H.M. McConnell, *Condensed complexes of cholesterol and phospholipids.* Biophys J, 1999. **77**(3): p. 1507-17.

62. McConnell, H.M. and A. Radhakrishnan, *Condensed complexes of cholesterol and phospholipids.* Biochim Biophys Acta, 2003. **1610**(2): p. 159-73.

63. Subramanian, S.; McConnell, H. M., *Critical mixing in monolayer mixture of phospholipid and cholesterol.* Journal Phys. Chem., 1987. **91**: p. 1715-1718.

64. Huang, C., J.T. Mason, and I.W. Levin, *Raman spectroscopic study of saturated mixed-chain phosphatidylcholine multilamellar dispersions.* Biochemistry, 1983. **22**(11): p. 2775-80.

65. Fox, C.B., G.A. Myers, and J.M. Harris, *Temperature-controlled confocal Raman microscopy to detect phase transitions in phospholipid vesicles. Appl Spectrosc, 2007. **61**(5): p. 465-9.*

66. Koan, M.M. and G.J. Blanchard, Gauging the effect of impurities on lipid bilayer phase transition temperature. J Phys Chem B, 2006. **110**(33): p. 16584-90.

67. Jacobs, R.E.; White, S. H., *Behavior of hexane dissolved in dioleoylphosphatidylcholine bilayers: an NMR and calorimetric study.* J Am Chem Soc, 1984. **106**(23): p. 6909-12.

68. Lemmich, J.; Mortensen, K.; Ipsen, J. H.; Hoenger, T.; Bauer, R.; Mouritsen, O. G., *The effect of cholesterol in small amounts on lipid-bilayer softness in the region of the main phase transition.* Eur Biophys J, 1997. **25**(4): p. 293-304.

69. Rowat A.C.; Keller D.; Ipsen, J.H., *Effects of farnesol on the physical properties of DMPC membranes.* Biochimica et biophysica acta, 2005. **1713**(1): p. 29-39.

70. Bondar, O.P., G. Melnykovych, and E.S. Rowe, *Effects of farnesol on the thermotropic behavior of dimyristoylphosphatidylcholine.* Chem Phys Lipids, 1994. **74**(1): p. 93-8.

71. Huang, W. and D.G. Levitt, *Theoretical calculation of the dielectric constant of a bilayer membrane.* Biophys J, 1977. **17**(2): p. 111-28.

72. Di Biasio, A. and C. Cametti, *Dielectric properties of aqueous zwitterionic liposome suspensions.* Bioelectrochemistry, 2007. **70**(2): p. 328-34.

73. Tocanne, J.F.; Teissie J., *Ionization of phospholipids and phospholipid-supported interfacial lateral diffusion of protons in membrane model systems.* Biochim Biophysica Acta, 1990. **1031**(1): p. 111-42.

74. Shepherd, J.C.W.; Bueldt, G., *Zwitterionic dipoles as a dielectric probe for investigating head group mobility in phospholipid membranes.* Biochimica et Biophysica Acta, Biomembranes, 1978. **514**(1): p. 83-94.

75. Bernik, D.L.; Zubiri, D.; Tymczyszyn, E.; Disalvo, E. A., *Polarity and Packing at the Carbonyl and Phosphate Regions of Lipid Bilayers.* Langmuir, 2001. **17**(21): p. 6438-6442.

76. Sackmann, E. and H. Trauble, *Studies of the crystalline-liquid crystalline phase transition of lipid model membranes. I. Use of spin labels and optical probes as indicators of the phase transition.* J Am Chem Soc, 1972. **94**(13): p. 4482-91.

77. Flewelling, R.F. and W.L. Hubbell, *The membrane dipole potential in a total membrane potential model. Applications to hydrophobic ion interactions with membranes.* Biophys J, 1986. **49**(2): p. 541-52.

78. Stuchly, M.A.; Stuchly, S. S.; Liburdy, R.P.; Rousseau, D. A., *Dielectric properties of liposome vesicles at the phase transition.* Phys. Med. Biol., 1988. **33**(11): p. 1309-1324.

79. Sujatha, J.; Mishra, A. K., *Effect of ionic and neutral surfactants on the properties of phospholipid vesicles: investigation using fluorescent probes.* J. Photochem. Photobiol. A: Chem., 1997. **104**: p. 173-178.

80. Kaiser, R.D.; London, E., *Location of diphenylhexatriene (DPH) and its derivatives within membranes: comparison of different fluorescence quenching analyses of membrane depth.* Biochemistry, 1998. **37**: p. 8180-8190.

81. Lakowicz, R.L., *Principles of Fluorescence Spectroscopy, Second Edition.* Plenum, Publishers, 1999. **233 Spring str. New York, N. Y.** (10013).

82. Klymchenko, A.S., et al., *Bimodal distribution and fluorescence response of environment-sensitive probes in lipid bilayers.* Biophys J, 2004. **86**(5): p. 2929-41.

83. Furlong, S.T., K.S. Thibault, and R.A. Rogers, *Fluorescent phospholipids preferentially accumulate in sub-tegumental cells of schistosomula of Schistosoma mansoni.* J Cell Sci, 1992. **103 (Pt 3)**: p. 823-30.

84. Pucadyil, T.J., S. Mukherjee, and A. Chattopadhyay, *Organization and dynamics of NBD-labeled lipids in membranes analyzed by fluorescence recovery after photobleaching.* J Phys Chem B, 2007. **111**(8): p. 1975-83.

85. Zubrzycki, I.Z.; Xu, Y.; Madrid, M.; Tang, P., *Molecular dynamics simulation of a fully hydrated dimyristoylphosphatidylcholine membrane in liquid- crystalline phase.* Journal of Chemical Physics, 2000. **112**(7): p. 3437-3441.

86. Bursing, H.; Ouw, D.; Kundu, S.; Vohringer, P., *Probing solvation Dynamics in liquid water and at phospholipid/ water interface with femtosecond photon-echo spectroscopies.* Physical Chemistry Chemical Physics, 2001. **3**(12): p. 2378-2387.

87. Mazeres, S., et al., *7-nitrobenz-2-oxa-1,3-diazole-4-yl-labeled phospholipids in lipid membranes: differences in fluorescence behavior.* Biophys J, 1996. **71**(1): p. 327-35.

88. Sykora, J.;Slavicek, P.; Jungwirth, P.; Barucha, J.; Hof, M., *Time-Dependent Stokes Shifts of Fluorescent Dyes in the Hydrophobic Backbone Region of Phospholipid Bilayer: Combination of Fluorescence Spectroscopy and Ab initio Calculations.* Journal of Physical Chemistry B, 2007. **111**(21): p. 5869-5877.

89. Prendergast, F.G.; Haugland, R. P.; Callahan, P. J., *1-[4-Trimethylamino)phenyl]-6-phenylhexa-1,3,5 triene: Synthesis, fluorescence properties, and use as a fluorescence probe of lipid bilayers.* Biochemistry, 1981. **20**: p. 7333-7338.

90. Kazuhiko, K., Jr.; Suguru K.; Akira I., *Dynamic Structure of Biological and Model Membranes: Analysis by Optical Anisotropy Decay Measurement.* Adv. Biophys., 1984. **17**: p. 147-203.

91. Kazuhiko, K., Jr.; Suguru K.; Akira I., *A Theory of Fluorescence Polarization decay in membranes.* Biophysical Journal, 1977. **20**: p. 289-305.

92. Chattopadhyay, A., *Chemistry and biology of N-(7-nitrobenz-2-oxa-1,3-diazol-4-yl)-labeled lipids: fluorescent probes of biological and model membranes.* Chem Phys Lipids, 1990. **53**(1): p. 1-15.

93. Huster, D., et al., *Dynamics of membrane penetration of the fluorescent 7-nitrobenz-2-oxa-1,3-diazol-4-yl (NBD) group attached to an acyl chain of phosphatidylcholine.* Biophys J, 2001. **80**(2): p. 822-31.

94. Brown, R.S.; Brennan, J. D.; Krull, U.J., *Self-quenching of nitrobenzoxadiazole labeled phospholipids in lipid membranes.* Journal of Chemical Physics, 1994. **100**(8): p. 6019-27.

95. McIntyre, J.C.; Sleight, R.G., *Fluorescent Assay for Phospholipid Membrane Asymmetry.* Biochemistry, 1991. **30**(51): p. 11819-11827.

96. Langner, M. and S.W. Hui, *Dithionite penetration through phospholipid bilayers as a measure of defects in lipid molecular packing.* Chem Phys Lipids, 1993. **65**(1): p. 23-30.

97. Alakoskela, J.-M.; Kinnunen, Paavo K. J., *Control of Redox Reaction on Lipid Bilayer Surfaces by Membrane Dipole Potential.* Biophys J, 2001. **80**: p. 294-304.

98. Alakoskela, J.-M.; Kinnunen, Paavo K. J., *Probing phospholipid main phase transition by fluorescence spectroscopy and surface redox reaction.* Journal of Physical Chemistry B, 2001. **105**(45): p. 11294-11301

99. Abreu, M.C.S.; Moreno,M.J.; Vaz, W.L.C., *Kinetics and Thermodynamics of Association of a Phospholipid Derivative with Lipid Bilayer in Liquid-Disordered and Liquid-Ordered Phases.* Biophys J, 2004. **87**: p. 353-365.

100. Moreno, M.J., L.M. Estronca, and W.L. Vaz, *Translocation of phospholipids and dithionite permeability in liquid-ordered and liquid-disordered membranes.* Biophys J, 2006. **91**(3): p. 873-81.

101. Benvegnu, D.J.; McConell, Harden M., *Surface dipole densities in lipid monolayers.* Journal of Physical Chemistry, 1993. **97**(25): p. 6686-91.

102. Gruber, H.J. and H. Schindler, *External surface and lamellarity of lipid vesicles: a practice-oriented set of assay methods.* Biochim Biophys Acta, 1994. **1189**(2): p. 212-24.

103. Moscho, A., et al., *Rapid preparation of giant unilamellar vesicles.* Proc Natl Acad Sci U S A, 1996. **93**(21): p. 11443-7.

104. Girard, P., et al., *A new method for the reconstitution of membrane proteins into giant unilamellar vesicles.* Biophys J, 2004. **87**(1): p. 419-29.

105. Leonard, A.; Celine, E.; Laguerre, M.; Pebay-Peyroula, E.; Neri, W.; Pott, T.; Katsara, J.; Dufourc, E. J., *Location of Cholesterol in DMPC Membranes. A comparative Study by Neutron Diffraction and Molecular Mechanics Simulation.* Langmuir, 2001. **17**(6): p. 2019-2030.

106. Sackmann, E., *Physical basis of self-organization anf function of membranes: Physics of vesicles.* Structure and Dynamics of Membranes: From Cells to Vesicles. R.Lipowski and E. Sackmann, eds., 1995(Elsvier, Amsterdam): p. 213-304.

107. Chattopadhyay, A. and E. London, *Parallax method for direct measurement of membrane penetration depth utilizing fluorescence quenching by spin-labeled phospholipids.* Biochemistry, 1987. **26**(1): p. 39-45.

108. Akashi, K.; Miyata, H.; Itoh, H.; Kinosita, K., Jr., *Formation of giant liposomes promoted by divalent cations: critical role of electrostatic repulsion.* Biophys J, 1998. **74**(6): p. 2973-82.

109. Bentz, J., N. Duzgunes, and S. Nir, *Temperature dependence of divalent cation induced fusion of phosphatidylserine liposomes: evaluation of the kinetic rate constants.* Biochemistry, 1985. **24**(4): p. 1064-72.

110. Monti, J.A., S.T. Christian, and W.A. Shaw, *Synthesis and properties of a highly fluorescent derivative of phosphatidylethanolamine.* J Lipid Res, 1978. **19**(2): p. 222-8.

111. Raghuraman, H., S. Shrivastava, and A. Chattopadhyay, *Monitoring the looping up of acyl chain labeled NBD lipids in membranes as a function of membrane phase state.* Biochim Biophys Acta, 2007. **1768**(5): p. 1258-67.

112. Klymchenko, A.S.; Mely, Y.; Demchenko, A.P., Duportail, G., *Simultaneous probing of hydration and polarity of lipid bilayers with 3-hydroxyflavone fluorescent dyes.* Biochimica et Biophysica Acta, 2004. **1665**: p. 6-19.

113. Heimburg, T., *Mechanical aspects of membrane thermodynamics. Estimation of the mechanical properties of lipid membranes close to the chain melting transition from calorimetry.* Biochim Biophys Acta, 1998. **1415**(1): p. 147-62.

114. Mabrey, S. and J.M. Sturtevant, *Investigation of phase transitions of lipids and lipid mixtures by sensitivity differential scanning calorimetry.* Proc Natl Acad Sci U S A, 1976. **73**(11): p. 3862-6.

115. Langner, M. and S. Hui, *Effect of free fatty acids on the permeability of 1,2-dimyristoyl-sn-glycero-3-phosphocholine bilayer at the main phase transition.* Biochim Biophys Acta, 2000. **1463**(2): p. 439-47.

116. Arvinte, T.; Cudd, A.; Hildenbrand, K., *Fluorescence studies of the incorporation of N-(7-nitrobenz-2-oxa-1,3-diazo-4-yl)-labeled*

phophatidylethanolamines into liposomes. Biochim Biophys Acta, Biomembranes, 1986. **860**((2)): p. 215-28.

117. Chattopadhyay, A. and S. Mukherjee, *Fluorophore environments in membrane-bound probes: a red edge excitation shift study.* Biochemistry, 1993. **32**(14): p. 3804-11.

118. Ramachandran, R., R.K. Tweten, and A.E. Johnson, *Membrane-dependent conformational changes initiate cholesterol-dependent cytolysin oligomerization and intersubunit beta-strand alignment.* Nat Struct Mol Biol, 2004. **11**(8): p. 697-705.

119. Chattopadhyay, A. and E. London, *Spectroscopic and ionization properties of N-(7-nitrobenz-2-oxa-1,3-diazol-4-yl)-labeled lipids in model membranes.* Biochim Biophys Acta, 1988. **938**(1): p. 24-34.

120. Saha, S.; Samanta, A., *Photophysical and Dynamic of NMR Studies on 4-Amino-7-nitrobenz-2-oxa-1,3-diazole Derivatives: Elucidation of the Nonradiative Deactivation Pathway.* Journal of Physical Chemistry A, 1998. **102**(41): p. 7903-7912.

121. Halstenberg, S., et al., *Cholesterol-induced variations in the volume and enthalpy fluctuations of lipid bilayers.* Biophys J, 1998. **75**(1): p. 264-71.

122. Genz, A., J.F. Holzwarth, and T.Y. Tsong, *The influence of cholesterol on the main phase transition of unilamellar dipalmytoylphosphatidylcholine vesicles. A differential scanning calorimetry and iodine laser T-jump study.* Biophys J, 1986. **50**(6): p. 1043-51.

123. Vist, M. R.; Davis, J. H., *Phase equilibria of cholesterol/dipalmitoylphosphatidylcholine mixtures: 2H nuclear magnetic resonance and differential scanning calorimetry.* Biochemistry, 1990. **29**(2): p. 451-64.